A model-based reconstruction of recent Siberian climate - focusing on snow cover

Dissertation

zur Erlangung des Doktorgrades

der Naturwissenschaften im Fachbereich

Geowissenschaften

der Universität Hamburg

vorgelegt von

Katharina Klehmet

aus Dresden

Hamburg

2014

Als Dissertation angenommen vom Fachbereich Geowissenschaften

der Universität Hamburg

auf Grund der Gutachten von Prof. Dr. Hans von Storch

und Dr. Burkhardt Rockel

Hamburg, den 28.01.2014

Prof. Dr. Christian Betzler
Leiter des Fachbereichs Geowissenschaften

Abstract

Snow cover is an important feature of the terrestrial landscape in Siberia. Variability and changes of snow cover have profound implications for surface energy and water balance, first due to its high short-wave albedo, high thermal emissivity and low heat conductivity, and second due to the control of evaporation, water storage, soil moisture, river discharge and freshwater transport. The snow properties affect moreover the soil temperature and thus the thermal state of permafrost and the biogeochemical cycle.

Monitoring of Siberian climate parameters, including those for snow cover, is complicated by the lack of in situ measurements, especially in the arctic regions. The sparse station density and limited length of data records makes it difficult to obtain a detailed regional overview of past and ongoing changes. The need of long-term climate information with less spatial and temporal gaps has motivated the effort to generate a model-based reconstruction of recent Siberian climate using the regional model COSMO-CLM (CCLM).

Although CCLM has been used for several areas, no simulations have been conducted for Siberia before. Therefore, different sensitivity experiments have been performed to identify important regional-specific processes and related adjustments that can be used for a specific model configuration for Siberia. These adjustments are an increased soil column depth down to 92 m, the application of the multi-layer snow model and the reduction of the minimal heat diffusion that has implications on the turbulence parameterization to better account for the stable conditions during the winter high pressure system.

One hindcast simulation has been conducted from 1948-2010 at about 50 km grid spacing using NCEP-R1 as driving global reanalysis to obtain a reconstruction of 63 years and to investigate long-term regional changes of climate parameters focusing on snow cover. A second climate reconstruction has been performed for comparison using ERA-40 reanalysis as forcing that range from 1958-2001.

Concerning the temporal evolution of reconstructed climate parameters, both hindcast simulations show considerable discrepancies prior 1970s. These discrepancies can be related to the varying large-scale atmospheric information of the driving global reanalyses (NCEP-R1 and ERA40). The temporal uncertainties in NCEP-R1 before 1979, mainly in southern parts of the domain, and in ERA40 before 1968, have strong implications on the regional climate reconstruction. Consequently, the reconstructed datasets cannot be used for the whole model domain and over their entire simulation period.

Near-surface temperature is in good accordance with observations in summer and spring but shows an overestimation in winter mainly in the central and northeastern part. There

is a tendency of CCLM to overestimate seasonal precipitation in the southern and north-eastern regions in winter, spring and fall whereas during summer an underestimation is evident in southern and western regions.

In terms of snow cover, snow water equivalent (SWE) is one important parameter to consider. CCLM-NCEP1 is able to provide more realistic SWE information from 1987-2010 relative to the global driving data NCEP-R1 and thus show a clear added value when compared with the satellite-derived SWE product of ESA GlobSnow as reference. The temporal consistency of CCLM is higher than that presented by ERA-Interim and NCEP-R2.

In general, changes and interannual variations of mean SWE are characterized by strong spatial and seasonal variability. According to CCLM-NCEP1, regional averages for the period of 1981-2010 show only minor changes of SWE during fall, whereas during winter and spring stronger changes occur with varying patterns throughout the region. Both hindcasts show stronger interannual variations of snow cover extent during the transition seasons spring and fall than in winter. During spring a negative tendency is evident since the early 1980s, which has ceased in recent years.

Contents

1 Introduction

1.1 Motivation

Siberia, a vast region extending from the polar to the temperate and subtropical latitudes of Russia, is characterized by one of the most continental climates on earth. Being a region where temperature rise has been among the most pronounced globally (Groisman et al. 2009), Siberia is a hot spot of climate change. According to Roshydromet (2008) the temperature increase in Russia was 1.29°C for the last 100 years (1907-2006) compared to the global average of 0.74°C (IPCC 2007).

Moreover, Siberia is the one of the world's largest cold regions characterized by some outstanding components of the cryosphere. More than 60 % of the Russian's terrestrial surface is underlain by permafrost (Anisimov and Reneva, 2006) and seasonal sea ice is characteristic of the adjacent Arctic Ocean. In addition, terrestrial snow cover is a key component of the cryosphere and plays an important role in the entire climate system by modifying surface energy and water balance (Alexander et al., 2010; Cook et al., 2008). This extensive, rapidly and seasonally changing cryospheric variable is critical in shaping the land surface of Siberia during the prolonged cold season (Bulygina et al., 2009).

Numerous studies indicate that Siberian snow cover and its changes have the potential to influence large-scale atmospheric circulation (Allen and Zender, 2011; Cohen et al., 2012). Evidence that Eurasian snow cover may feed back to Arctic and North-Atlantic Oscillation was discussed by Alexeev et al. (2012). A review of recent studies on Arctic snow was published within the SWIPA (Snow, Water, Ice and Permafrost in the Arctic) report by Callaghan et al. (2011) to highlight its importance. The higher albedo of snow-covered compared to snow-free surfaces leads to an increased reflectance of solar radiation and a near-surface cooling (Stieglitz et al., 2003; Vavrus, 2007). Additionally, the low thermal conductivity of snow makes it a good insulator that limits the heat exchange between soil and atmosphere. Changes in snow accumulation, extent, timing, duration and density have profound implications for soil temperatures and, therefore, for permafrost thermal state (Shkolnik et al., 2010; Stieglitz et al., 2003; Zhang et al., 2005), ecology and biogeochemical cycles (Sturm et al., 2005). Moreover, snow cover plays an important role within the hydrological cycle that controls evaporation, water storage, soil moisture, river discharge and freshwater transport to the Arctic Ocean (Groisman and Amber, 2009; Troy et al., 2012; Yang et al., 2003).

The documentation of changes and variability of terrestrial snow cover in Siberia is fundamental for climate change detection and understanding of snow-climate interactions. Several studies have focused on the assessment of snow cover extent using satellite-derived products or in situ measurements of snow depth or snow water equivalent (SWE; the equivalent depth of liquid water that would result from melting the snow pack) (Bulygina

et al., 2011; Shmakin, 2010). According to Bulygina et al. (2011) an overall tendency of increasing maximum values of SWE was evident since 1966 over Siberia, whereas a decreasing length of snow season was observed.

However, the analysis of long-term changes and trends of climate parameters for all of Russia is hampered by the lack of reliable observational data (Bulygina et al., 2011; Ge and Gong, 2008). The availability of continuous, homogeneous in situ snow observations in Siberia is restricted because of a sparse meteorological network and incomplete data records (Brown et al., 2003; Khan et al., 2008; Serreze et al., 2003). Furthermore, the documentation still lacks regional detail (Brown and Mote, 2009), especially for snow variables describing the amount and accumulation of snow, such as SWE, that are characterized by complex spatial distribution (Callaghan et al., 2011). Estimates of historical SWE from remote sensing are still difficult to derive (Takala et al., 2009) and show large discrepancies from reanalysis products (Khan et al., 2008).

To overcome this problem, regional hindcasts obtained using regional climate models (RCMs) are useful for filling the spatial gaps between sparse weather stations and deliver multi-decadal climatologies of various meteorological parameters – including SWE – on a uniformly spaced grid. These reconstructions provide dynamically consistent data that is continuous in time. Additionally, they offer greater spatial and temporal resolution than observations alone. To perform regional hindcasts, large-scale atmospheric fields of global reanalysis data are taken as initial and boundary conditions over a limited area (Giorgi, 1990; Giorgi and Mearns, 1999). This technique of dynamical downscaling allows a more detailed representation of regional aspects, e.g. land-sea contrast, local orography, land-cover and small-scale atmospheric features. It is expected that this technique leads to a better description of regional climate than that presented by coarsely resolved global reanalyses.

There have been several efforts to apply RCMs over Siberia. Most consider a pan-Arctic domain that includes northern parts of Siberia (e.g., Rinke et al., 2010). Within the SHEBA (Surface Heat Budget of the Arctic Ocean) project, an ensemble was evaluated to quantify the scatter among different RCMs and to assess the reliability of their Arctic simulations (Rinke et al., 2006). The Polar Weather Research and Forecasting (Polar WRF) model (e.g., Bromwich et al., 2009) was used to provide a high resolution (10 km) Arctic System Reanalysis for 2000-2011. Shkolnik et al. (2010) used the MGO (Main Geophysical Observatory) regional climate model for permafrost and snow cover studies. Furthermore, Brun et al. (2012); Liston and Hiemstra (2011) performed regional snow simulations over pan-Arctic or Siberia using detailed snow pack models coupled to a land-surface scheme, forced by global hydro-meteorological data.

1.2 Objectives

The objective of this work is to use the whole model system of the regional climate model COSMO-CLM (CCLM) with its land–atmosphere interactions to obtain a regional climate hindcast over Siberia for the longest possible period until present (1948–2010), that can be used to investigate long-term regional changes of snow cover, with a focus on SWE and snow extent. Therefore, NCEP-R1 is used for the primary driving global reanalysis as more recent global reanalysis projects provide only noticeably shorter periods. For comparison, a second climate reconstruction is aimed to derive using ERA40 reanalysis as forcing that range from 1958-2001.
The following questions are addressed within this work:

- What does an optimized model configuration of CCLM for Siberia look like?
- How reliable are the derived regional climate model hindcasts and their forcings over Siberia with respect to their temporal consistency?
- Is CCLM able to represent realistic climate conditions in Siberia for recent years?
- How do snow water equivalent over Siberia differ by different reanalyses and can CCLM add value?
- What are the characteristics of change patterns of snow cover for the past decades in Siberia?

To answer these questions, initially a model configuration of CCLM for Siberia is defined and tested, as the standard setup is mainly optimized for Europe. The adjusted model setup is then used to conduct regional climate hindcast simulations for Siberia.

1.3 Structure of Thesis

In Chapter 2 the physical and basic climatological features of the area of investigation are introduced. An overview of the regional climate model CCLM with its important characteristics used in this study is given in Chapter 3. Chapter 4 addresses the model configuration for Siberia and necessary sensitivity studies that have been undertaken to determine the setup. In Chapter 5 aspects of temporal reliability of derived hindcasts and the underlying forcings are presented. A basic evaluation of simulated parameters is provided in Chapter 6, investigating the ability of CCLM to represent climate characteristics in Siberia. A large-scale added value assessment of simulated snow water equivalent and comparison to a set of reanalyses is conducted in Chapter 7. Chapter 8 focuses on the investigation of regional change patterns of terrestrial snow cover in Siberia over recent decades. Finally, conclusions and the outlook are presented.

2 Siberia and its Climate Characteristics

2.1 Geographical Location and Physical Features

Siberia, a vast landmass between ∼45°N to ∼75°N and ∼70°E to ∼150°E, covers an area of about 10 million km^2, almost 60 % of the Russian Federation. It accounts for approximately 11 % of the global terrestrial land surface (Groisman and Gutman, 2012) and thus encompasses one of the largest continuous land areas on Earth (Shaw, 1999). The geographic location approximates an area that stretches east of Ural Mountains to the mountain ranges of the Pacific watershed and from the borders of Kazakhstan, Mongolia and China in the south to the Arctic Ocean in the north. Siberia ranges from subtropical and temperate latitudes in the south to the subpolar and polar latitudes in the north.

Investigation Area

In this work the defined area of Siberia and the area of investigation does not encompass the exact domain according to the geographical expression. Fig. 2.1 presents the Siberian model domain of the CCLM hindcast simulation on a lat/lon grid and subregions considered throughout this work. It covers a region in Siberia that spans from the Laptev Sea and Kara Sea to northern Mongolia and northern China and from the West Siberian Lowland to the border of Sea of Okhotsk. The subregions are: Arctic-West (AW), Arctic-East (AE), Mid-West (MW), Mid-Mid (MM), Mid-East (ME), South-West (SW) and South-East (SE), representing the Arctic (northwards of the Arctic Circle), subarctic regions and those of the mid-latitudes.

Regional orographic features

Regional variations of climate are strongly determined by the specification of Siberian orography. The relief is characterized by mountains and intermontane basins. Important physical features are the Central Siberian Plateau and several lowlands, as e.g. are the West Siberian Plain and the lowland of the Lena river basin (Lydolph, 1977). Furthermore, several mountain ranges separate the basins as e.g. the Verkhoyansk Mountains north-east of Lena river basin and of the southern domain including Altai, West Sayan, Eastern Sayan Mountains and the Stanovoy Range north-east of Lake Baikal. The north-eastern part of the model domain is characterized by Yana ridge and Kolyma Mountains. The West Siberian Plain extends east from the Ural Mountains to the valley of the Yenisei. It is a vast basin with an average elevation below 200 m (Wood, 1987). The land cover is dominated by swamps and taiga forests along the rivers (Groisman and Gutman, 2012). East of the Yenisei valley is the Central Siberian Plateau, an enormous highland with a general elevation of about 500-700 m and maximum height of 1.700 m north-west in the Putorana mountains (Wood, 1987). The edges of that plateau are steep (Wood, 1987), especially in the west due to an escarpment. The dominant land cover is coniferous forest.

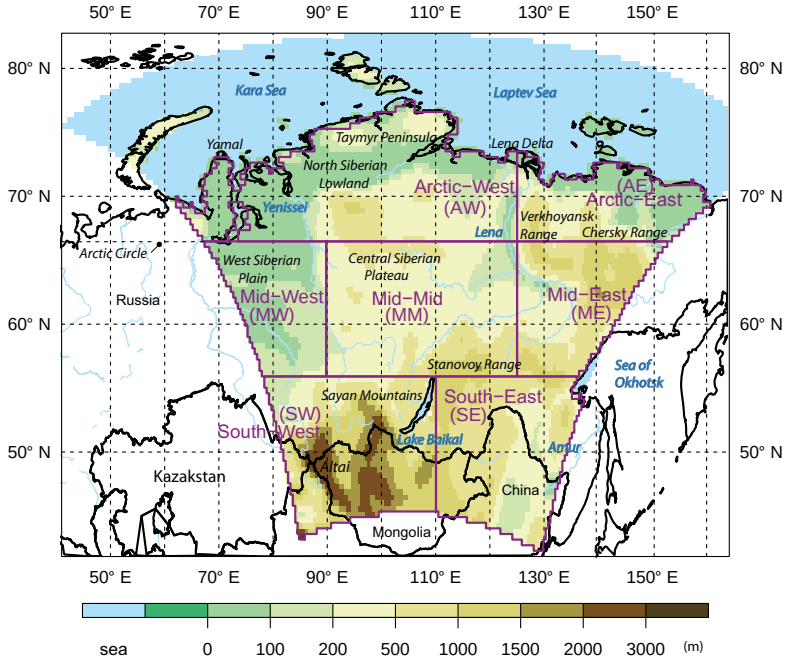

Figure 2.1: Orography [m] of model domain of CCLM (coloured area) for Siberia and considered subregions (purple) on lon/lat grid.

Important mountain ranges include the Sayan and adjacent mountains. In the south-east between Krasnoyarsk and Irkutsk, the Sayan mountains are seperated by a deep tectonic through (Wood, 1987). Lake Baikal is a large waterfilled rift valley of about 636 km length and the deepest fresh-water lake on Earth. Characteristic lowlands include the lowland of the Lena river basin and the North Siberian lowland that stretches north of the slopes of the Putorana mountains between the Lena Delta and the West Siberian Plain (Wood, 1987). Vegetation of the North Siberian Plain is a mixture of trees, bushes with tundra grasses and moss (Wood, 1987). The northernmost part of the region is the lowland of the Taimyr peninsula reaching into the Arctic Ocean. The land cover of this Peninsula and adjacent coastlands is tundra.

General characteristics and their climate effects

Several physical factors are responsible for the formation of typical characteristics of Siberian climate. An important feature is the enormous size of the Siberian land surface with its wide latitudinal extension and a relatively northern position (most of the territory is situated north of 50°N) (Wood, 1987). Due to the large extent of land mass, many regions are far from the influence of adjacent Pacific or Atlantic Ocean. The specific arrangements of mountains and lowlands lead to the creation of unique regional climate characteristics. The vicinity of the Arctic Ocean leads to a cooling effect of the nearby coastal areas during summer and even more so during winter when the Arctic Ocean is covered by sea ice. The maritime influence of the Pacific Ocean is limited as cold currents

are predominant and high mountain ranges along the coast acts as a barrier (Dewdney, 1971). Even in winter the maritime influence is limited as offshore winds prevail. Relief features act as barriers in the eastern and southern part whereas the interior is open northward to the influences of the Arctic Ocean and westwards to the moist air masses that originate from the Atlantic (Shaw, 1999). For most of Siberia, all of these factors create an extreme continental climatic regime, characterized by cold winters and short warm summers and relatively small amounts of rainfall (Shaw, 1999; Dewdney, 1971). For some peripheral areas, such as parts of Central Asia and Russian Far East, different climatic characteristics are predominant. The huge deficit of energy in subarctic and arctic regions is supplemented by atmospheric circulation which determines the spatial and temporal characteristics of the climate in Siberia (Przybylak, 2003; Serreze and Barry, 2005). All of these factors favour specific vegetation types and soil conditions, greatly influenced by permafrost.

2.2 Basic characteristics of Siberian Climate

Atmospheric Circulation

During winter, surface and near-surface circulation is mainly dominated by the Siberian High pressure system which controls the climatic regime of the region and acts as an important atmospheric centre (Przybylak, 2003). This low-level feature is mainly driven by radiative cooling of the surface and is, on average, strongest in January and February (Serreze and Barry, 2005). Its centre is situated near Lake Baikal (Przybylak, 2003). The high pressure system extends to the north-east where a secondary centre establishes across the Lena river basin (Lydolph, 1977) and is limited to the east by the Pacific Ocean. The thermally induced Siberian High represents a shallow pressure system of approximately 1.5 km height. Above, a predominant trough ranges from the Barents Sea south-eastwards and to the Aleutian low in the north-east and the Icelandic low situated in the north-west. An important influence during winter is the Icelandic low for the western and northern parts, inducing Atlantic depressions that move eastwards. If the Siberian High has a strong extension to Europe, the depressions are blocked and forced to move northwards to the Arctic regions, mainly along the Lena and Kolyma rivers (Przybylak, 2003).

In April, when solar heating is stronger, the Siberian High is less developed and its centre moves to the west (Serreze and Barry, 2005). During summer the high pressure system is replaced by a shallow, diffuse low-pressure system (Przybylak, 2003; Serreze and Barry, 2005). In the northern part a frontal zone establishes from ∼60-70°N (Serreze and Barry, 2005).

The mid-tropospheric (500hPa) circulation of the northern high latitudes is characterized mainly by a cyclonic vortex that is predominant for most of the year, but is weaker during summer time (Serreze and Barry, 2005). Due to dynamically induced perturbation by

the Ural Mountains and the radiative gradient between land and ocean, the mean flow exhibits a weak trough and a ridge over central Asia (Serreze and Barry, 2005).
The dominant mode of winter atmospheric circulation variability is related to the Arctic Oscillation (AO) (Thompson and Wallace, 1998; Allen and Zender, 2011) and North Atlantic Oscillation (NAO) (Hurrell, 1995). The AO is characterized by fluctuation of sea level pressure between the Arctic and anomalous pressure of opposite sign over the North Pacific (Allen and Zender, 2011). This atmospheric oscillation pattern strongly influences surface temperature, precipitation and winds in Eurasia (Allen and Zender, 2011). Atmospheric variability is also determined by the Scandinavian pattern (SCAND) that consists of a circulation center over Scandinavia and eastern Russian and western Mongolia.

Air Temperature

The temperature regime in Siberia is strongly determined by its position and vastness of land area. Main influences are the energy balance (incoming solar radiation, strong energy loss during winter) and atmospheric circulation. Regional variations occur due to effects of local relief features. In general, a strong continental climate is predominant, i.e. the annual temperature range is large due to low temperatures in winter and high during summer. Low temperatures in winter are, except for the northwest, associated with the Siberian Anticyclone (mean values below -40°C in January) (Serreze and Barry, 2005) which is associated with clear, and cold weather. A west-east temperature gradient occurs representing the increasing continentality towards inland. In basins and valleys, cold air lakes can produce a specific local climate (Serreze and Barry, 2005). In central Siberia a special feature during winter is the strong low-level temperature inversion (temperature increase with height) that is elevated up to 1200 m during January-March (Serreze and Barry, 2005) which is characteristic for the stable atmospheric conditions of the Siberian High. This near-surface feature is weaker during May-September (Serreze and Barry, 2005). During summer the temperatures are, in general, high. Hot air advection can take place from Mongolia and China whereas cold air masses reach the coast from the Arctic.

Precipitation

In general, annual average precipitation mostly range from 200-600 mm with higher values along the mountain ranges and lower along the arctic coast in the north-eastern part of the domain (Lydolph, 1977). Precipitation totals are low especially in regions where the influence of moist air masses from the Atlantic or Pacific is limited. Northward, towards the Kara Sea, precipitation decreases due to the decay of the cyclone track (Serreze and Barry, 2005). In general, from November-March, solid precipitation (snow) is predominant. During summer the cyclone activity increases in the northern areas and convection takes place leading to a summer maximum. 60-70° N is characterized by pronounced cyclone activity due to the barocline Arctic frontal zone (Serreze and Barry, 2005).

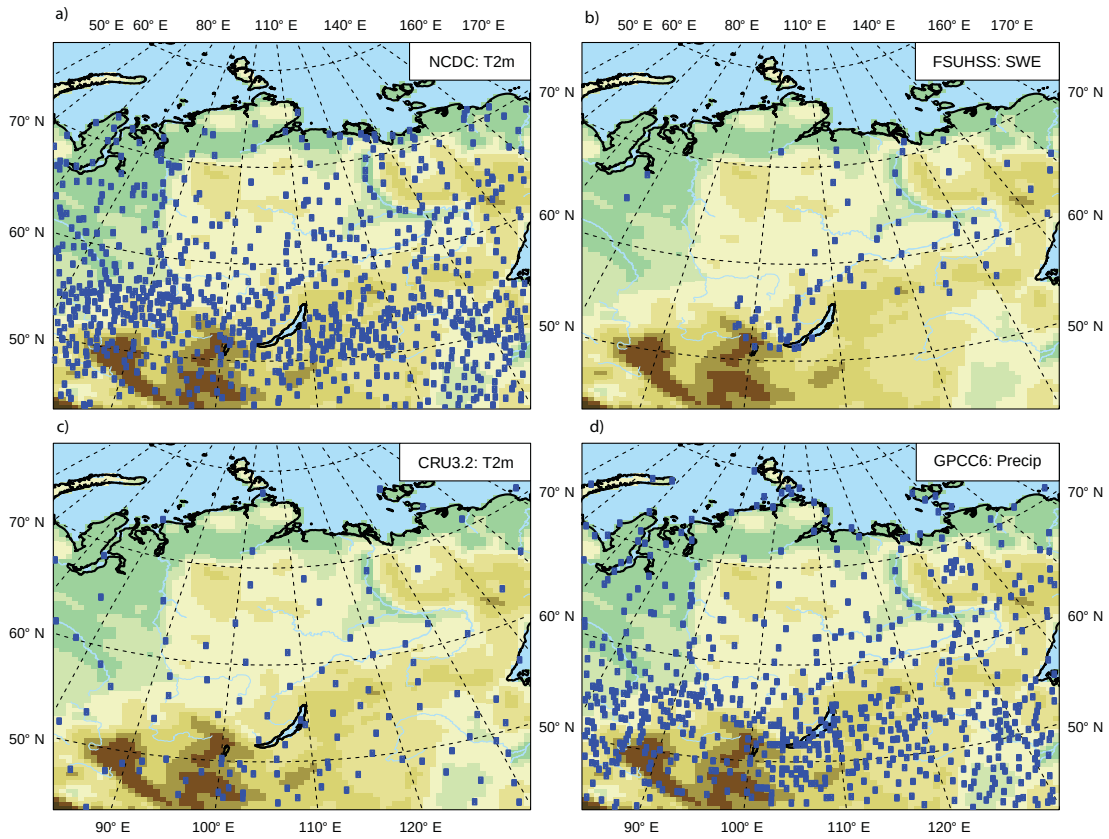

Figure 2.2: Distribution of available in situ measurements of four different datasets. a) Stations with 2 m air temperature measurements of NCDC dataset, b) transect measurements of SWE provided by FSUHSS, grid boxes with measurements of 2 m air temperature of c) CRU3.2 and d) precipitation of GPCC6.

2.3 Sparseness of in situ measurements

Scientific understanding and documentation of past and ongoing changes and variability of climate variables such as temperature, precipitation, soil temperature or snow requires sufficient long-term information that is consistent and homogeneous over time. Moreover, to present a detailed overview, data records with sufficient temporal and spatial coverage are necessary.

However, data supply in Siberia is constrained by a sparse station network of in situ measurements, unevenly distributed stations, data that often suffer from limited length and incomplete records or inhomogeneous measurement techniques (Adam and Lettenmaier, 2008; Groisman and Rankova, 2001; Serreze et al., 2003). Station density of meteorological variables is rather sparse, especially in the arctic regions (ACIA, 2005; Roshydromet, 2008). Fig. 2.2a and 2.2b presents the distribution of available stations provided by NCDC for 2 m air temperature and SWE data of FSUHSS snow transect measurements. The data coverage of 2 m air temperature measurements is largest in the southern parts of Siberia and Mongolia but sparse in the arctic regions. SWE transect measurements of FSUHSS are seldom and not distributed over the entire domain. More snow measurements exist,

offered by different services, but still the overall coverage is sparse.

Reliable measurements of certain variables at high-latitudes, e.g. precipitation, snow-depth or SWE are especially difficult to obtain due to problems of gauge-undercatch of wind induced losses or redistribution (Adam and Lettenmaier, 2008; Serreze et al., 2003). Altogether, this leads to a rather coarse description of contemporary changes and variability that lacks detail in presenting the spatial and altitudinal heterogeneity (Adam and Lettenmaier, 2008; Shmakin and Popova, 2006; Shulgina et al., 2011).

Several attempts have been made to generate historical long-term data sets with sufficient spatio-temporal coverage on an evenly distributed grid. For several variables there are globally gridded climatologies of observed station data as e.g. provided by the Climate Research Unit (CRU, Mitchell and Jones, 2005) or Global Precipitation Climatology Center (GPCC, Schneider et al., 2013). Station data was interpolated onto a regular grid of e.g. 0.5° (Mitchell and Jones, 2005). Fig. 2.2c and 2.2d show the maximal number of stations distributed over the considered Siberian domain that are incorporated as sources to construct these databases. The CRU TS 3.2 dataset (from here CRU3.2) for 2 m air temperature is based only on few stations, especially along the poor observed arctic coast. More station data were available for the precipitation dataset of GPCC (version 6: from here GPCC6, Fig. 2.2d). The number of stations are minimal for the northern high latitudes. Areas of the final grids that are based on a small number of observations are estimates that only likely represent real conditions. The source-related limitations are a clear disadvantage when using these gridded databases over certain areas in Siberia.

Another shortcoming in the observing system in Siberia, that affects the in situ observation quality, is the shrinkage of station network around 1990. In the following years, the station coverage was only about half of what it was in the 1980s. After the disintegration of the Soviet Union, many stations were closed (Adam and Lettenmaier, 2008; Khan et al., 2008; Serreze et al., 2003) or were not accessible in the late 1980s and early 1990s. In recent years the number of stations with information e.g. for 2 m of the daily station data ('Global Summary of the Day') provided by the National Climatic Data Center (NCDC) or by CRU have increased (Fig. 2.3). According to Mitchell and Jones (2005), this development is mainly due to improvements in the exchange of information by the Global Climate Observing System (GCOS). In contrast, the network of precipitation measurements used in GPCC has decreased in the last years (Fig. 2.3). SWE measurements provided by Former Soviet Union Hydrological Snow Surveys (FSUHSS) ended at 1996.

After 1970 satellite observations could partly compensate for the deficiencies of Siberian network of meteorological observing stations (Clifford, 2010; Khan et al., 2007). However, the spatio-temporal coverage depends on the satellite overpass and algorithms to derive estimates. Certain problems arise e.g. to deliver information by remote sensing of snow parameters, such as water equivalent, grain size, and depth especially in forest and

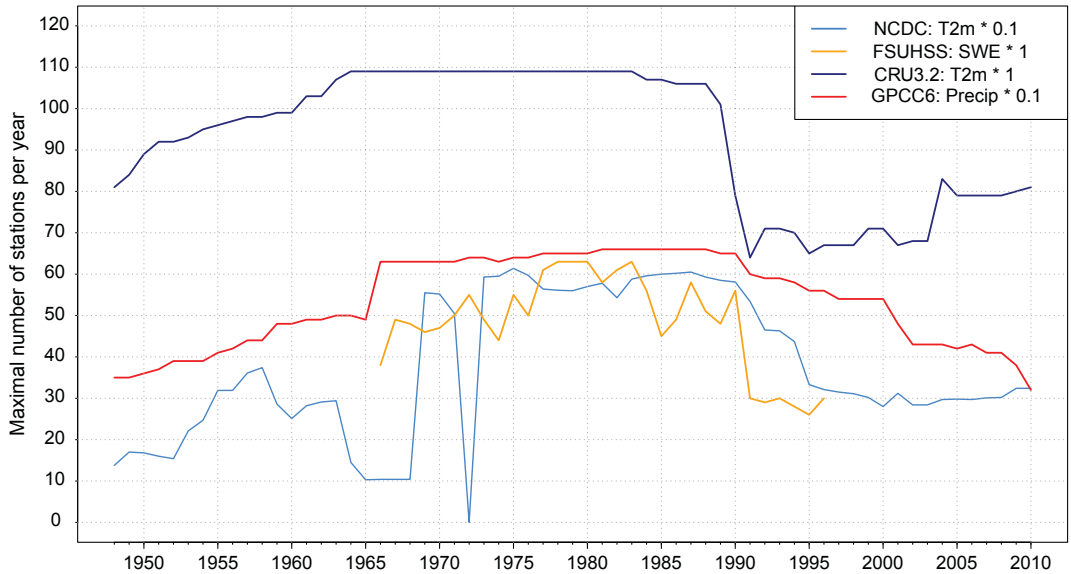

Figure 2.3: Maximal number of stations per year for 2m air temperature (T2m) of NCDC dataset, SWE of FSUHSS, 2m air temperature of CRU3.2 and precipitation (Precip) of GPCC6.

mountainous areas (Takala et al., 2011).

Further potential data sources, trying to fill observational data voids, are reanalyses. Using a fixed assimilation scheme, past observations are incorporated into an atmospheric numerical weather prediction model to provide a dynamical consistent three dimensional dataset for various variables on a uniformly spaced grid (Bromwich et al., 2007). However, it is known that outputs of different reanalyses can differ considerably at some locations (e.g., Bromwich et al., 2007; Simmons et al., 2004; Sterl, 2004) and can suffer from temporal discontinuities (Bengtsson et al., 2004). Moreover, the usability of snow information from reanalyses is limited by the coarse resolution and errors in the assimilation of snow observations (Callaghan et al., 2011; Khan et al., 2008). Even though some recent reanalysis products offer an increasing spatial resolution, the long-term products that predate 1979 are still on a coarse resolution, which limits the use for multi-decadal regional climate change studies.

There is a considerable need to construct datasets with less spatial and temporal gaps than what has been available to date. To overcome the sparseness of in situ observations over often remote areas of Siberia, we use the RCM CCLM to conduct a climate reconstruction over the period of 1948 to 2010, producing detailed regional historical climatologies.

3 The Regional Climate Model COSMO-CLM (CCLM)

3.1 General Description

To perform the regional climate hindcast simulations, the nonhydrostatic regional climate model CCLM (COSMO-CLM: http://www.clm-community.eu, Rockel et al. (2008)) is used. CCLM is the numerical weather prediction model COSMO (Steppeler et al., 2003) in climate mode, originally developed by the Deutscher Wetterdienst (DWD).

The dynamical part of the limited-area model CCLM is based on primitive thermo-hydrodynamical equations (e.g. conservation laws for momentum, mass and heat for the compressible nonhydrostatic flow of the atmosphere, Schaettler et al., 2008). The atmospheric prognostic variables are pressure deviation from the standard atmosphere, wind components, temperature, specific humidity and cloud water content (Schaettler et al., 2008). To solve the differential equations of the model, a horizontal, vertical and temporal discretization is applied (Roeckner, 2003). For the horizontal discretization, CCLM uses an Arakawa C-grid, accordingly scalar model variables (temperature, pressure and humidity variables) are defined in the center of the grid box. Vertically, a Lorenz grid is used, for which pressure and wind-vector components are defined at the border of the grid boxes (Schaettler et al., 2008). Due to the convergence of the meridians, the grid distances get smaller to the north which results in varying horizontal resolutions away from the equator (Roeckner, 2003). This feature is especially strong in the vicinity of the poles. To overcome this problem, the grid boxes, for which the model equations are solved, are defined on a rotated latitude-longitude coordinate system. This is achieved by rotating the north pole to bring the equator and the prime meridian through the model domain. For the vertical, a generalized terrain-following height coordinate (here: Gal-Chen) is used (Schaettler et al., 2008).

For the initial and boundary conditions, CCLM uses meteorological fields that are either provided by GCM simulations, re-/analyses or CCLM simulations with coarser horizontal resolutions (double nesting). Large-scale fields are e.g. wind speed, atmospheric temperature and pressure are interpolated at the RCM grid. At the lateral boundary in a sponge zone of 8 grid boxes, the prognostic variables are adopted to the driving data, based on the relaxation scheme after Davies (1976). At the top of the model domain, Rayleigh damping is applied. At the lower boundary, CCLM obtain information on the Earth' land surface from external datasets. These are e.g. orography, land use and land cover characteristics, soil type and deep soil temperature. The information about sea or ice surface temperature and sea ice extent enters CCLM either by interpolating from the driving data or by a coupled regional ocean model. To date there is no coupled system for the Arctic in CCLM available. Therefore, CCLM takes interpolated values of the forcing data. In contrary to the initialisation, in which the forcing fields are taken for the whole model domain only at

the start of the simulation, the forcing data of the lateral boundaries and over the ocean is used here every 6 hours throughout the entire simulation period.
The CCLM-Community offers an optimized model configuration and parameter setup for Europe. This includes a specific configuration of physical parameterizations for resolving sub-grid scale processes. In this study, one aim is to provide an optimal model setup for Siberia that has not been available for CCLM. Therefore, the specific regional features and processes that determine Siberian climate need to be realistically represented. Important aspects are e.g. the representation of stable atmospheric conditions in the Siberian high pressure system, thermal effects of deep reaching permafrost soils and a realistic treatment of snow cover. Together, this implies a special consideration of land-surface treatment, including soil and snow aspects, and boundary layer processes in CCLM. In Chapter 4, sensitivity experiments are presented. These were undertaken to determine an optimized model setup for Siberia. As such, changes in parameter settings and physical parameterizations according to the regional peculiarities are considered. An overview of the general treatment of land-surface and boundary layer processes in CCLM is provided. Subsequently the effects of changes in underlying parameterizations in the performed test experiments are described.

3.2 Turbulence Parameterization

Turbulent fluxes are necessary to consider the description of atmospheric flow. They describe the exchange of heat, humidity and momentum between the atmosphere and surface. The turbulence parameterization used here for vertical turbulent transports is based on a diagnostic closure scheme – the 1-D TKE-Based closure scheme. A second-order closure at level 2.0 after Mellor and Yamada (1982) is applied for the vertical turbulent transport. The stability and roughness-length dependent surface flux formulation for the prandtl-layer is based on Louis (1979). A more detailed description was given by Doms et al. (2011).

3.3 Land-surface Treatment

The coupling between land and atmosphere in CCLM requires the knowledge of surface fluxes as the lower boundary condition. For the calculation of the energy and water fluxes in CCLM, the multi-layer soil and vegetation model TERRA-ML is applied as the standard land-surface scheme (Doms et al., 2011). It considers hydrological and thermal processes within the soil and surface and the specific characteristics of vegetation. These aspects are necessary to derive the temperature and specific humidity of the ground, which are needed for the calculation of the stability and roughness-length dependant surface fluxes. Soil in TERRA-ML, in a standard setup, is subdivided in 10 non-equidistant vertical soil layers that increase with thickness down to a depth of about 11.5 m for which

temperature and water content are calculated. The solution of the differential equations requires characteristic hydraulic and thermal parameters of the classified soil texture. In TERRA-ML, different soil horizons within the vertical soil profile are not taken into account. The thermal and hydraulic parameters are defined for only one texture per grid box that is valid for the whole soil column. 8 types with corresponding soil characteristics are defined in a standard setup. There are 5 types corresponding to soil texture (sand, sandy loam, loam, loamy clay and clay) and 3 additional ones (ice, rock, and peat). The hydrological processes for ice and rock are neglected (Doms et al., 2011).

Vegetation and Land-use

Vegetation in TERRA-ML is not explicitly included. Rather an external dataset of land cover (e.g. GLC2000) is used and specific plant characteristics are derived from the dominant land cover and land use type. These characteristics are fractional area covered by plants (plant cover), leaf area index (LAI) and roughness length. The interpolation between maximum and minimum values for LAI and plant cover enables the consideration of an annual cycle for these parameters (Doms et al., 2011).

Soil Processes

Soil hydrology in TERRA-ML is considered for three reservoirs: the interception reservoir (i.e. water that is held by vegetation and at soil surface), snow pack (including frozen surface water and rime) and soil layers until the holding capacity is reached. Furthermore, processes for the exchange and transport, as e.g. by infiltration, percolation, capillary movement and melting of snow as well as upward transport by plants, are included to solve the mass budget equations for the different water reservoirs. Precipitation serves as the incoming water source from the atmosphere, whereas soil looses water due to evaporation and transpiration (Doms et al., 2011). A further sink of the water amount is given by the runoff formation. The vertical transport of water between the soil layers is described by the Richards equation (e.g., Hillel, 1980) (3.1).

Soil temperatures of all soil layers are calculated using the heat conduction equation:

$$\frac{\delta T_{SO}}{\delta t} = \frac{1}{pc}\frac{\delta}{\delta z}\left(\lambda \frac{\delta T_{SO}}{\delta z}\right) \tag{3.1}$$

with T_{SO} as soil temperature, pc as heat capacity, λ as heat conductivity, t as time and z as height of layer.

The lowest layer acts as boundary condition for temperature, prescribed by a climatological mean near-surface temperature that is constant in time. Radiation, sensible and latent heat fluxes form the upper boundary condition and couple soil (or snow) and atmosphere. Further processes, as e.g. melting of falling snow, freezing of rain, melting of snow in the snow pack, freezing of water in the interception reservoir and freezing (thawing) of water

(ice) in the soil layers are considered (Doms et al., 2011).

Snow Cover

For the heat conduction, the calculation of snow temperature for an extra snow layer is regarded when a snow cover has more than 0.01 m depth. In a standard version, CCLM includes a single-layer snow scheme. Is a snow layer present, preliminary soil temperatures and snow temperatures are calculated. The snow surface temperature is then interpolated from the mean snow temperature and the temperature of the soil surface. In regions such as Siberia, snow cover plays an important role. Therefore, DWD introduced, in a preliminary version, a multi-layer snow model within TERRA-ML. Still under development it includes the following:

The temperature of snow pack T_{sn} changes with time t according to Equation 3.2:

$$\rho_{sn} C_{sn} \frac{\delta T_{sn}}{\delta t} = \frac{\delta}{\delta z} \lambda_{sn} \frac{T_{sn}}{\delta z} + L\left(F\left(z\right) - M\left(z\right)\right) + R \tag{3.2}$$

where ρ_{sn} and C_{sn} are the density and specific heat capacity of snow, λ_{sn} is the heat conductivity of snow, L is latent heat of freezing, M and F are melting and refreezing rates, and R is radiative heating. The time rate of change of the specific liquid water content, W_{liq}, is given by Equation 3.3:

$$\frac{\delta W_{liq}}{\delta t}\left(z\right) = M\left(z\right) - F\left(z\right) - q\left(z\right) \tag{3.3}$$

and the specific total water (liquid and solid) content W_{tot} by Equation 3.4:

$$\frac{\delta W_{tot}}{\delta t}\left(z\right) = -q\left(z\right) + P \tag{3.4}$$

where q is the rate of liquid water percolation and P is the precipitation rate. Snow density may vary at any time step, according to the following Equation 3.5:

$$\begin{aligned} \frac{\delta \rho_{sn}}{\delta t} = & \left(M\left(z\right) - F\left(z\right)\right)\left(\rho_w - \rho_i\right) + \\ & P \rho_{sn} \frac{1 - \frac{\rho_{sn}}{\rho_{fr}}}{W_{tot}} - \frac{q \rho_w}{W_{tot} - q} + \sigma\left(t\right) \end{aligned} \tag{3.5}$$

where ρ_w, ρ_i and ρ_{fr} are the densities of water, ice and fresh falling snow respectively and $\sigma\left(t\right)$ is gravitational compaction and compaction resulting from metamorphism.

Snow heat capacity, C_{sn}, is calculated by Equation 3.6:

$$C_{sn} = W_{liq} \rho_w C_w + \left(W_{tot} - W_{liq}\right) \rho_{dry} C_i \tag{3.6}$$

where C_w and C_i are the specific heat capacity of water and ice. Snow heat conductivity λ_{sn}

depends on snow density ρ_{sn}. It therefore changes with height and time and is calculated using an empirical formula after 3.7:

$$\lambda_{sn} = 2.22 \left(\frac{\rho_{sn}}{\rho_i} \right)^{1.88} \tag{3.7}$$

where ρ_i is the density of ice. The density of fresh snow is derived in the same way as in the single-layer snow model according to Equation 3.8:

$$\rho_{fr} = \rho_{frmin} + (\rho_{frmax} - \rho_{frmin}) \frac{T_{air} - T_{min}}{T_0 - T_{min}} \tag{3.8}$$

with ρ_{frmin}=50 kg/m^3, ρ_{frmax}150 kg/m^3,T_{min}=258.16 K = 273.16 - 15.0 K, T_0=273.16 K. A time dependent snow albedo a_s is included by using an aging condition S_{age} given by Equation 3.9:

$$0 \leq S_{age} \leq 1 \tag{3.9}$$

The snow albedo is given by:

$$a_s = a_{s,max} S_{age} + a_{s,min}(1 - S_{age}) \tag{3.10}$$

where $a_{s,max}$=0.7 and $a_{s,min}$=0.4. S_{age} has the value 1 in case of fresh snow and 0 for old snow.

S_{age} varies with time depends on constant ageing and on falling snow according to the Equation 3.11:

$$\Delta S_{age} = S_{age} \left[\frac{P_{snow}}{P_{norm}} - \frac{\Delta t}{\tau_\alpha} \right] \tag{3.11}$$

with P_{snow} as snowfall rate and P_{norm}=5 mm/24 h. S_{age}=1 when there is no snow.

The upper boundary condition at the snow surface is the heat flux formed as sum of net solar and infrared radiation and sensible and latent heat fluxes. In addition, heat conductivity flux into the snow layer and the flux of heat from freezing rain that is released, is considered. The lower boundary condition is the prescribed soil temperature of the lowest soil layer as the heat conduction equations is solved for the entire column of snow and soil. In case the temperature of one layer exceeds the melting point, snow melts. The whole solid part of the layer melts if enough heat is available, otherwise only a part of the layer melts.

Freezing and Thawing

Processes of freezing and thawing are considered after the calculation of the heat conduction equation and melting of snow. Freezing (thawing) occurs when the calculated temperature is below (above) a certain threshold. The freezing point cannot be used as threshold, as unfrozen water can be available within the soil even when soil temperatures

are below the freezing point. Therefore, a specific threshold is considered as function of the unfrozen volumetric water content ωl after Warrach (2000) based on a suggestion by Flerchinger and Saxton (1989). In that sense, the liquid water content depends on the temperature and on the hydrological characteristics of the soil (e.g., the air entry potential at saturation ψ_s, and the pore-size distribution index b, Brooks and Corey, 1966) which are soil-texture dependent according to Cosby et al. (1984). The equilibrium temperature T_*, used as threshold temperature, is calculated according to Equation 3.12:

$$T_* = T_0 \left[1 - \frac{g\psi_s}{L_f} \left(\frac{\omega PV}{\omega l} \right)^b \right]^{-1} \tag{3.12}$$

where g is gravitational acceleration and ωPV as volume of voids. After the calculation of the energy amount that is necessary to melt ice or freeze liquid water the change of water/ice can be determined before the final soil temperature is calculated.

3.4 Spectral Nudging

Optionally in CCLM, spectral nudging can be used after von Storch et al. (2000). Spectral nudging, which was introduced by Waldron et al. (1996) and applied to climate simulations by von Storch et al. (2000), has been employed to force the RCM to stay close to the driving large-scale information, not only at the lateral boundaries but also within the entire model domain. In large domains, the RCM simulated large-scale circulation can deviate from the one prescribed by the forcing fields. Therefore, spectral nudging terms are added to the model equations. The nudging term depends on the difference of spatial scales between the regional and global data. In CCLM it is possible to choose the time step of how often nudging terms are added. Additionally, a height-dependent nudging coefficient is used starting in atmospheric levels above 850 hPa (Feser et al., 2011; Müller, 2004). Consequently, spectral nudging is strongest in the uppermost levels. With decreasing height the nudging gets less so that the RCM can develop its own dynamics in the lower troposphere where regional features such as orography play a dominant role (von Storch et al., 2000). A detailed description of spectral nudging was given by Müller (2004). Spectral nudging has been implemented in several RCMs (e.g., Alexandru et al., 2009; von Storch et al., 2000) and evaluated in numerous studies (e.g., Miguez-Macho et al., 2005; Weisse and Feser, 2003).

4 Defining the Model Configuration

4.1 Introduction

For CCLM, standard model configurations are mainly optimized and tested for simulations over Europe and recently used for CORDEX regions. The application of CCLM in a different region such as Siberia requires several adjustments and changes in the model parameters and inclusion of physical processes reflecting those predominant in the considered region. The parameter settings and the model setup strongly influence the output of the model simulations as e.g. stated by Meissner et al. (2009). In CCLM several parameters can be changed affecting the dynamics and physical parameterizations (Schaettler et al., 2008). Therefore, a suitable model configuration for Siberia has to be identified and tested to obtain reliable hindcast simulations.

In a first test simulation for Siberia, CCLM showed a strong winter warm bias in the 2 m air temperature, especially in the northern parts of the model domain which will be presented in more detail in the following. To reduce the warm bias on the one the hand and to identify insufficient and inappropriate model parameterizations for that region on the other hand, further test and sensitivity experiments are needed.

Climate conditions in Siberia are influenced by interactions of various region-specific processes and features that determine the soil-surface-atmosphere interactions as e.g. soil processes in permafrost, strong low-level temperature inversion in the planetary boundary layer (PBL), seasonal variation of snow-cover and its impact on surface albedo among many others, as mentioned in previous sections. It is difficult to identify key processes in the model which are responsible for the bias as many interactions and coupling mechanisms occur when changing one parameter in the setup. The final settings of physical parameterizations and parameters need to consider the unique regional features that determine Siberian climate.

The present study aims to examine the sensitivity of simulated 2 m air temperature and sensible and latent heat fluxes for five different combinations of parameter settings to determine potential underlying processes that might be responsible for the temperature bias. Based on these findings, the objective is to adjust and refine the configuration for a better model performance.

4.2 Data and Methods

To identify an appropriate model version and configuration for climate simulations over Siberia, several 10 year period (1990-1999) test simulations are carried out. We start with the model version CCLM-4.14, with a spatial resolution of 0.44° using NCEP-R1 (Kalnay et al., 1996; Kistler et al., 2001) as driving reanalysis. NCEP-R1 is available in a grid spacing of $1.875° \times 1.875°$ (~ 210 km). A 3-D variational TS2 scheme is used

as spectral statistical interpolation and various observations (e.g., upper air rawinsonde observations of temperature, horizontal wind, and specific humidity; operational Television Infrared Observation Satellite (TIROS), Operational Vertical Sounder (TOVS), vertical temperature soundings from NOAA) are assimilated (Kalnay et al., 1996; Kistler et al., 2001).

For the evaluation, the bias of 2 m air temperature for the period of 1995-1999 against CRU3.2 data is calculated. CRU3.2 (Mitchell and Jones, 2005) is used as one observational reference data. It was provided by the Climate Research Unit (CRU) of the University of East Anglia and delivers gridded monthly fields of several climate parameters (e.g. near-surface temperature, precipitation, cloud cover) on a regular lon/lat grid in 0.5 degree resolution from 1901 to present. The underlying interpolation method used to obtain historical fields on a regular grid based on homogenized station data is described by Mitchell and Jones (2005). In addition, station count files are available to provide an overview of which grid boxes station data were available and incorporated in the data set production. As previously mentioned in Chapter 2.3, CRU3.2 is only based on few stations over Siberia. Therefore, only those station grid boxes of CRU3.2 and corresponding grid boxes in CCLM and considered reanalyses (NCEP-R1, ERA40, ERA-Interim) are selected.

The ERA-Interim reanalysis is the latest version of the ECMWF forecast system that is available for 1979-2010 in a resolution of ($\sim$ 80 km) (T255) (Dee et al., 2011). The former reanalysis ERA40, provided by the ECMWF, is available from 1958-2001 in a horizontal resolution of 1.25° (Uppala et al., 2005).

Furthermore, the average of selected grid boxes per subregion and considered time period are calculated. To account for the uncertainty of the observational data, station data of 'Global Summary of the Day' provided by the National Climatic Data Center (NCDC) are added in the comparison as second reference data. Again the nearest neighbor grid boxes of CCLM and reanalyses are selected from the daily means of the datasets. Missing days in NCDC data are excluded in the gridded datasets. To account for the general height dependance of air temperature, normally a height correction needed to be applied when differences of elevation occurred in the compared datasets. Due to the strong temperature inversion during winter time, the uniform lapse rate of $-0.65°C/100$m could not be used. Therefore, the height differences between CRU/NCDC and CCLM or reanalyes have to be considered in the comparisons.

In a second step, the model sensitivity is investigated by comparing single sensitivity experiments with control simulations. To save some computing time, certain experiments are conducted in a spatial resolution of 0.88° (approximately 100 km). An overview of the model simulations carried out in this study is presented in Table 4.1. In a first test simulation CCLM-4.14 is used, which is named as $\mathrm{CRTL}_{0.44}$. To investigate the effect of increased soil column depth to better account for the temperature gradient in permafrost

Experiment Acronym	Model	Spatial Resolution	Specification
$CTRL_{0.44}$	CCLM-4.14	0.44	Control run of 0.44° spatial resolution
SOILC_mS	CCLM-4.14	0.44	Increase of soil-column depth, multi-layer snow
$CTRL_{0.88}$	CCLM-4.14	0.88	Control run of 0.88° spatial resolution
HIST	CCLM-4.14	0.88	External field of soil type changed to histosols
TSOIL	CCLM-4.14	0.88	Increase of 10°C in initial field of soil temperature
$CTRL_{0.88}$	CCLM-4.16	0.88	Control run of 0.88° spatial resolution
TURB	CCLM-4.16	0.88	Reduced minimal heat diffusion
$TURB\_mS_{0.88}$	CCLM-4.16	0.88	Reduced minimal heat diffusion, multi-layer snow
$TURB\_mS_{0.44}$	CCLM-4.16	0.44	Reduced minimal heat diffusion, multi-layer snow

Table 4.1: Overview of experiment runs and their different setups.

soil, SOILC_mS is conducted with a soil depth down to 92 m. This experiment is conducted by additionally applying the multi-layer snow model (mS) to consider the strong importance of snow cover in that region. The sensitivity of surface fluxes and air temperature to organic material (HIST) is investigated by changing the entire external field of prescribed soil type to Histosols. Furthermore, it is of interest to analyze whether changes in the prescribed temperature of the deepest soil layer has an impact (TSOIL). To better account for the stable atmospheric conditions in the high pressure system that prevail during winter in Siberia, a sensitivity experiment with a reduced minimal diffusion coefficient (TURB) is performed. The influence of considering the multi-layer snow parameterization is additionally regarded ($TURB\_mS_{0.88}$, $TURB\_mS_{0.44}$). The control and sensitivity runs of CCLM are performed using NCEP-R1 as lateral boundary condition. Afterward, the final model setup for CCLM-4.16 is presented which is used later on for the long-term hindcast simulations.

4.3 Overestimation of Winter Near-surface Temperature

The difference for the annual variation between the test simulation of CCLM-4.14 and CRU3.2 illustrates a strong warm bias in winter near-surface air temperature, mainly in the arctic and subarctic regions. In Fig. 4.1 the bias is shown for six subregions. The strongest overestimation compared to CRU3.2 reaches 11 K in December in the subregion AE. This warm bias is still evident in the central regions in ME up to 10 K during December. Lowest temperature warm bias occur in the MW and SW with maximum values of approximately 3 K. Moreover, the direct comparison of monthly differences of the forcing reanalysis NCEP-R1 and of reanalysis data of ERA40 and ERA-Interim compared to CRU3.2 in Fig. 4.1 illustrates that NCEP-R1 exhibits already a winter warm bias, except in the southern regions (here shown for SW). Especially in the arctic subregions, the winter warm bias is stronger than presented by ERA40 and ERA-Interim. This is consistent

with the results published in ACIA (2005) in which seasonal differences in the surface air temperature between NCEP-R1 and ECMWF reanalyses for the period 1979-1993 show strong warm winter biases of NCEP-R1.

Figure 4.1: Monthly mean differences of 2 m air temperature [K] of selected grid boxes per subregion of CCLM ($CRTL_{0.44}$), NCEP-R1, ERA40, ERA-Int against CRU station grids for the years 1995-1999 and NCDC stations (dashed magenta). Magenta bars represent the number of stations found during the considered months per subregion (CRU (solid), NCDC (hatched)). h-diff is the height difference in m between station/station grid and CCLM/reanalyses.

Although NCEP-R1 already introduces a warm bias during the winter months, CCLM overestimates the air temperature even more. To understand which processes might be misrepresented in CCLM for that region, the sensitivity of the near-surface air temperature of CCLM was tested to changes in the parameter settings that reflect the consideration of physical processes according to the regional peculiarity of Siberia. Besides the effects on the 2m air temperature, the sensitivity of surface fluxes (sensible and latent) was

considered exemplary for three subregions (AE, ME, SW).

4.4 Sensitivity Studies for Bias Reduction

4.4.1 Soil Column Depth and Multi-layer Snow Cover

Permafrost soils are an important regional feature in Siberia. Their depth reach from less than a meter to more than 1000 m in the arctic regions or even 1500 m in eastern Siberia as e.g. documented by Ershov (1998). Permafrost represent an important component of local and regional land-atmosphere interactions in that region (Frauenfeld et al., 2004). Within the active layer, freezing and thawing control the transportation and exchange of heat flux between soil and atmosphere (Frauenfeld et al., 2004; Lachenbruch and Marshall, 1986). Furthermore, permafrost influences the moisture balance through evapotranspiration (Saito et al., 2007).

Several studies, using GCM land surface schemes, mentioned the improved effect on long-term soil temperature simulations when deeper soil columns are considered (Alexeev et al., 2007; Dankers et al., 2011; Nicolsky et al., 2007; Lawrence et al., 2008a). Saito et al. (2007) suggested the use of a total depth of soil column greater than 15 m. According to this study, more soil layers and therefore a deeper soil column is important for the exchange of energy flux from the atmosphere to the ground and for the distribution of energy (Saito et al., 2007). Different studies were performed focusing mainly on permafrost and soil simulations. In order to enhance the representation of yearly cycle and long-term dynamics in subsurface temperature, Alexeev et al. (2007) suggested to increase the soil depth in the LSM to at least 30 m or even deeper soils. In contrast, Dankers et al. (2011) found that the increased soil thickness of 60 m led only to small changes on the simulation of permafrost and active layer thickness.

A further major cause of winter cold bias of near-surface air temperature might be due to an unsophisticated representation of snow cover in the model. Snow cover has an insulating effect, i.e. the heat exchange between surface and atmosphere is restricted. To the contrary, a small or absent snow cover leads to reduced or no insulation and decreasing soil temperatures (Saito et al., 2007) which again alters the surface energy budget. Further impacts of snow were previously mentioned in the introduction. According to Saito et al. (2007), snow cover is one of the major causes of thermal biases for simulations in cold regions.

In general, the vertical stratification of the snow pack is physically more correct in multi-layered snow schemes than in single-layer models (Brun et al., 1992). According to Waliser et al. (2011), the consideration of physical processes e.g. the heat transfer, snow compaction and refreezing of snow melt water, is too simple in single-layer snow models. Moreover, the absence of partial melting within the snow column is a major drawback in single-layer models as stated by Waliser et al. (2011). In reality, snow surface can be

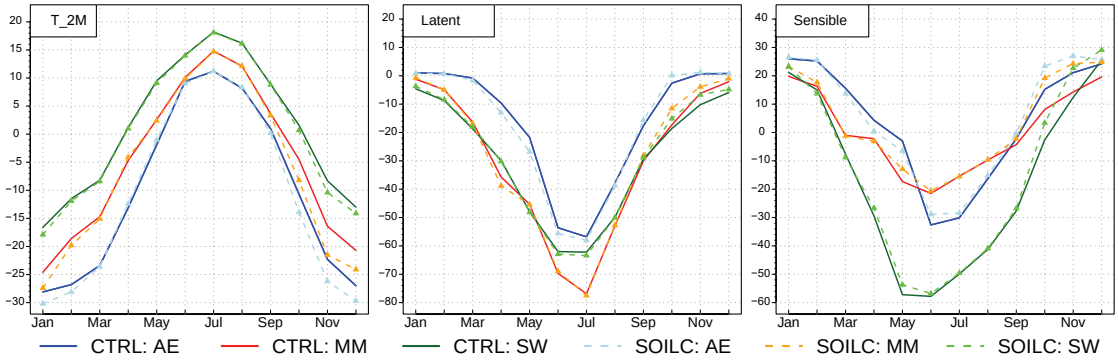

Figure 4.2: Mean annual cycle (1995-1999) of 2 m air temperature [°C], latent and sensible heat flux [W/m^2] for the control run CRTL$_{0.44}$ and the experiment SOILC_mS over three subregions (AE, MM, SW).

above the freezing point whereas snow temperatures at the bottom are below the melting point. This has strong influence of long-term snow variations and snow retreat during the ablation period (Waliser et al., 2011). Several studies showed that multi-layer snow models produce better results in the simulation of long-term snow cover variations. Due to the improved treatment of physics within the snow pack in multi-layer models, the onset of snow melting during spring started earlier. That is often delayed in many single-layer models (Slater et al., 2001) which effects the entire surface energy balance. However, besides the stratification of snow, an important role for snow simulations plays the simulation of temperature and precipitation. Therefore, it is necessary to examine whether the multi-layer snow treatment has an effect on the energy budget and thus on the air temperature or whether the effect is negligible and does not produce better results compared to the single-layer scheme.

For the sensitivity experiment presented here, the the multi-layer snow model with 2 snow layers is applied and compared against the control run which considered a snow pack with only one snow layer. In addition, interest focuses on the effect on increased total soil thickness on near-surface conditions. For this sensitivity experiment, 3 more soil layers are added to the standard layer depth of 11.5 m to extend the soil column to a depth of 92 m. The thickness of the hydrological active layer was set to 10 m. The soil type and corresponding thermal and hydrological soil parameters are prescribed for the entire soil column and do not change with depth.

Compared to CTRL$_{0.44}$, the temperature 2m air temperatures decrease - most pronounced in the subregion AE by a temperature reduction of nearly 5°C. Towards the southern subregion the temperature change decreased in winter. The effect of reduced lower temperatures persisted longest in the arctic subregion from September to March/April whereas in the subregion SW only changes from October to March are evident. The latent heat flux responds to the snow layer changes only slightly, mainly between March and July in AE and March and May in MM with increased downward fluxes. This might be due to

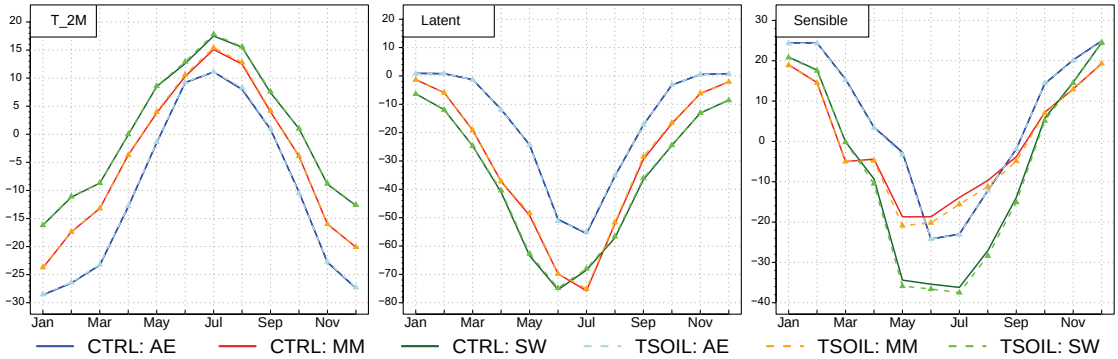

Figure 4.3: Mean annual cycle (1995-1999) of 2 m air temperature [°C], latent and sensible heat flux [W/m^2] for the control run CRTL$_{0.88}$ and the experiment TSOIL (+10K) over three subregions (AE, MM, SW).

the increased water availability due to snow melting. The application of multi-layer snow model caused a distinct effect of the sensible heat flux in month September to December with an increase compared to the sensitivity experiment in which only the minimal heat diffusion was changed. The sensible heat flux increases most pronounced in October.

The inclusion of increased soil column depth and multi-layer snow model could reduce the winter warm bias of 2m air temperature and therefore is considered in the final model setup.

4.4.2 Initial Condition of Soil Temperature

In the sensitivity experiment TSOIL, the sensitivity of 2 m air temperature to initial condition for soil temperature at the bottom of the soil column is investigated. In TERRA-ML the initial condition is prescribed by the climatological mean of near-surface temperature derived from the global dataset CRU. The heat flux into the soil at the lowest layer is needed for the solution of heat conduction equation and establishing the initial temperature profile. However, the surface temperatures do not represent the realistic state of the frozen ground conditions in permafrost soils. The question arises whether this precondition influences near-surface conditions.

Previous studies using the Community Land Model assessed how soil temperature initial and boundary conditions effect soil temperatures in permafrost soils. Lawrence et al. (2008b) investigated the influence of warm, cool and cold initial condition by conducting different experiments. They suggested only minor effect of initial soil temperature condition on the spin-up of soil temperatures. In addition, Nicolsky et al. (2007) studied the effect on the bottom boundary condition on the temperature dynamics in the upper soil layers.

However, in these studies the main focus was on the effect on soil temperatures in permafrost dynamics or warming of near-surface permafrost soil. Here in this study, the focus is on the potential effect of the initial soil temperature condition on near-surface air tem-

perature using the coupled land-atmosphere model system of TERRA-ML and CCLM. The assessment of sensitivity of air temperature to initial soil temperature conditions of lowest soil layer is of interest to determine if this factor might be one reason for the existing winter warm bias of 2 m air temperature.

For this study, two sensitivity experiments are conducted and compared to the control run. The model setups differ compared to the control run only by the prescribed initial soil temperature at the lowest soil layer. The tests are performed with warm (+10 K) and cool (-10 K) initial conditions, in which 10 K are added or subtracted from the original prescribed mean temperature field for all grid boxes.

As illustrated in Fig. 4.3, exemplary for the case with +10 K, changes in the lowest soil boundary temperature have only minor effects on the simulated 2 m air temperature, latent and sensible heat fluxes. The annual variations of the sensitivity experiment with a temperature increase of 10 K at the soil bottom is exemplary presented against the control simulation but is similar to the sensitivity experiment with decreased bottom soil temperature of -10 K. Only during summer is the sensible heat flux reduced in the middle and southernmost subregion. These results are consistent with the results obtained by Nicolsky et al. (2007) stating that the bottom boundary condition in a depth of 100 m has only minimal effect on the temperature dynamics in the upper 20-30 m of the soil. As shown here, the effect is even more reduced on near-surface temperature. Therefore, it can be concluded that the thermal bias in the RCM simulation cannot be reduced by modifying the initial field of soil temperature.

4.4.3 Representation of Soil Organic Matter

Organic material plays an important role in permafrost soils. The uppermost soil layers of 0.2-0.3 m depths of many permafrost regions consists of organic matter (Nicolsky et al., 2007) which has thermal and hydraulic properties distinct from mineral soil. During summer, moist organic material has an isolating effect, whereas in winter dry and frozen conditions prevail that favor the heat exchange between soil and atmosphere(Lawrence and Slater, 2008). Therefore, organic material influences the heat balance, temperature and moisture regime of permafrost soils and thus land-atmosphere interactions.

Previous studies showed some improvements in the model experiments when organic matter was considered. Lawrence and Slater (2008) analyzed the sensitivity of a GCM to inclusion of soil organic matter and found a warming effect on summer Arctic surface air temperatures. This is in contrast to the study by Rinke et al. (2008). They used the RCM HIRHAM and assessed the sensitivity of arctic climate to the organic layer on top of mineral soil (Rinke et al., 2008). Their results suggested a cooling of surface air temperature in Siberia mainly in summer, due to increased ground evaporation, and even an effect on large-scale atmospheric circulation. In a more recent study by Dankers et al. (2011)

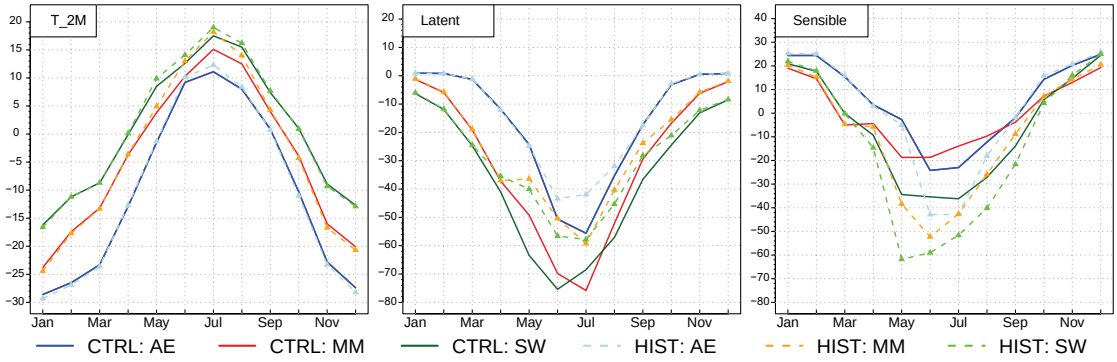

Figure 4.4: Mean annual cycle (1995-1999) of 2 m air temperature [°C], latent and sensible heat flux [W/m^2] for the control run CRTL$_{0.88}$ and the experiment HIST over three subregions (AE, MM, SW).

the land surface model JULES was used in which the properties of organic material vary with depth. They found a reduction of soil temperatures in the upper soil layers during summer. In winter they found a temperature increase due to lower thermal conductivity and therefore improved isolating effects to cold air temperatures. However they concluded a limited effect on the annual average by the consideration of organic matter.

TERRA-ML does not consider a layered structure of different soil horizons within the soil-column. As mentioned in Chapter 3, a soil type is defined per grid box that implies thermodynamic and hydrological properties for the entire soil column from the surface down to the lowest soil layer. A sensitivity experiment is performed representing an extreme-case in which the external dataset for soil is changed to Histosols for all grid boxes, which does not represent any real soil type distribution. However, some conclusions can be drawn about the effect of organic matter on climate simulations for Siberia. The aim is to investigate the impact and differences on near-surface climate in that region when organic material is predominant in comparison to mineral soil consideration.

Compared to the control run, the changed soil ground properties have a minor effect on the winter temperatures but a stronger response is simulated during summer, as presented in the averaged annual variation in Fig. 4.4. During winter, CCLM responds with a slight cooling especially in the arctic subregion and a heating in the summer months which is strongest in the subregion MM. Effect in the latent heat flux is strongest during summer for the southern and middle subregion. In the southern subregion the reduced downward latent heat flux, i.e. the increased upward heat flux starts earliest for all subregions in May and ends latest in November. Due to the southernmost location the temperatures are lowest throughout the year in SW and more water can be evaporated. To the contrary, the sensible heat amount going upward is reduced, i.e. an increase in the downward flux.

The consideration of organic matter led to changes in summer air temperature and latent and sensible heat flux. However, in TERRA-ML it is not possible so far to include organic matter on top of mineral soil. In addition, the effect on the reduction of winter air

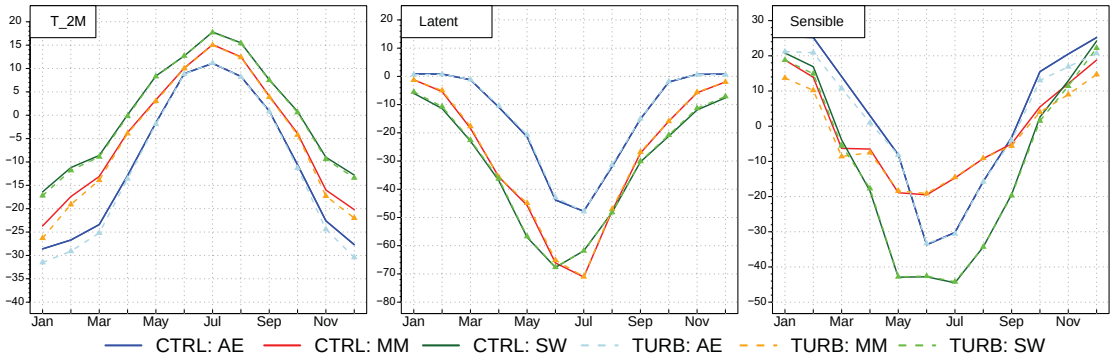

Figure 4.5: Mean annual cycle (1995-1999) of 2m air temperature [°C], latent and sensible heat flux [W/m^2] for the control run CRTL$_{0.88}$ and the experiment TURB over three subregions (AE, MM, SW).

temperature is negligible. Therefore, changes regarding organic material are not further considered in the final model setup.

4.4.4 Minimal Heat Diffusion

During winter, Siberian climate is characterized by strong surface cooling due to a negative radiation balance. Very low temperatures at the lower troposphere are the consequences, together with air subsidence in the middle troposphere that favors the near-surface temperature inversion. At the surface layer a stable stratified boundary layer establishes (Cuxart et al., 2006), characterized by a weak turbulent mixing and a downward directed heat flux (Byrkjedal et al., 2008). Heat fluxes are driven by static stability, lapse rate and wind speed (Byrkjedal et al., 2008). The higher the winds the more the turbulent conditions occur in the PBL and more downward heat flux appears increasing the surface temperatures. Insufficient presentation of fluxes in the turbulence parameterization effects surface air temperatures (SAT) (Byrkjedal et al., 2008). Model simulations used in ACIA (2005) tend to overestimate the SAT in regions characterized by low surface temperatures (Byrkjedal et al., 2008; Kiehl and Gent, 2004). According to Cuxart et al. (2006) many turbulence parameterizations in GCMs overestimates turbulent fluxes, highlighting shortcomings in the description of the boundary-layer, and this has strong implications, especially in regions dominated by temperature inversions. One option to reduce these fluxes is to tune the parameterization to achieve better results (Byrkjedal et al., 2008; Saha, 2006; Viterbo et al., 1999).

The purpose of the sensitivity experiment performed here (TURB) using an updated version of CCLM-4.16, is to investigate the influence of reduced minimal heat diffusion, given as tuning parameter (changed to 0.1), on near-surface air temperature. The question arise whether reduced turbulent heat fluxes and vertical mixing in the model lead to more stable conditions in the lower troposphere and thus reduce near-surface temperatures during the winter season.

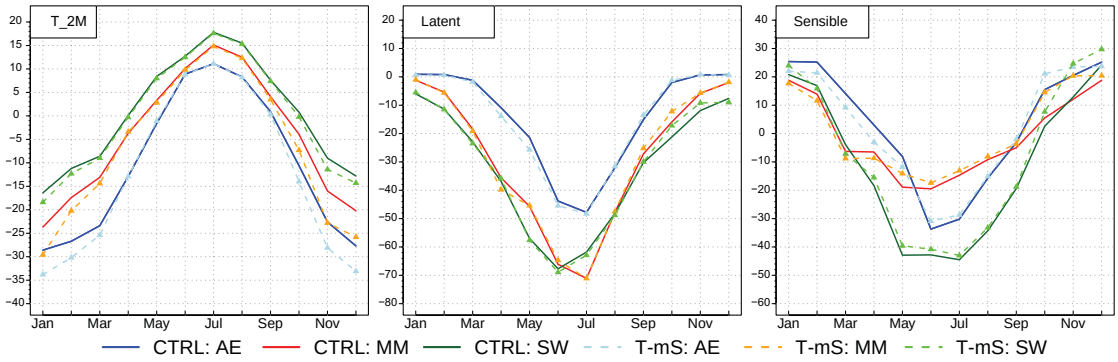

Figure 4.6: Mean annual cycle (1995-1999) of 2m air temperature [°C], latent and sensible heat flux [W/m^2] for the control run CRTL$_{0.88}$ and the experiment TURB_mS$_{0.88}$ over three subregions (AE, MM, SW).

Fig. 4.5 shows the annual cycle of 2m air temperature, latent and sensible heat fluxes for the sensitivity runs and control simulations averaged over three selected subregions for the period of 1995-1999. In all three subregions the winter 2 m air temperature has decreased. The temperature decrease during wintertime is strongest in the northern subregions with a maximum of 4 K and gets less in the southern regions. During summer, no effect on the temperature is visible. As no changes affecting the land-surface or vegetation had been made, no changes in the latent heat flux occur. To the contrary, the changed setting effects the sensible heat flux. In the northern subregion the upward heat flux is strongest mainly during the winter months. During summer, the simulated sensible heat flux is not sensitive to reduced minimal heat diffusion.

In the next step, the response of near-surface air temperature on changed minimal heat diffusion together with the inclusion of the multi-layer snow model is investigated. The effect varies throughout the year and subregions (Fig. 4.6).

Compared to Fig. 4.5, in which only the heat diffusion tuning parameter has changed, the temperature decrease is even stronger during the winter months - most pronounced in the subregion AE by a temperature reduction of nearly 5°C. Towards the southern subregion the temperature change compared to the control run decreased in winter. The effect of reduced lower temperatures persisted longest in the arctic subregion from September to March/April whereas in the subregion SW only changes from October to March are evident. The latent heat flux responds to the snow layer changes only slightly, mainly between March and July in AE and March and May in MM with increased downward fluxes. This might be due to the increased water availability due to snow melting. The application of multi-layer snow model caused a distinct effect of the sensible heat flux in month September to December with an increase compared to the sensitivity experiment in which only the minimal heat diffusion was changed. The sensible heat flux increases most pronounced in October about 8 W/m^2 in AE and about 10 W/m^2 in SE. Even higher increase occurs in SW in November up to 15 W/m^2.

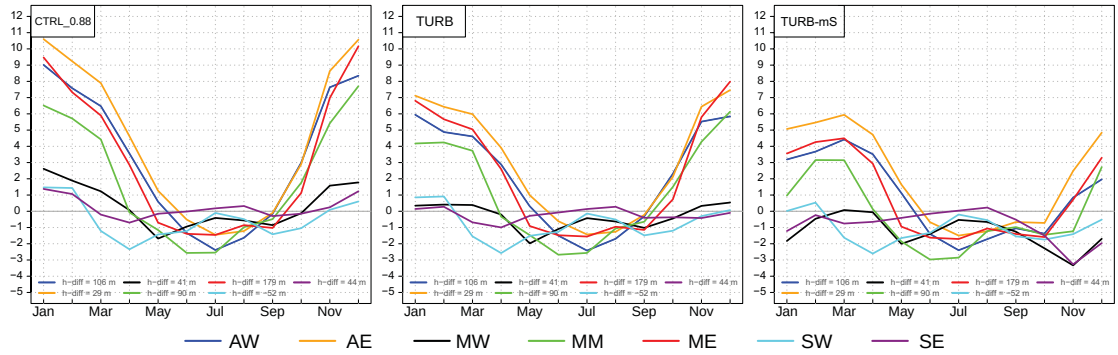

Figure 4.7: Monthly differences of 2 m air temperature [K] from selected grid boxes per subregion of three CCLM experiments in 0.88° resolution ($CTRL_{0.88}$, TURB, $TURB\_mS_{0.88}$) against CRU station grids for the years 1995-1999.

These sensitivity experiments illustrate that a reduction of the minimal heat diffusion leads to a cooling of near-surface winter temperatures and a better representation of the stable conditions in the PBL. Therefore, this modification in the tuning parameter is considered in the final model setup to better capture low temperatures in the stratified boundary layer together with the application of the multi-layer snow model.

4.5 Final Model Setup for Siberia

After the performance of several sensitivity experiments and test simulations in 0.88° and 0.44° spatial resolutions, using two different model versions, one final model setup, namely TURB_mS, is able to reduce the winter 2 m air temperature warm bias considerably. Fig. 4.7 presents the differences of 2 m air temperatures in the mean annual cycle of the first test run using $CTRL_{0.88}$ and CRU3.2 as reference data. Again, station grid boxes of CRU and the corresponding grid boxes of CCLM are selected and averaged per subregion over the period 1995-1999. Amplitudes of differences vary from region to region and month to month. In Fig. 4.7 the strong warm bias during the winter months for AE is illustrated ranging up to 11K.

After the reduction of minimal heat diffusion to 0.1, the increase of soil column depth to 92 m, the application of multi-layer snow model the bias could be reduced as shown in Fig. 4.7 (TURB_mS). As the spatial resolution of the performed long-term hindcasts should be 0.44°, the final results of TURB_mS for 0.44° is shown in Fig. 4.8. In addition, it illustrates that the annual variation of bias is somewhat modified due to the higher resolution.

Even though an improvement with respect to 2 m air temperature can be achieved, a large warm bias remains for subregions, e.g. AE and a cold bias occurs for subregions as e.g. MW. Nevertheless, the model configuration of $TURB\_mS_{0.44}$ is used to perform the final long-term hindcast simulations, on the one hand driven by NCEP-R1 from 1948-

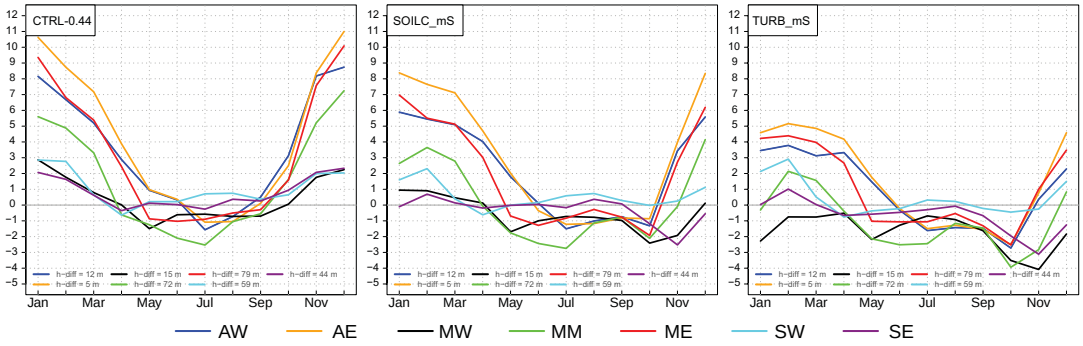

Figure 4.8: Monthly differences of 2 m air temperature [K] from selected grid boxes per subregion of three CCLM experiments in 0.44°resolution ($CTRL_{0.44}$, SOILC_mS, $TURB\_mS_{0.44}$) against CRU station grids for the years 1995-1999.

2010 (CCLM-NCEP1) and on the other hand driven by ERA40 from 1958-2001 (CCLM-ERA40). Both reconstructions are stored at the Climate and Environmental Retrieval and Archive (CERA) database of the World Data Center Climate (WDCC) (`http://cera-www.dkrz.de/WDCC/ui/Entry.jsp?acronym=COSMO-CLM_siberia`).

A problem for accurate model adjustment is still the reliability of the observational reference data used, which itself provide uncertainty. This is especially the case for the arctic regions of Siberia.

Besides these specific changes in the parameter settings made here for Siberia, Runge-Kutta is used as time-integration scheme. Additionally, Tiedtke convection scheme and spectral nudging is applied, i.e. the nudging terms were added every third time step.

5 On the Temporal Reliability of Hindcasts and their Forcings

5.1 Introduction

In numerous regional climate model applications, reanalyses are used as forcing and are often assumed to be 'perfect boundary conditions'. This assumption should not be accepted per se, especially when temporal consistency for the downscaled effort is expected (Brands et al., 2011).

One should be aware of certain issues when dealing with reanalyses. One important issue is the inhomogeneity aspect as discussed in several studies (e.g. Bengtsson et al., 2004; Screen and Simmonds, 2010; Sterl, 2004; Thorne and Vose, 2010). Underlying causes include changes in the quantity and quality of assimilated observations over time due to changed observing systems (as e.g. the use of global radiosonde data in 1958 and satellite observations since the late 1970s (Bengtsson et al., 2004; Bromwich and Fogt, 2004)).

Furthermore, in some regions over the globe, reanalyses, compared to each other, show large discrepancies in spatio-temporal distribution and temporal variability of certain variables. This occurs especially in regions where continuous long-term observations are sparse as e.g. in Polar Regions (Bromwich et al., 2007; Sterl, 2004). Several studies illustrated differences between NCEP-R1 and ERA40 reanalyses over the Northern Hemisphere and Eurasia e.g. for air temperature (Simmons et al., 2004), precipitation of the Arctic north of 45°N (Serreze and Hurst, 2000; Serreze et al., 2005), and China (Gao et al., 2008; Liu et al., 2012; Zhao and Fu, 2006) or snow water equivalent for Russian watersheds (Khan et al., 2008), surface or sea level pressure (Inoue and Matsumoto, 2004; Wu et al., 2005) and geopotential heights (Brands et al., 2011; Huang et al., 2011; Wu et al., 2005; Zhao and Fu, 2009). Some studies mentioned different assimilation schemes (Bengtsson et al., 2004; Bromwich and Fogt, 2004) as potential cause for temporal dissimilarities. Important in terms of dynamical downscaling of reanalyses are the documented discontinuities and discrepancies of variables that are used as forcing e.g. tropospheric temperature and humidity (Brands et al., 2011) and winds (Wu et al., 2005).

However, the published assessments of reanalysis discrepancies were restricted to certain variables and seasons and did not consider the effect on dynamical downscaling results. Temporal dissimilarities and thus uncertainty of the forcings might have profound impact on the downscaling effort and should be employed with caution, especially when climate change analysis is intended.

In this chapter, the aim is to analyze the temporal consistency and reliability of derived regional climate model hindcasts for Siberia (one driven with NCEP-R1 and the other by ERA40) by assessing their degree of agreement. The same is done with the two reanalyses used as forcings to investigate to what degree the potential uncertainty is already inherent

in the underlying RCM lateral boundary conditions. In case of strong disagreement of the two reanalyses, at least one reanalysis does not reflect real climate conditions. This comparison is used as estimator of reanalysis uncertainty. If the hindcasts show a similar pattern of disagreement, it illustrates that they are sensitive to uncertainty given by the forcing and should consequently be regarded as unreliable.

Here, the uncertainty of the reanalysis NCEP-R1 and ERA40 is assessed in more detail than done for Siberia in previous studies. Additionally, a set of surface and upper-level variables that are important forcing variables are considered over all seasons. Furthermore, as recommended by Brands et al. (2011), the sensitivity of derived hindcasts to the choice of reanalysis data in terms of past interannual variability and interdecadal changes is investigated. This knowledge is of importance for assessing the reliability of forcing data and the hindcast's quality to clarify which variables, periods, seasons and regions are usable for further analyses when temporal consistency is needed.

5.2 Data and Methods

Temporal reliability and uncertainty of performed climate hindcast simulations and underlying forcings are investigated by assessing their degree of similarity and discrepancy of the interannual variability and interdecadal changes. The agreement or disagreement is considered separately between CCLM-NCEPR1 and CCLM-ERA40 on the one hand and between NCEP-R1 and ERA40 on the other hand, for the period from 1960 to 2001 in which all datasets provide data. The magnitude of dissimilarity for different atmospheric forcing variables that play an important role in the dynamical downscaling procedure are used as measure for the uncertainty given by the global data. The sensitivity of derived hindcasts to reanalysis uncertainty is investigated in the same way.

The assessment is done for mean sea level pressure (MSLP), tropospheric temperature T, geopotential FI, specific humidity QV and horizontal wind components which are here considered at 850, 500 and 200 hPa. This study gives a regional and seasonal overview to what extent both forcings and hindcasts differ or agree in terms of their temporal atmospheric information.

To discuss interannual variations, all analyses are carried out for standard seasons (DJF, MAM, JJA, SON). Regional averages are presented for several subregions as introduced in Fig. 2.1. Several aspects of data analysis are presented: One the one hand interannual variations are presented as time series of seasonal means for the time period of 1959-2001 where both NCEP-R1 and ERA40 and both hindcasts provide data, averaged over the considered subregions. On the other hand, changes in the mean spatial patterns are shown, presenting the seasonal differences of 2 periods (1959-1979 minus 1980-2001).

To examine the similarity of both reanalyses and both hindcasts, the bias, their correlation and their centered root-mean-square difference (crmsd) of seasonal means for each

subregion and variable are calculated. To obtain a final metric of agreement, all the three measures are aggregated to one after checking whether the single values are above or below a certain threshold. If the value is greater than the threshold, the considered seasonal value for a certain subregion is set to 1 - otherwise to 0 and averaged at the end. For the bias, the threshold is dependent on the considered variable: 3 hPa for MSLP and 3 gpdm for FI, 2°C for T, 0.5 W/m^2 for QV and 1m/s for U and V. For the correlation coefficient the threshold is 0.5. In case of crmsd, the threshold is 0.5 for all variables except QV with 0.3. This similarity assessment is performed for 4 different time periods - each 10 years: for 1959-1968, 1969-1978, 1979-1988, 1989-1999. These periods are chosen to present interdecadal discrepancies for NCEP-R1 and ERA40 and the corresponding hindcasts.

5.3 Results and Discussion

5.3.1 Spatial patterns of inter-period discrepancies of MSLP

It is known from the study by Inoue and Matsumoto (2004) that strong discrepancies occur in the inter-period differences (1980/1999 - 1960/1979) between NCEP-R1 and ERA40 in the Lake Baikal region and over Mongolia for summertime (JJA) mean sea level pressure (MSLP). They conclude spurious variations of NCEP-R1. However, this comparison of reanalyses has only been conducted for the summer season.

To illustrate the seasonal evolution in these inter-period difference patterns between the periods 1980/1999-1960/1979 for NCEP-R1 and ERA40, additional DJF, MAM and SON are presented in Fig. 5.1. Furthermore, both hindcasts CCLM-NCEP1 and CCLM-ERA40 are added to this comparison to show the effect on the dynamical downscaling approach. The spatial distribution of inter-period differences of both reanalyses reveal dissimilarities in all seasons, most pronounced during JJA in the southern regions and a better agreement in the northern high latitudes. The conducted hindcasts reveal similar difference patterns compared to the forcings, although somewhat reduced in the magnitude.

As illustrated in Fig. 5.1, NCEP-R1 shows strongest inter-period differences in the summer season (JJA) with differences from 8 to 10 hPa in the southern region over Mongolia and near Lake Baikal as already mentioned by Inoue and Matsumoto (2004). This strong increase of MSLP during 1980/1999 shown by NCEP-R1 is not presented by ERA40 - to the contrary, MSLP increases slightly to 1 hPa and only in southwest and east of Lake Baikal a slight decrease of 1 hPa is evident. These discrepancies of NCEP-R1 and ERA40 are in line with the results given by Inoue and Matsumoto (2004). Similar results are reported in the spatial distribution of summer geopotential heights at 500 and 700 hPa by Zhao and Fu (2009). They presented differences of ERA40 and NCEP-R1 between 1958-1979 and 1980-2001.

In the NCEP driven hindcast, the inter-period difference pattern look similar to the one presented for NCEP-R1 but less pronounced with maximum values of 5 hPa. The smoother

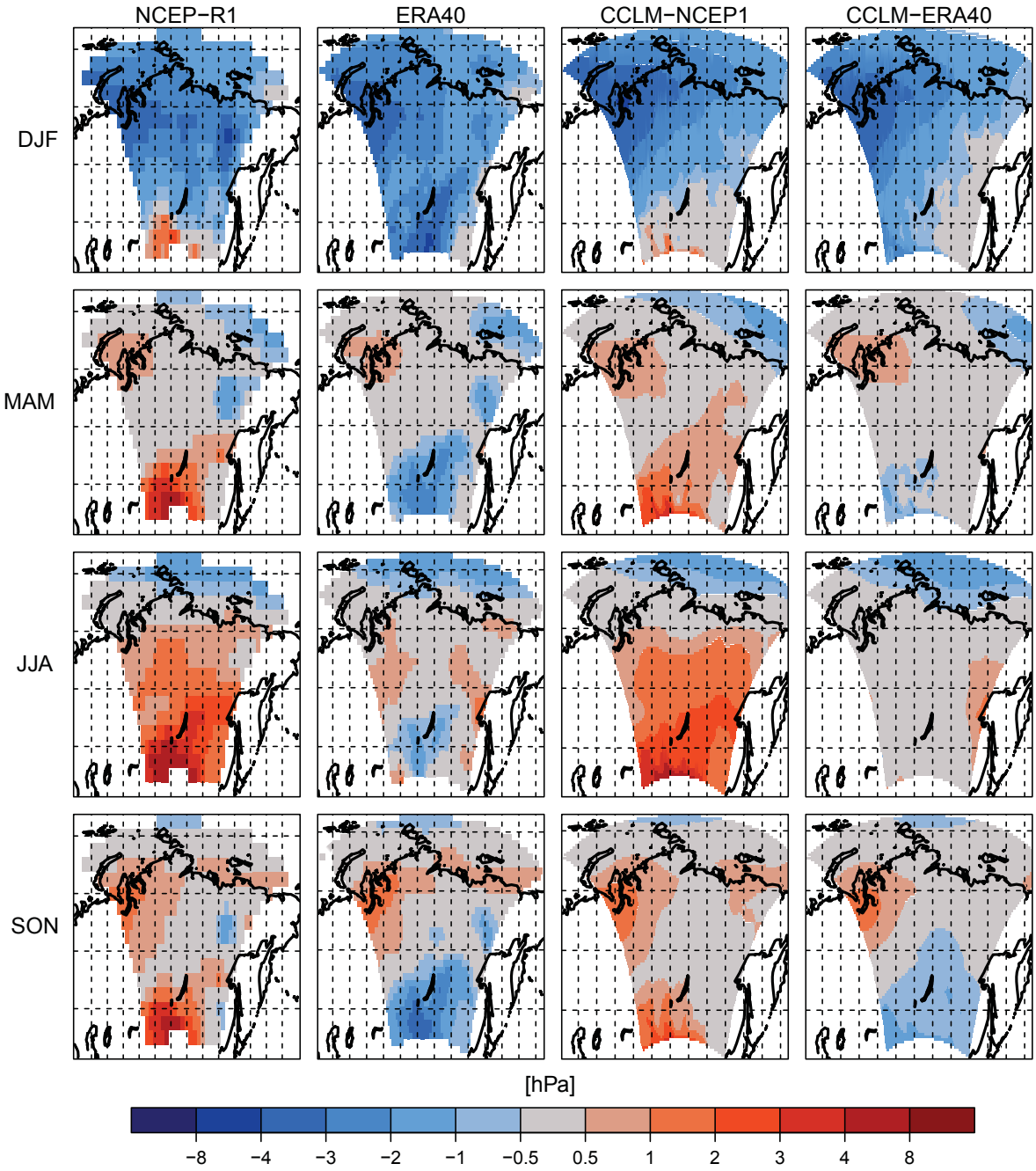

Figure 5.1: Seasonal inter-period differences (1980/1999-1960/1979) for MSLP [hPa] of NCEP-R1, ERA40, CCLM-NCEP1, CCLM-ERA40.

differences are also visible in the ERA40 driven hindcast that shows no decrease in MSLP anymore. Despite spectral nudging, CCLM was able to develop its own climatology within the large model domain. Near-surface variables were able to deviate from the prescribed large-scale forcings fields due to finer resolved orography and a different boundary layer parameterization than given in the reanalyses.

In the seasons DJF, MAM and SON, NCEP-R1 differ in the spatial patterns of difference fields of the two considered periods compared to ERA40 over the southern part. Both forcings show dissimilarities in their pressure fields and consequently in their large-scale atmospheric circulation patterns, mostly south of 60°N. The opposed patterns of MSLP changes throughout 1960/1979 and 1980/1999 are also strong during autumn (SON) in which NCEP-R1 reveals an pressure increase of up to 5 hPa and ERA40 a decrease of up to 4 hPa. Again, these discrepancies effect MSLP fields of the derived hindcasts that use the information of pressure fields as lateral forcing. But due to the model physics in the inner domain, CCLM established a smoother inter-period difference field, both in the NCEP-R1 driven and ERA40-driven simulation. In the ERA40 driven hindcast the RCM physics even led to opposed inter-period difference patterns. As shown for SON, in ERA40 MSLP decreases in the second period whereas CCLM-ERA40 does not show this feature. In general, the maximum MSLP differences during the two periods are shifted southward both in CCLM-NCEP1 and CCLM-ERA40.

The strong discrepancies of inter-period differences between NCEP-R1 and ERA40 were investigated by Inoue and Matsumoto (2004). They compared their results of summertime MSLP with the distribution based on monthly mean SLP grid data provided by CRU. The inter-period differences of CRU did not show the increase between the two periods as illustrated in NCEP-R1. To the contrary, the patterns were similar to the decreases in MSLP around Mongolia presented in ERA40. Therefore, they concluded that the MSLP increases of NCEP-R1 might be unrealistic. Which years are affected most will be analyzed more in depth in the following by presenting interannual variations of MSLP for three selected subregions (AE, ME and SW).

5.3.2 Temporal variability of reanalyses and hindcasts

Seasonal comparison for MSLP

As previously shown in the spatial patterns of inter-period discrepancies, a strong discrepancy occurs between NCEP-R1 and ERA40 in the southern part of the model domain. In a next step, it is necessary to determine how the similarity and discrepancy evolve throughout the years. For the region of 40-60°N and 90°-120°E a comparison between these reanalyses together with some station data was already undertaken for mean JJA SLP by Inoue and Matsumoto (2004). It covers a domain that corresponds roughly to the subregions SW and parts of MW, MM and SE also under consideration here.

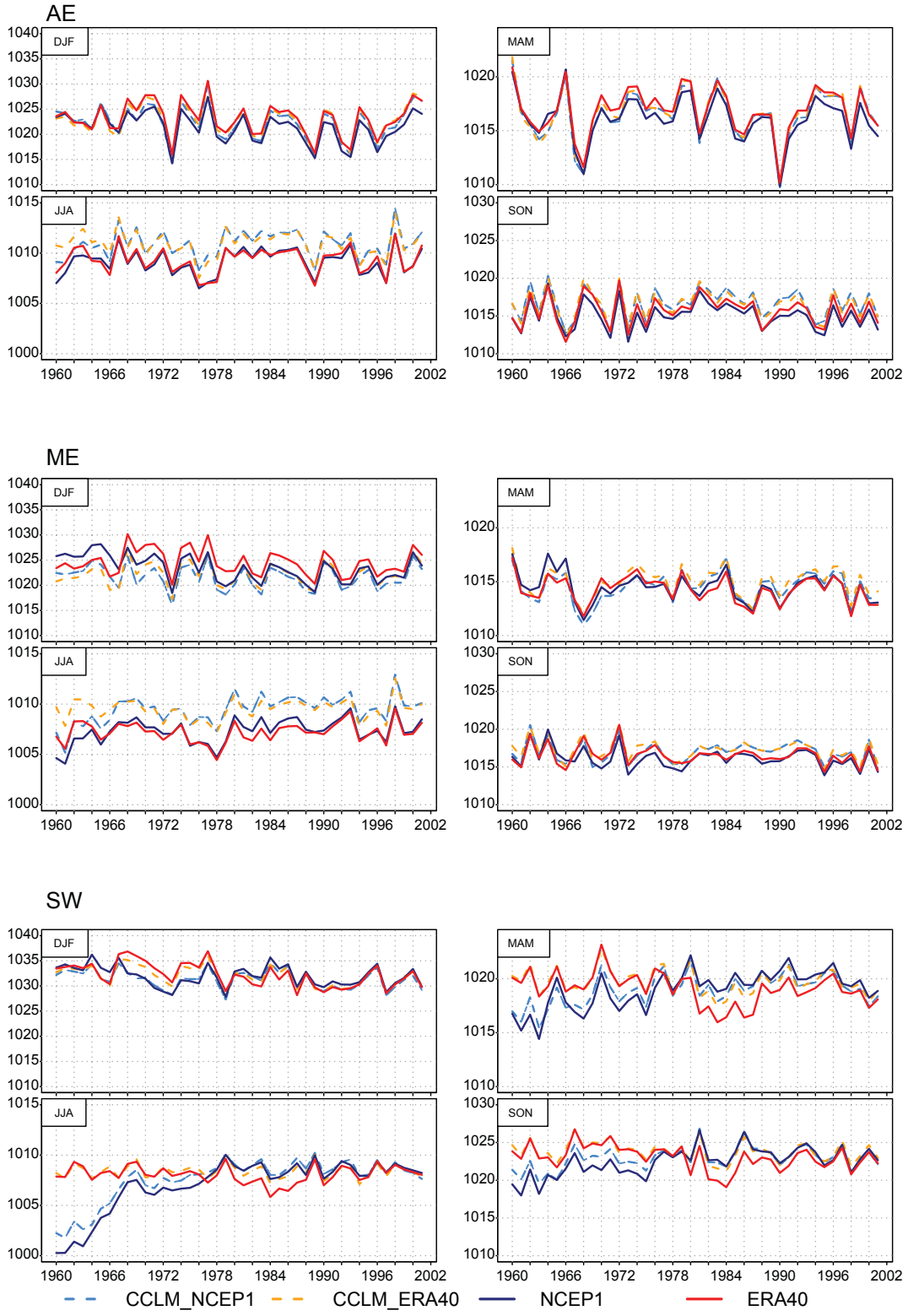

Figure 5.2: Interannual variations of MSLP [hPa] for NCEP-R1, ERA40, CCLM-NCEP1, CCLM-ERA40 considered for the subregions AE, ME and SW.

In this study, the interannual MSLP comparison of reanalyses is extended to all four seasons showing, in addition, the similarity and dissimilarities in terms of temporal variations of downscaled hindcasts and their sensitivity to the forcings. In the following, the focus is put on the interannual variations of MSLP using the following measures: temporal correlation, bias and centered root mean square error of MSLP for both reanalyses and hindcasts of four decades given in Table 5.1 to provide a interdecadal comparison. The focus is put on the subregions AE, ME and SW representing latitudinal variations from north to south (5.1).

For the subregion AE the reanalyses agree well in their interannual variability from 1959-2001 throughout the different seasons. According to Fig. 5.1, the highest bias throughout the seasons occur during DJF in the period of 1969-1978 with -2.4 hPa. The temporal correlation for the considered periods and seasons are between 0.9 and 1. The highest crmsd occur during the first period of 1959-1968 in DJF with 0.9 hPa. The hindcasts show, in general, a smaller bias than the forcings, except for the first period in DJF and JJA. In these cases the sign of bias is reversed in the following years.

For ME during DJF, the temporal correlation between reanalyses is lowest during first period with 0.6 and a crmsd with 1.7 hPa. Hindcasts show a better agreement with 0.9 correlation during the first period and a crmsd of 1.1 hPa. Throughout all periods the bias between the reanalyses is higher than between the hindcasts as already shown in AE. Both between the forcings and hindcasts in the first period NCEP and CCLM-NCEP present higher values (positive bias) than ERA and CCLM-ERA which is vice versa (negative bias) in the following periods .

Strongest discrepancies in the year-to-year and interdecadal variability between the forcings and between the hindcasts occur in the southern subregion SW, especially during the first period in MAM, JJA and SON. The highest bias occurs between the forcings in JJA during the first period with -5.5 hPa and between the hindcasts of -4.3 hPa as illustrated in Table 5.1. This is also evident with the low temporal correlations in that period with 0.3 of the forcings and 0.4 of the hindcasts. Most pronounced are the differences in the year 1960 (Fig. 5.2) with more than 7 hPa between NCEP-R1 and ERA40. Until 1979 MSLP of NCEP-R1 increases to 1010 hPa and gets closer to ERA40. This strong difference between NCEP-R1 and ERA40 prior 1979 and slight approximation was already mentioned by Huang et al. (2011) investigating the discrepancies between reanalyses in the interdecadal variation of the southeast Asian cold surge. Several studies have dealt with possible causes (Salstein et al., 2008; Sterl, 2004; Sturaro, 2003). Potential reasons are the changes in the observing system especially in 1958 with the establishment of global radiosonde network and at the end of 1970s with the use of satellite observations that effects the amount and quality of assimilated observations (Huang et al., 2011). Additionally, the different assimilation schemes between reanalyses might be a cause of the discrepancies (Bengtsson et al.,

2004). According to Sterl (2004), NCEP-R1 produced earlier than ERA40, has excluded newer observations to ensure a consistent output.

When the bias of forcings changes the sign in some periods, some special behavior of forcing discrepancies occur. This is very pronounced e.g. in the third period in MAM, JJA and SON. In the periods before, ERA40 shows higher MSLP than NCEP-R1 and afterwards this feature changes suddenly. This also happens with the hindcasts but less pronounced, as in general the biases are smaller than found for the forcings. The ERA40-hindcast does not completely follow the sudden decreasing trend of ERA40 from 1979-1987. The slightly decreasing trend of ERA40 from 1980-1987 is also evident but less pronounced in the surface pressure anomalies of the station averages illustrated by Inoue and Matsumoto (2004). After 1988 the two reanalyses reveal similar patterns of interannual variations. The hindcasts follow both their forcings in terms of temporal variability. It is evident from Fig. 5.2 that the year-to-year variability of averaged JJA MSLP for the subregion SW shown by the NCEP-R1 data shows the same two increases in pressure during the 1960 and 1970s as presented by Inoue and Matsumoto (2004). These positive trends cannot be observed in ERA40. In their study they conclude that the sudden increases of MSLP in NCEP-R1 over Mongolia before 1979 are likely spurious and do not represent real surface conditions. A possible reason for the MSLP increase over Mongolia during the 1960s was pointed out to be the 'psfc problem', already stated by Kistler et al. (2001). But this problem did not appear anymore after 1968 anymore.

Summertime variations of upper-level variables

These different characteristics of temporal discrepancy and similarity from north to southern subregions are not only visible in MSLP but also in other variables throughout the vertical profile of the atmosphere. In Fig. 5.3 the interannual variations for FI500, T850, U500 and QV850 for the subregions AE, ME, and SW are presented. Again, a north-south gradient with increasing discrepancies between the reanalyses and hindcasts occur as already stated for MSLP. For the geopotential height and the U-wind component at 500 hPa, NCEP-R1 and CCLM-NCEP-R1 have lower values than ERA40 and CCLM-ERA40 until 1976 (for FI500) and 1964 (for U500). Afterwards, both reanalyses and hindcasts get closer together. In contrast to QV500 in SW - here NCEP1 stays throughout the entire period higher than ERA40. In that subregion during the summer season the ERA40 driven hindcast is closer to its forcing than the NCEP1 driven hincast to NCEP-R1.

The NCEP-R1 and ERA40 time series presented for the subregion SW of the geopotential height at 500 hPa look similar to the same variables for regions over China, as illustrated by Zhao and Fu (2009). Additionally, they compared against observations showing that ERA40 is in better agreement to the observations prior the 1970s than NCEP-R1.

Reanalyses		DJF				MAM				JJA				SON			
		Period:				Period:				Period:				Period:			
		1.	2.	3.	4.	1.	2.	3.	4.	1.	2.	3.	4.	1.	2.	3.	4.
Corr	AW	1	1	1	1	1	1	1	1	1	1	1	1	1	1	1	1
	AE	0.9	1	1	1	1	1	1	1	0.9	1	1	1	1	1	1	1
	MW	1	1	1	1	1	1	1	1	1	1	1	1	1	1	1	1
	MM	0.8	1	1	1	1	1	1	1	0.8	1	1	1	1	1	1	1
	ME	0.6	1	0.9	1	0.9	1	1	1	0.6	1	0.9	1	0.8	1	0.9	1
	SW	0.3	0.9	0.9	1	0.6	0.7	0.8	0.9	0.3	0	0.8	1	0.7	0.4	0.8	0.9
	SE	0.5	0.9	0.7	0.9	0.9	0.9	0.9	1	0.7	0.9	0.9	1	1	1	0.7	1
Bias	AW	-0.3	-1.6	-1.4	-1.1	-0.3	-0.9	-0.8	-0.6	-0.6	-0.2	-0.1	0	-0.3	-0.6	-0.4	-0.4
	AE	-0.3	-2.4	-1.9	-1.9	-0.1	-1.1	-0.8	-1	-0.4	-0.2	0.1	-0.2	-0.2	-1	-0.5	-0.8
	MW	-1.1	-1.8	-1.5	-1.2	-0.5	-0.6	-0.5	-0.3	-0.6	-0.1	0	0	-0.7	-0.6	-0.6	-0.5
	MM	0.1	-2.9	-2.1	-1.7	-0.3	-0.7	-0.2	-0.1	-2.2	-0.4	0.1	0	-0.9	-1.2	-0.6	-0.7
	ME	1.9	-2.4	-2.1	-1.5	0.7	-0.5	0.3	0.1	-1	0.2	0.7	0.2	0.1	-1.1	-0.3	-0.3
	SW	0.1	-3.1	1.2	0.6	-2.8	-1.7	2.2	1.2	-5.5	-1.2	1.4	0.3	-3.5	-2.2	1.9	0.7
	SE	1.4	-2.6	0	0	-1.4	-1.1	0.8	0.6	-3.8	-0.8	0.5	0.2	-1.8	-1.7	0.5	0.2
Crmsd	AW	0.6	0.5	0.3	0.3	0.2	0.2	0.2	0.2	0.2	0.1	0.1	0.1	0.3	0.2	0.2	0.2
	AE	0.9	0.5	0.4	0.4	0.4	0.2	0.2	0.4	0.6	0.2	0.1	0.3	0.6	0.3	0.2	0.3
	MW	0.4	0.4	0.2	0.2	0.1	0.1	0.2	0.1	0.2	0.1	0.1	0.2	0.1	0.2	0.2	0.1
	MM	1.3	0.5	0.5	0.5	0.2	0.1	0.3	0.2	0.9	0.1	0.1	0.2	0.2	0.2	0.3	0.4
	ME	1.7	0.6	0.5	0.3	0.7	0.2	0.4	0.1	1	0.2	0.3	0.2	0.9	0.2	0.4	0.2
	SW	1.8	0.8	0.9	0.3	1.2	1	0.9	0.4	2.2	0.9	0.5	0.2	1.1	1.1	1	0.4
	SE	1.8	0.4	0.8	0.4	0.5	0.3	0.5	0.3	1.4	0.3	0.3	0.2	0.3	0.3	0.6	0.3

Hindcasts		DJF				MAM				JJA				SON			
		Period:				Period:				Period:				Period:			
		1.	2.	3.	4.	1.	2.	3.	4.	1.	2.	3.	4.	1.	2.	3.	4.
Corr	AW	1	1	1	1	1	1	1	1	1	1	1	1	1	1	1	1
	AE	0.9	1	1	1	1	1	1	1	0.9	1	1	1	1	1	1	1
	MW	1	1	1	1	1	1	1	1	0.9	1	1	1	1	1	1	1
	MM	1	1	1	1	1	1	1	1	0.7	0.9	1	1	1	1	1	1
	ME	0.9	1	1	1	1	0.9	1	1	0.7	1	1	1	1	1	1	1
	SW	0.7	1	1	1	0.6	0.9	1	1	0.4	0.5	1	1	0.9	0.7	1	1
	SE	0.9	0.9	1	1	0.9	0.9	1	1	0.5	0.9	1	1	0.8	0.9	0.9	1
Bias	AW	0.8	-0.4	-0.3	-0.4	0.1	-0.2	-0.2	0	-0.5	0.1	0.1	0.2	0.4	0.2	0.3	0.6
	AE	0.8	-0.9	-0.6	-0.8	-0.1	-0.3	-0.2	-0.2	-0.9	0.3	0.2	0.2	0.1	0	0.2	0.4
	MW	-0.1	-0.9	-0.4	-0.3	-0.5	-0.4	-0.2	-0.1	-1.1	-0.1	0.2	0.2	-0.3	-0.3	0	-0.1
	MM	0.3	-1.3	-0.6	-0.8	-0.9	-0.7	-0.3	-0.3	-2.3	-0.2	0.3	0.4	-0.7	-0.5	0	-0.1
	ME	1.1	-1.3	-0.8	-0.9	-0.7	-0.9	-0.3	-0.4	-1.6	0.2	0.4	0.4	-0.5	-0.6	0	0
	SW	-0.7	-2	0.1	-0.3	-2.7	-1.1	0.3	0	-4.3	-0.6	0.6	0.4	-2.7	-1.3	0.3	-0.2
	SE	0.1	-1.5	-0.5	-0.7	-1.5	-0.9	-0.1	-0.3	-3.1	-0.1	0.7	0.3	-1.6	-0.9	0.1	-0.3
Crmsd	AW	0.8	0.4	0.2	0.3	0.4	0.2	0.2	0.2	0.2	0.2	0.2	0.2	0.3	0.3	0.3	0.2
	AE	1	0.4	0.2	0.4	0.5	0.3	0.3	0.2	0.6	0.3	0.2	0.2	0.5	0.3	0.3	0.3
	MW	0.4	0.3	0.2	0.2	0.1	0.2	0.1	0.1	0.5	0.2	0.1	0.1	0.1	0.4	0.1	0.2
	MM	0.8	0.4	0.2	0.4	0.2	0.3	0.2	0.2	1	0.3	0.1	0.1	0.3	0.4	0.2	0.2
	ME	1.1	0.4	0.1	0.2	0.5	0.4	0.2	0.2	1	0.2	0.2	0.1	0.5	0.4	0.2	0.3
	SW	1.1	0.5	0.3	0.2	0.9	0.5	0.4	0.2	1.8	0.6	0.2	0.2	0.6	0.6	0.4	0.2
	SE	0.9	0.4	0.2	0.3	0.6	0.4	0.3	0.2	1.8	0.3	0.3	0.1	0.7	0.5	0.3	0.1

Table 5.1: Seasonal values of temporal correlation (Corr), bias [hPa], centered root mean square difference [hPa] (Crmsd) of MSLP of used reanalyses (NCEP-R1 and ERA40) and both hindcasts (CCLM-NCEP1, CCLM-ERA40) for four different periods (1.period: 1959-1968, 2.period: 1969-1978, 3.period: 1979-1988, 4.period: 1989-1999).

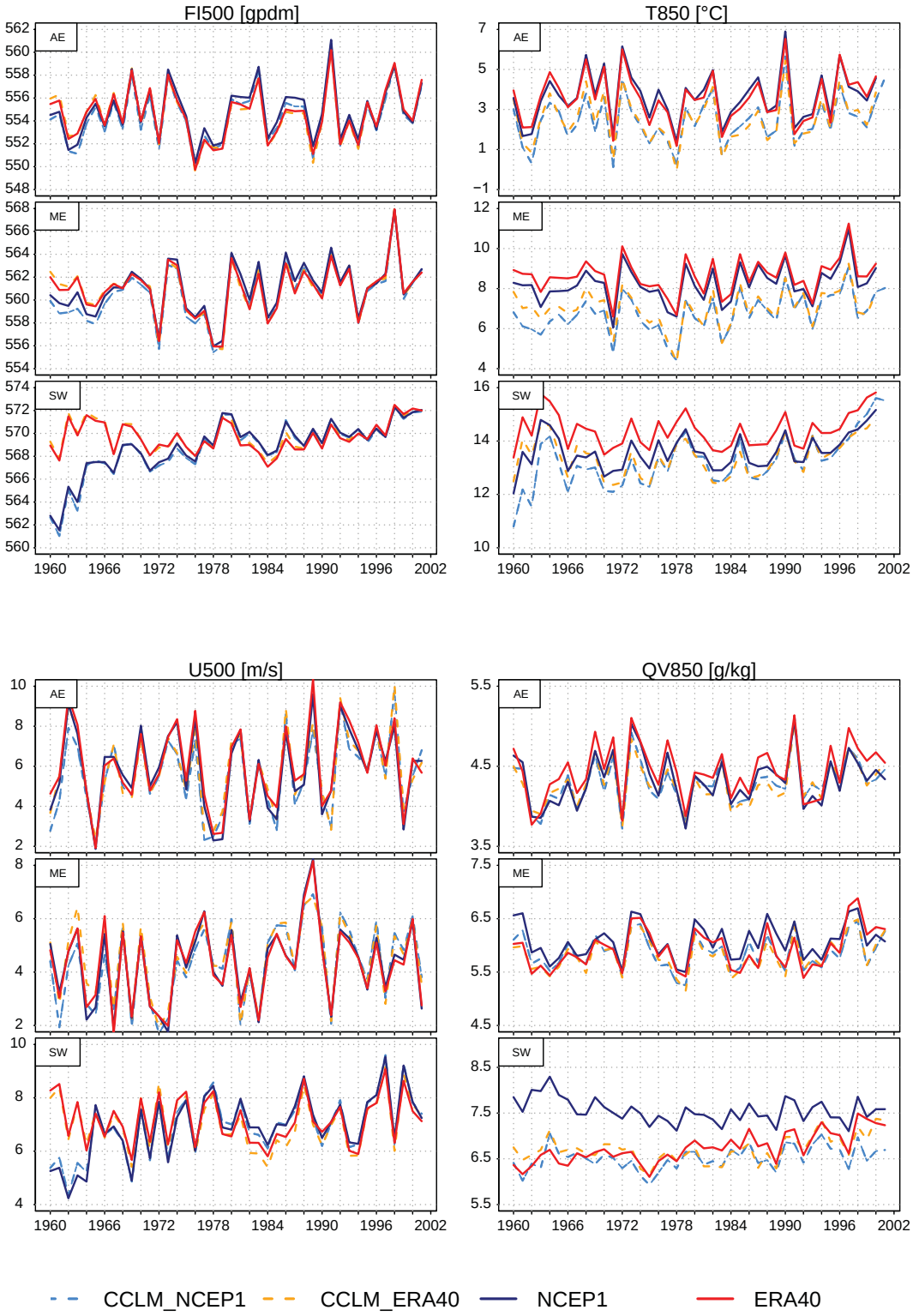

Figure 5.3: Summertime variation of both hindcasts and used forcings for FI500, T850, U500, QV850 averaged over three subregions (AE, ME, SW).

5.3.3 Interdecadal similarity assessment

As mentioned previously, the objective was to perform a similarity test between both reanalyses and both hindcasts separately. The aim was to provide an overview about the decadal agreement or disagreement of two distinct reanalyses in their large-scale atmospheric information that reflects data reliability or uncertainty. Additionally, this test was also performed for both hindcasts to evaluate their degree of similarity or discrepancy and their sensitivity to the reanalyses uncertainty. The aggregated similarity metric is presented for all analyzed variables, seasons and subregions for each of the four periods (1959-1968, 1969-1978, 1979-1988, 1989-1999). A strong decadal discrepancy of the two reanalyses or the derived hindcasts indicates a high uncertainty of the considered datasets. At least one of the reanalyses or hindcasts does not show real conditions. All three single measures exceed the threshold, the considered decade and variable is colored in red (see Table 5.2) due to strong discrepancy between either the forcings or both hindcasts. Therefore, these affected years should be used with caution or excluded in further studies. It is apparent that both reanalyses show only small discrepancies in the arctic subregions AW and AE and subarctic subregions MW, MM and ME. In the southern subregions SW and SE, the strongest differences, and thus uncertainties, between the global datasets occur mainly in the first and second period. These discrepancies are especially pronounced during JJA for MSLP, FI850, U850 and U500, QV850, V850 during the first period. Altogether, the RCM hindcasts reveal similar uncertainty in the southern subregions that reflects the direct transfer of large-scale uncertainty of atmospheric variables to the regional scale. However, in some periods the number of aggregated metric is different from the metric of the similarity-check between the reanalyses. This shows that the output of the RCM is somewhat different from the forcings due to its own model dynamics.

The results of regional characteristics for seasonal similarity are in detail illustrated in Table 5.2. In the left part of Table 5.2, the comparison is presented for the two considered reanalyses. Small discrepancies between reanalyses occur in the arctic and subarctic regions AW, AE, ME, MM and MW mainly in the first two periods for all seasons. For the majority of considered variables the compared datasets are in good agreement in the last 3 periods. Except for FI200, small differences of 0.3 are mostly throughout all the periods and seasons. Small differences are visible for U200 in AW and U500 in AE in the last period during DJF. A discrepancy between the reanalyses with 0.7 occurs during JJA in the subregion MM for U500 and U200. Except for the first period, the overall agreement is good and the reliability of global atmospheric information throughout these periods is given.

Strongest uncertainties in the global data occur in the subregion SW during JJA. The decadal agreement is considerably weak in SW for MSLP, FI850, FI500, all considered U-levels and QV850 in the first period. Dissimilarities are also found in JJA during the

second period for MSLP and FI850 that are decreasing during the 3rd. period. However, not only JJA is affected. Additionally, in DJF in the first two decades, MSLP and FI850 show strong differences. For FI500 and U500 this is evident in the second decade. During the spring season MAM, most discrepancies occur in the first decade for FI850, FI500, T850, U850, U500 and U200. For SON dissimilarities are evident in the first period for FI500, U200 and for U500 in the first and second period the reanalyses show differences. A somewhat smaller degree of discrepancy than presented in SW can be observed in the subregion SE. Again the summer season JJA has the highest degree of discrepancy for MSLP, FI850, V850 and V500. There are also DJF differences in MSLP, U850 and V850 are predominant.

The right part of Table 5.2 reveals the regional overview for seasonal similarity characteristics between the derived hindcasts. In addition to showing the degree of agreement, this assessment indicates the sensitivity of downscaled hindcasts to the reanalyses uncertainty. In the arctic and subarctic regions the majority of downscaled variables show similar patterns of similarity and discrepancy as the reanalyses throughout the seasons.

For certain variables the hindcasts show a better agreement than presented by the reanalyses. This is e.g. the case for AE during DJF for U850 during the second and third period and V500 in DJF and V200 in MAM in the first period. Similar patterns are evident for the subregion MM during DJF for MSLP: the forcings show small differences throughout all periods, whereas the hindcats reveal no tested discrepancy after the first period. This occurs again, e.g. in the subregion ME for MSLP in DJF, in JJA for U850 or e.g. in SW for MSLP and FI850 in DJF and MAM. A pronounced reduction of discrepancy is evident in SW for QV850 during MAM and JJA where a good agreement is given between the hindcasts.

In contrast to the reduction of discrepancy, there are cases where the degree of similarity or dissimilarity stays the same as e.g. shown in ME during the autumn season SON. However, for certain variables the discrepancies between the hindcasts are even more pronounced than in the forcings as e.g. seen for V200 in the first period of MAM and JJA or in the subregion SE for V500 in MAM in the first period.

As seen for MSLP in the subregion SW with pronounced discrepancies between the reanalyses during the first two periods as e.g. in DJF, the reduction of differences show that the RCM can dampen the discrepancy due to its own model physics in the inner model domain. In other cases where the discrepancies are strongest between the forcings as in JJA for MSLP, this does not seem possible.

It should, however, be noted, that these results of the similarity test are based on subjective thresholds. Depending on the chosen thresholds the similarity in the temporal correlation, bias and centered root mean square is ranked. The final metric shown in Table 5.2 is affected by these thresholds that determine the degree of discrepancies.

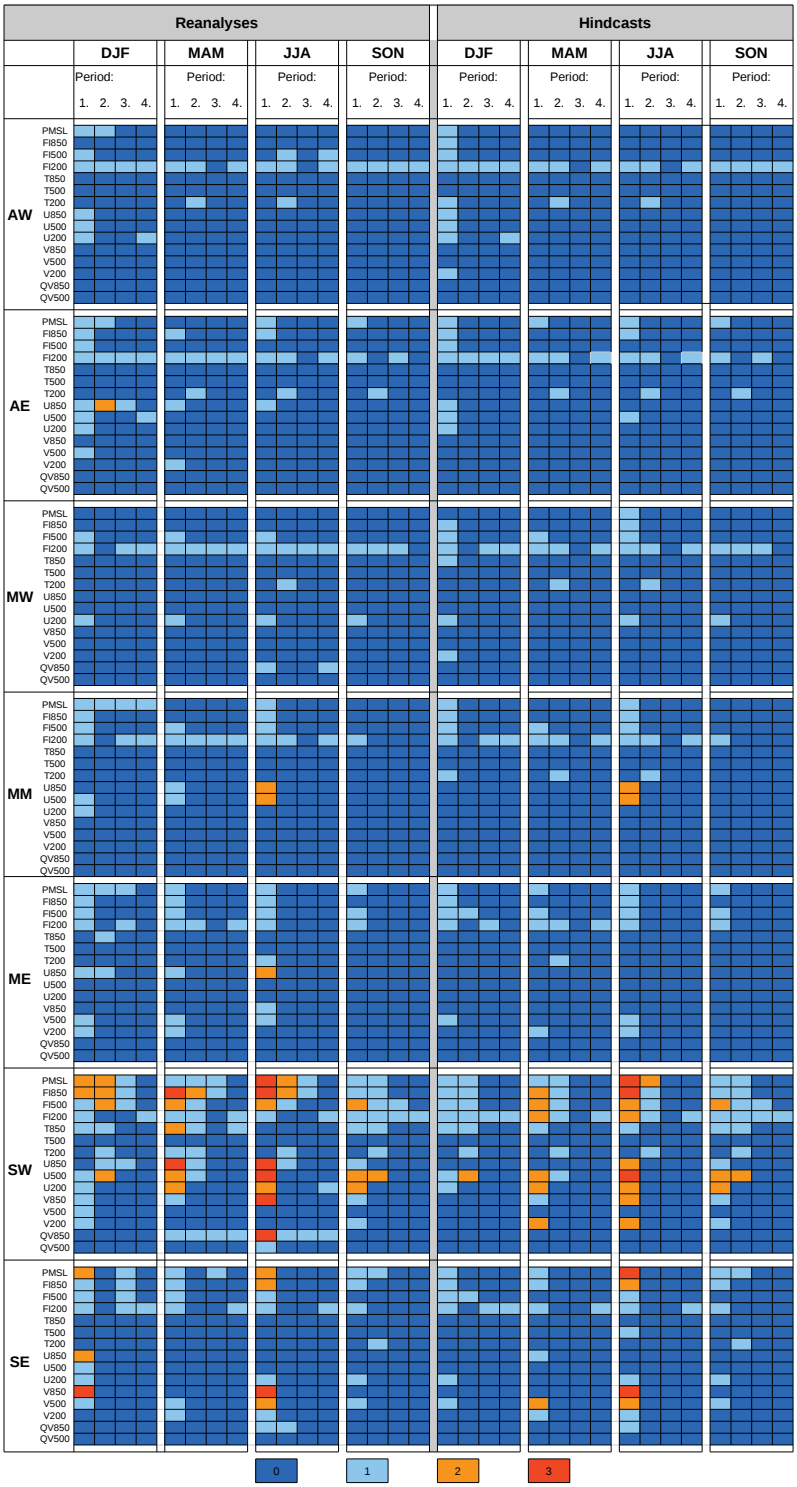

Table 5.2: Seasonal aggregated measure of agreement between both reanalyses and hindcasts illustrated for all 7 subregions and considered periods for 6 variables at the given levels. Dark blue: good agreement according to set thresholds, light blue: disagreement in one measure, orange: disagreement in two measures, red: disagreement in three measures.

In general, the first two periods are the strongest affected. Affected variables do not show the same dissimilarity score throughout the regions and seasons, rather they vary from season to season and decade. A good agreement according to this similarity test is given for the last 2 analyzed periods with small discrepancies for FI200, F850 and QV500. As shown in the Table 5.2, three cases occur: the arctic regions with almost no discrepancies, some of the middle domains with a little bit higher degree of dissimilarity and for certain variables strong discrepancies as e.g. in the subregion SW.

5.4 Conclusion

This study analyzes the temporal consistency and reliability of derived regional climate model hindcast for Siberia driven with NCEP-R1 by assessing the degree of agreement with a second hindcast driven with ERA40. The same investigation is done with the forcings themselves.

According to Inoue and Matsumoto (2004) and Zhao and Fu (2009), NCEP-R1 strongly overestimates interdecadal changes prior the 1970s occurring in the southern region near Lake Baikal for summertime MSLP and geopotential heights at 500 and 700 hPa. This study provides a comprehensive overview of the degree of agreement and disagreement in terms of atmospheric information of employed reanalyses in Siberia. Therefore, different variables (surface and upper-level), important for downscaling, were assessed in terms of interdecadal changes and variability for seasonal and regional similarity. The reliability of the two chosen forcings for Siberia was investigated in more seasonal detail than done so far. Moreover, this analysis additionally presents the sensitivity of downscaled hindcasts to the reanalyses uncertainty.

The analysis shows that for a set of variables, the two hindcasts can differ considerably in terms of interannual variability prior the 1970s in the southern parts of the model domain especially during summer season and that those large temporal discrepancies can be related to the varying large-scale atmospheric forcing of NCEP-R1 and ERA40. In certain regions such as southern Siberia, reanalyses cannot be assumed to be a 'perfect' boundary per se. They suffer from inhomogeneities and spatial and temporal discrepancies, particularly in regions where in situ observations are sparse. This is the case even for certain middle-tropospheric variables such as FI850, FI500, U500 which are important for dynamical downscaling and spectral nudging purposes. Therefore, it is, in general, necessary to first assess the temporal consistency of the used reanalyses for the considered region to identify the causes of temporal inconsistency of derived hindcasts or to identify the best possible reanalysis for the region under investigation.

This assessment gives an overview of which variables, seasons, regions and years of the derived hindcasts and the reanalyses are usable or are of concern for the use of trend analysis and dynamical downscaling purposes. As shown, several variables of the forcings

show some uncertainty from 1960 to 1970s especially in the southern domain. The following analyses will be conducted after 1979 to exclude spurious variations and trends. Having the aim to derive long-term homogenous regional hindcast data, it is suggested that future work use ERA40 as forcing or exclude the southern parts of the NCEP-R1 driven hindcast when data prior to 1979 is needed. If regional climate hindcast data after 1979 is of interest, ERA-Interim would be a further option with possibly enhanced reliability.

6 Evaluation of Model-based Climate Reconstructions

6.1 Introduction

The purpose of this section is to evaluate the regional climate hindcast simulations conducted for Siberia in terms of skills and deficiencies in the representation of observed climate characteristics. The model output is compared to different kinds of observational datasets or reanalyses. As already mentioned in Chapter 2.3, observational data are limited for Siberia, especially in northern high latitudes, due a sparse station network. These limitations need to be taken into account within the evaluation.

The evaluation focuses on assessing the ability of the regional climate model in reproducing observed atmospheric patterns of MSLP, the vertical temperature profile, seasonal characteristics and annual differences to observational reference of near-surface temperature and precipitation. Additionally, seasonal trend patterns of 2 m air temperature and precipitation for 1981-2010 are compared to observations to investigate the agreement in reproducing recent changes. Furthermore, the interannual variations of certain climate extremes in terms of 2 m air temperature and precipitation are analyzed.

6.2 Data and Methods

First, the evaluation of simulated atmospheric circulation patterns over Siberia is addressed in comparison to ERA40. Spatial fields are considered by looking at mean sea level pressure averaged over 1980-1999. In this analysis, standard seasons (DJF, MAM, JJA, SON) are used. The vertical temperature profile for selected subregions during winter and summer season is compared against ERA-Interim for the years 1995-1999.

Spatial distribution of mean seasonal fields of 2 m air temperature and precipitation, as well as recent trends, are assessed by comparing CCLM-NCEP1 with selected grids of CRU3.2 and GPCC6 for the years 1981-2010 where station records were available and were incorporated within the interpolated datasets. Trends of the considered variables and seasons are calculated using a linear regression with the least squares method. Statistical significance are assessed using the non-parametric Mann-Kendall trend test (Mann, 1945; Kendall, 1975). Seasonal mean values are used to reduce autocorrelation within the time series.

The regional averaged bias of the annual cycle for 2 m air temperature and precipitation of both hindcasts are calculated in comparison to CRU3.2 and GPCC6 in the same way as already introduced in Chapter 4 for the period of 1979-2001. The corresponding nearest neighboring grid boxes of CCLM and considered reanalysis products (NCEP-R1, ERA40, ERA-Interim) are selected and averaged over six subregions. To assess the observational uncertainty, daily station data provided by NCDC is included in comparison to CCLM-NCEP1. As the application of a constant temperature lapse rate especially during winter

is not realistic due to the predominant temperature inversion, no height-correction for temperature is carried out. However, to take into account the different elevations of stations and the model orography, the differences of heights averaged over each subregion are shown.

Additionally, threshold-based indices for climate extreme events defined by the World Climate Research Programme (WCRP) Climate Variability and Predictability (CLIVAR) project's Expert Team on Climate Change Detection, Monitoring and Indices (ETCCDMI) (Karl et al., 1999; Peterson, 2005) are evaluated. As reference, the global land-base climate extremes dataset offered by ETCCDMI is used. Several indices of temperature and precipitation computed from daily station data are provided for different countries. They make use of quality controlled daily data. The indices extend only to 2001. The interannual variation of three selected indices are presented from the model output as well as from NCEP-R1, ERA40, ERA-Interim and are compared against the subregion-specific station data of ETCCDMI. The indices are: frost days (annual count of days when daily minimum temperature $< 0°C$), summer days (annual count of days when daily maximum temperature $> 25°C$) and R10mm (annual count of days when precipitation is $> 10\,mm$).

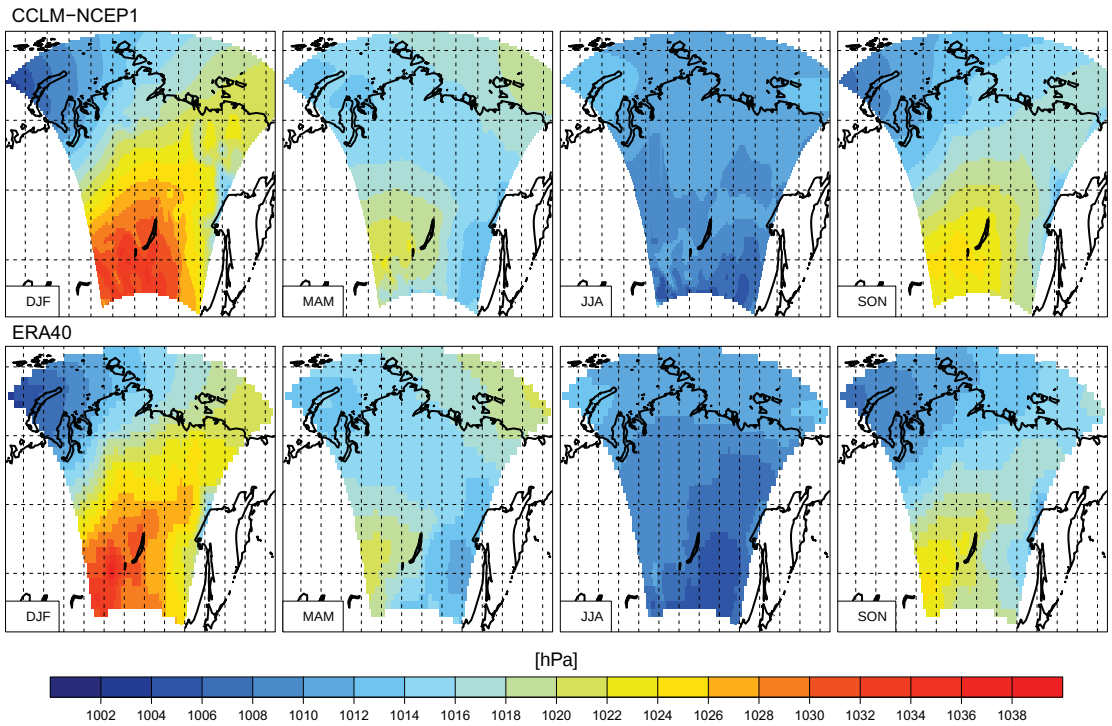

Figure 6.1: Seasonal mean (1980-1999) distribution of MSLP [hPa] for CCLM-NCEP1 and ERA40.

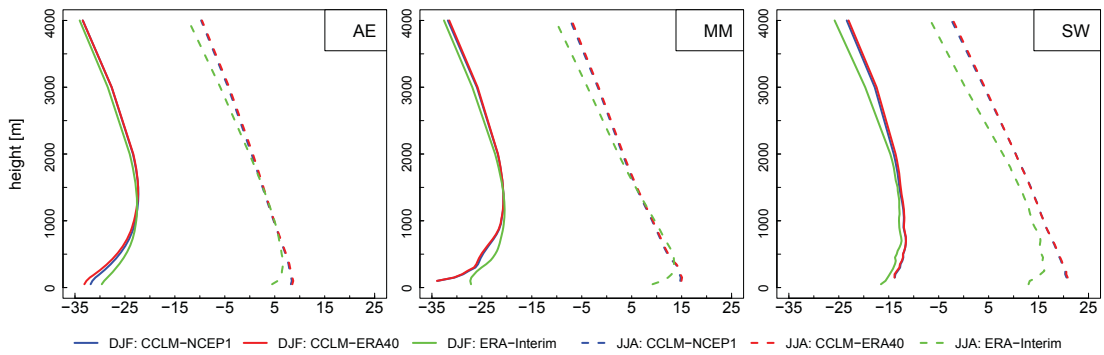

Figure 6.2: Vertical temperature profile of CCLM-NCEP1, CCLM-ERA40 and ERA-Interim for DJF (solid lines) and JJA (dashed lines) averaged over the period of 1995-1999.

6.3 Results

6.3.1 Atmospheric Patterns of Mean MSLP

Fig. 6.1 reveals the seasonal variation, showing high sea level pressure during the winter season DJF. In contrast to ERA40, in CCLM-NCEP1 high pressures of the Siberian high are extended more southeastward. Along the Verkhoyansk Mountains, CCLM-NCEP1 presents a bisection of high pressure system which is not visible in ERA40. Here the pressure decreases gradually from southwest to northeast. During JJA the lowest pressure occurs. During SON the high pressure system starts to establish in southwest.

6.3.2 Vertical Temperature Profile

In this section, the focus is on the representation of vertical temperature profile (Fig. 6.2). Temperature at different pressure levels of CCLM-NCEP1, CCLM-ERA40 and ERA-Interim is interpolated on height-levels above surface. In comparison to ERA-Interim, CCLM is able to reproduce the mean temperature vertical profile. During the winter season the temperature increase with height represents the characteristic feature of low-level temperature inversion that is predominant in the Siberian high pressure system.

6.3.3 Seasonal Patterns of Air Temperature and Precipitation

To evaluate the ability in reproducing the spatial distribution of mean seasonal 2 m air temperature and precipitation, the reconstructed climatologies over the period 1981-2010 are presented for CCLM-NCEP1 and selected grid boxes of CRU3.2 in Fig. 6.3 and of GPCC6 Fig. 6.4 respectively.

Generally, both datasets depict the strong seasonality with a large temperature range throughout the year showing extreme low temperatures during winter in northern regions and high temperatures during summer (Serreze and Barry, 2005). Compared to CRU3.2, CCLM shows good agreement in seasonal temperature fields with less discrepancies during

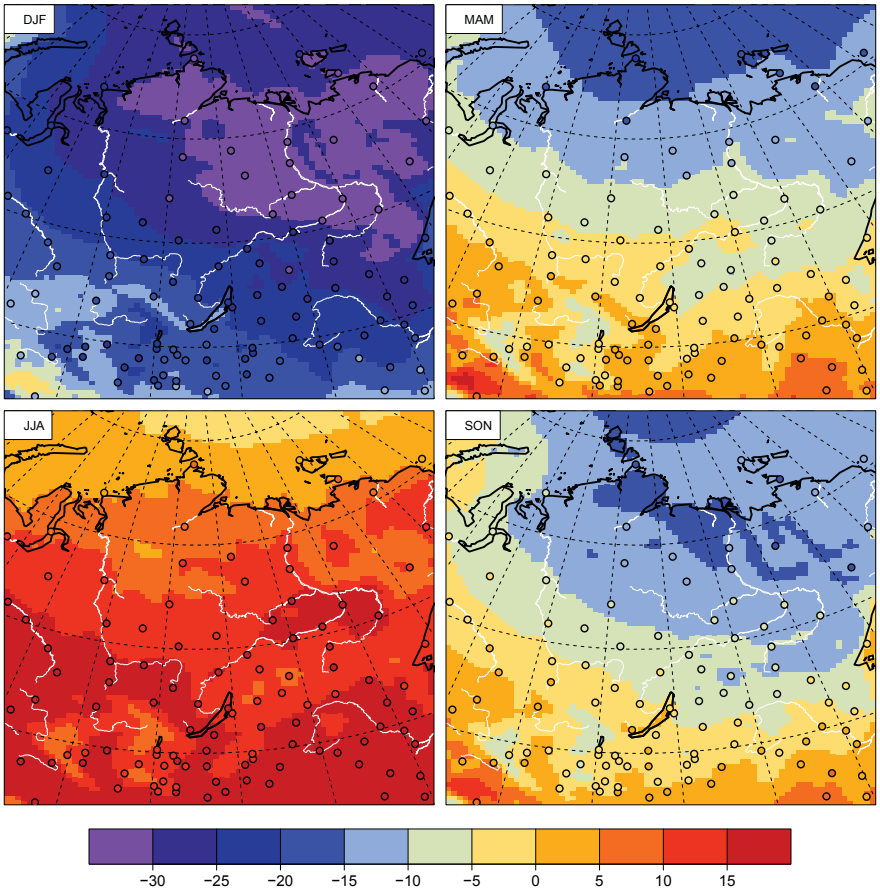

Figure 6.3: Seasonal mean of 2 m air temperature [°C] of 1981-2010 for CCLM-NCEP1 and CRU3.2 station grids (colored dots).

summer and spring but regional differences in winter and fall. During winter, CRU3.2 illustrates temperatures lower than -30°C more extended to the west at the Central Siberian Plateau and southwest towards the Stanovoy Range. In addition, a warm bias in CCLM is illustrated in the southwestern region. In contrast, CCLM tend to be colder than CRU3.2 compared to the depicted grid boxes in the southeastern part. During fall, temperatures between -15 to -10°C along the Lena river basin are extended more southwards than the observed in CRU3.2.

The agreement between CCLM-NCEP1 and GPCC6 for mean seasonal precipitation is presented in Fig. 6.4. Throughout all seasons, CCLM tend to overestimate precipitation along the coasts except for western parts in summer and fall. A pronounced overestimation is further illustrated in the southern and northeastern regions in DJF, MAM and SON whereas during summer an underestimation is evident in southern and western parts of the model domain.

To assess the differences for 2 m air temperature and precipitation in more detail, i.e. in comparison to the second hindcast simulation, the driving reanalyses and ERA-Interim and a second observational dataset, the bias of annual cycle variations averaged over six

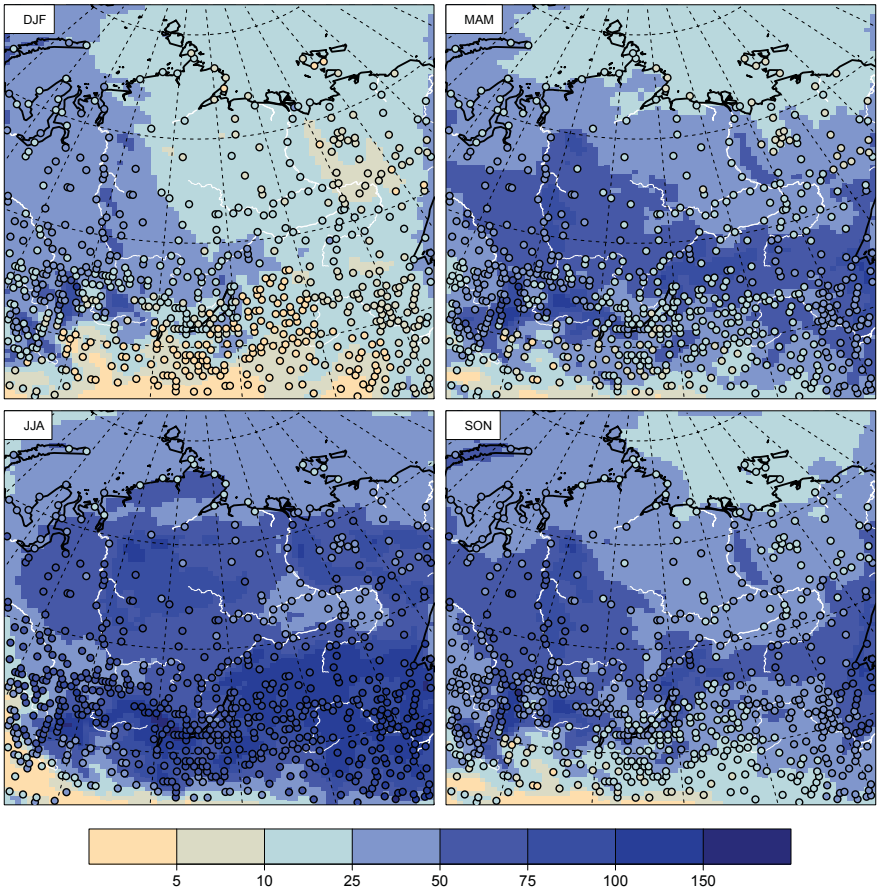

Figure 6.4: Seasonal sum of precipitation [mm/season] of 1981-2010 for CCLM-NCEP1 and GPCC6 station grids (colored dots).

subregions is presented in the following.

6.3.4 Annual Cycle of Bias of Air Temperature and Precipitation

A winter warm bias of CCLM occurs in all subregions except for MW most pronounced for AE (6K in January), AW (4K) and ME (4K) when compared to CRU3.2 grid boxes as presented in Fig. 6.5. However, the overestimation of CCLM-NCEP1 is smaller when evaluated against NCDC stations except for ME. In general, more stations are available per month within the considered period compared to CRU3.2 stations as illustrated in purple bars. The bias between CCLM-NCEP1 and the 2 selected observational reference datasests can vary considerably as e.g. in AW and AE. In these regions it is difficult to assure reasonable model evaluation due to the observational uncertainty range. The bias of CCLM is partly related to the forcings which show a warm bias when compared to CRU3.2 grid boxes.

During spring, a warm bias is still predominant in the arctic subregions, ME and partly in MM in CCLM. During summer and fall all subregions except of MW and SW present

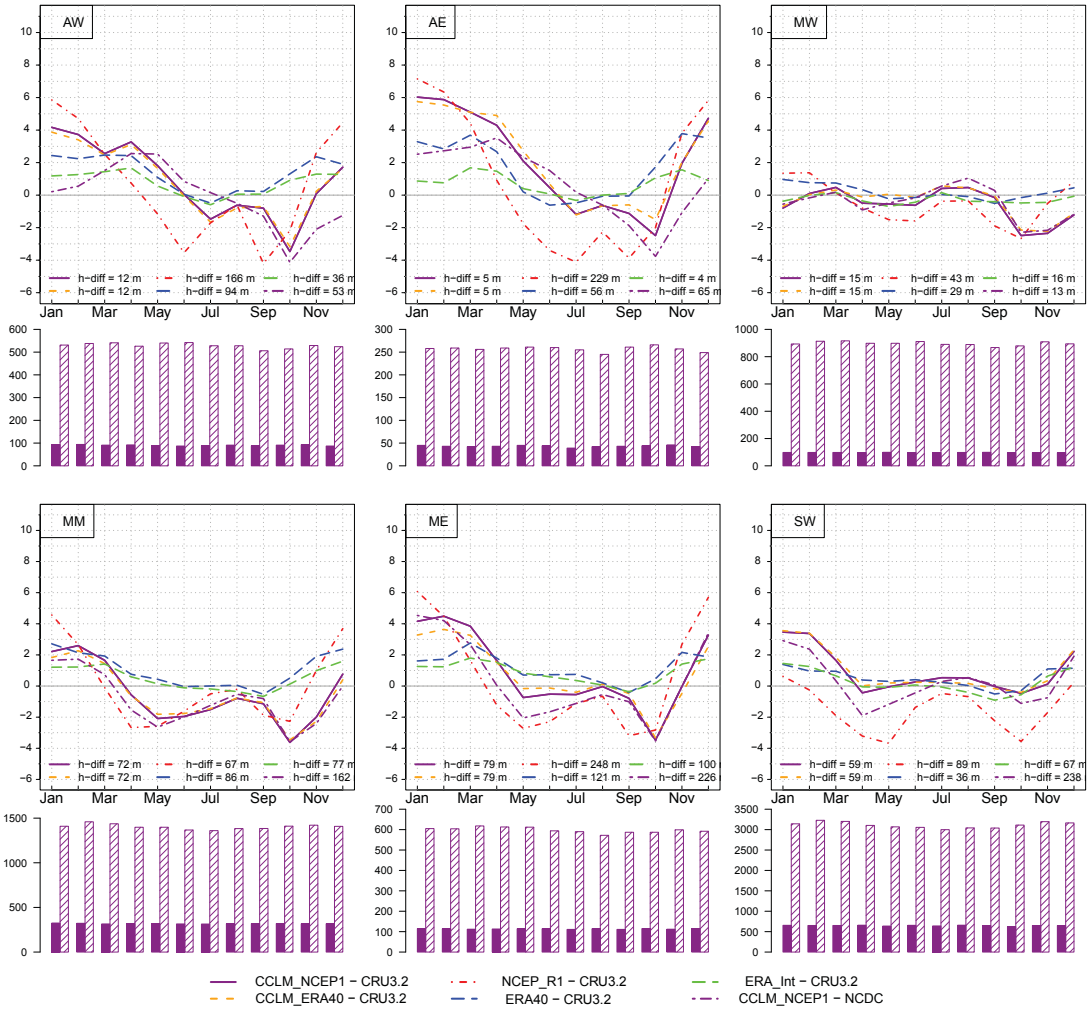

Figure 6.5: Bias of monthly means of 2m air temperature [K] for selected grid boxes per subregion of CCLM-NCEP1 and CCLM-ERA40, NCEP-R1, ERA40, ERA-Int(erim) against CRU3.2 station grids for the years 1979-2001 and NCDC stations (dashed purple). Purple bars represent the number of stations found during the considered months per subregion (CRU3.2, NCDC). H-diff illustrates height differences in m between station/station grid and CCLM/reanalyses.

a cold bias which is also presented by NCEP-R1 whereas this feature is not present in ERA40.

Fig. 6.6 depicts the bias in mean monthly sums of precipitation derived from both hindcasts, reanalyses and GPCC6 grid boxes. Each panel refers to one subregion starting with the arctic regions down to south-west. Except for AW, in all considered subregions NCEP-R1 reveal a strong wet bias during the summer months. In MW and ME, the NCEP-R1 bias exceeds 60 and 65 mm in July. In contrast, CCLM-NCEP1 does not follow its forcing and presents rather a fairly small overestimation compared to GPCC6 during July except for the western subregions with a large dry bias in MW. In general, CCLM produce an overestimation for most of the subregions throughout the annual cycle - most pronounced

Figure 6.6: Same as Fig. 6.5 but for precipitation sums [mm] in comparison to GPCC6 and NCDC station data.

during April in MW and MM up to 45 mm.

6.3.5 Changes of seasonal Temperature and Precipitation

To evaluate whether reconstructed seasonal trend patterns in terms of 2 m air temperature and precipitation are in good agreement with recent observed changes, CCLM-NCEP1 is compared against derived temperature trends of grid boxes from CRU3.2 (Fig. 6.7) and precipitation trends of GPCC6 (Fig. 6.8) in which in situ observations were incorporated. In general, CRU3.2 shows strong spatial variability in seasonal changes of 2 m air temperature over the years of 1981-2010 which is reproduced well by CCLM.

During wintertime, a cooling with maximum values of approximately 1.5 to 2°C per decade over western terrestrial areas is presented both in CRU and CCLM. However, the temperature decrease is less pronounced in CRU southwest in Mongolia and at the Central

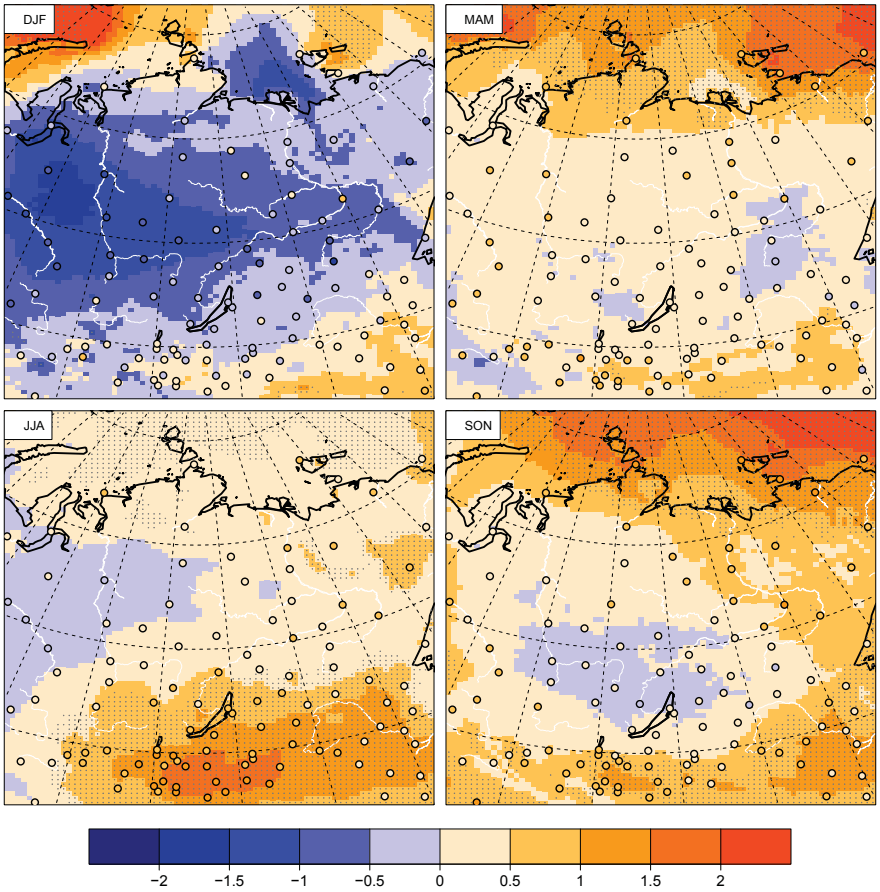

Figure 6.7: Seasonal trend patterns of 2m air temperature [°C/decade] of 1981-2010 for CCLM-NCEP1 and CRU3.2 grid boxes (colored dots). Significant trends of CCLM-NCEP1 at the 95% level are indicated by gray dots.

Siberian Plateau. The illustrated cooling is consistent with decreasing trends obtained by Cohen et al. (2012) for 1988-2010, that an analysis based on gridded CRU data at 5° spatial resolution. Therefore, over Siberia no regional-detailed patterns could be derived.

During spring, the overall trend is a slight temperature increase over land, which is stronger north of 70°N and over the Kara, Laptev and East Siberian Sea. These general patterns are presented both in CRU and CCLM, whereas CCLM illustrates some slight cooling as e.g. west of Lake Baikal which is not in concordance with CRU. At western Siberian Lowland and along the northern Lena river basin, CRU3.2 presents a stronger increase up to 1 °C decade^{-1} than what is illustrated by CCLM. During summer, both datasets show a negative trend along the Western Siberian Lowland and a statistically significant positive trend over Kara, Laptev and East Siberian Sea and south of 55°N. Statistically significant increases are strongest in southern regions ranging up to 1.5°C decade^{-1} in CRU3.2 and 2°C decade^{-1} in CCLM south of Lake Baikal in Mongolia and the Northeast of China. According to Tang and Leng (2012), the pronounced positive trend (1982-2009) over these regions was associated with a decrease in cloud cover and precipitation which

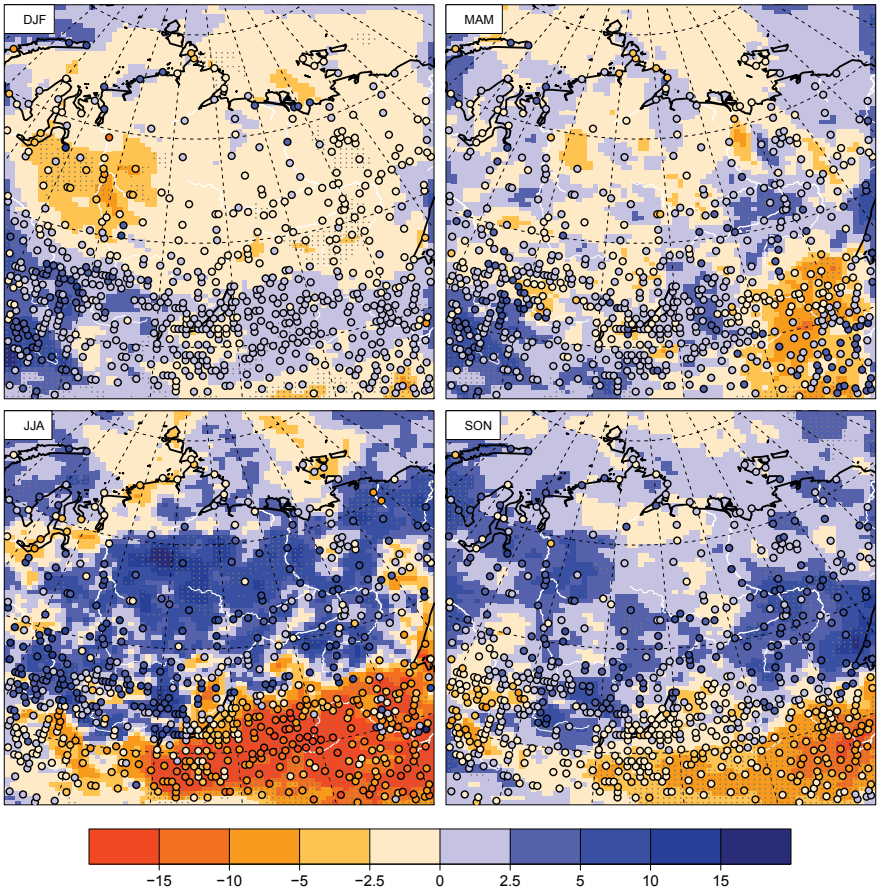

Figure 6.8: Seasonal trend patterns of total precipitation [mm/decade] of 1981-2010 for CCLM-NCEP1 and GPCC6 grid boxes (colored dots). Significant trends of CCLM-NCEP1 at the 95 % level are indicated by gray dots.

is consistent with the results for precipitation shown in the following Fig. 6.8. A reduced cloud cover lead to increases in the surface shortwave radiation. Ye and Fetzer (2010) reported decreases in total water vapor with increasing air temperature during summer across southern Eurasia, which is somewhat distinct from the water vapor temperature relation over colder regions.

Strongest temperature increases during fall occur again along the southern parts over Mongolia and Northeast of China but are less pronounced than during summer and over the Arctic Ocean of the Kara, Laptev and East Siberian Sea ranging up to 4°C decade^{-1} in CCLM. North and northwest of Lake Baikal a slight negative trend is presented by CCLM which is less spatially distributed in CRU and not statistically significant.

Winter precipitation trends are characterized by slight decreases north of 60°N and increases south of 60°N, both in GPCC6 and CCLM as illustrated in Fig. 6.8. The magnitude of trends is a bit higher in the western parts of the domain ranging -10 mm decade^{-1} along the western border of Central Siberian Plateau and +10 mm decade^{-1} in southwestern parts. During spring the trend patterns are not very strong, showing a strong inter-

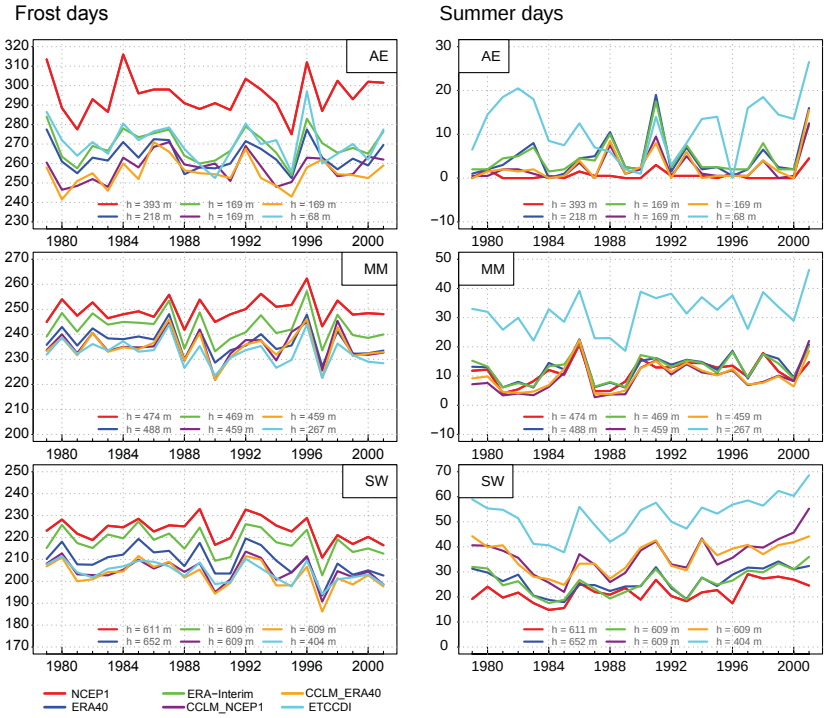

Figure 6.9: Time series of Frostdays and Summerdays compared to ETCCDMI stations for the period of 1979-2001.

regional variability of slight increases and decrease in CCLM. In the southeastern domain CCLM shows a more pronounced increase up to 10 mm decade^{-1} whereas in GPCC6 still a negative trend is predominant except of some stations. During summer both in CCLM and GPCC6 a strong precipitation increase is evident over land except for southeastern parts of the domain with a strong precipitation decrease. In fall, a precipitation decrease remains in the southeastern domain but less pronounced than during summer. Most of northern parts show a positive trend. A slight increase of precipitation is also illustrated over the Kara, Laptev and East Siberian Sea.

6.3.6 Variability of Temperature and Precipitation extremes

To investigate the ability of CCLM to capture threshold-based extreme values, the regional model output and all considered reanalyses are compared against the station-based extreme indices dataset provided by ETCCDMI for the period of 1979-2001. Fig. 6.9 presents time series of yearly frost days of CCLM and the driving data NCEP-R1 as well as ERA40 and ERA-Interim against the station based derived indices of ETCCDMI for three selected subregions (AE, MM and SW).

The decreasing number of frost days from north to south of the region indicates the temperature gradient from the arctic to temperate latitudes. NCEP-R1 shows more frost days than ERA-Interim, ERA40 and CCLM in all subregions. The year-to-year variability compared to ETCCDMI is well represented by CCLM-NCEP1 for the subregion MM and

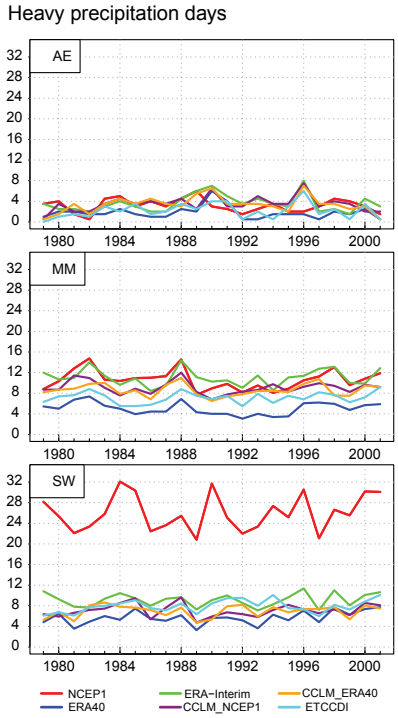

Figure 6.10: Time series of heavy precipitation days > 10mm compared to ETCCDI stations over the period of 1979-2001.

SW. Better representation of orographic detail might lead to this agreement, especially in the region of SW. NCEP-R1 strongly overestimates frost days in AE, MM and SW. This is consistent with a strong cold bias of NCEP-R1 for minimal air temperature from spring to fall season (not shown here) when compared to CRU3.2 and NCDC station data.

In terms of summer days, all considered gridded data sets show less summer days than derived by ETCCDMI, especially pronounced in MM and SW. Whereas in MM all gridded datasets are close together throughout the years, in SW both CCLM hindcasts are closer to yearly values of the station-based summer days. One reason might again be the finer resolved orography in CCLM.

Heavy precipitation days > 10 mm occur in general more often in central and southern regions than in the arctic region (Fig. 6.10). All gridded datasets present a similar number of days for MM and AE wheres NCEP-R1 strongly overestimates heavy precipitation days in SW.

6.4 Conclusion

The performance of both CCLM hindcasts (CCLM-NCEP1 and CCLM-ERA40) was evaluated in terms of spatial patterns of mean seasonal MSLP and vertical temperature profile in comparison to reanalyses. The bias of mean annual cycle of 2 m air temperature and precipitation averaged over six subregion was assessed against station data. On the one

hand, those grid boxes of the quality-controlled CRU3.2 and GPCC6 were selected that received station data, and on the other hand, daily station data provided by NCDC was used to provide an alternative comparison and highlight the observational uncertainty. Moreover, mean seasonal distribution and trend patterns of 2 m air temperature and precipitation of CCLM-NCEP1 and CRU3.2/GPCC6 were compared to analyze the ability in reproducing recent changes for the period 1981-2010. Furthermore, some threshold-based climate extreme indices were compared for three subregions against the ETCCDMI dataset.

In general, it is not unexpectedly, that large-scale atmospheric patterns as e.g. MSLP of CCLM are similar to reanalyses, as the RCM uses this information for initial and boundary conditions. Differences in the temperature magnitudes between the gridded data of CCLM, reanalyses and station data must be judged against the background of different heights between model orography and elevation of the station, of grid to station comparison with varying spatial resolution that cannot account for local effects and for discrepancies even in the observational reference data.

However, the general distribution of seasonal temperature and precipitation are well reproduced by CCLM. Compared to CRU3.2, CCLM shows good agreement in seasonal temperature fields with less discrepancies during summer and spring but regional differences in winter and fall. Strong overestimation is still evident in AE (range from 2.6 to 6 K in January compared to CRU3.2 and NCDC) and ME (approximately 4 K) during winter. Throughout all seasons, CCLM tend to overestimate precipitation in many parts along the coast. A pronounced overestimation is further illustrated in the southern and northeastern regions in DJF, MAM and SON whereas during summer an underestimation is evident in the southern and western parts of the model domain.

In general, CRU3.2 shows strong spatial variability in seasonal changes of 2m air temperature over the years of 1981-2010 which is well reproduced by CCLM. The pattern of strong winter cooling is depicted by CCLM but with a slight more eastward extension than presented by CRU3.2. Increasing temperature patterns south and southeast of Lake Baikal during summer and fall are reproduced by CCLM, however a bit more pronounced than CRU3.2.

7 Large-scale Added Value Assessment of Snow Water Equivalent

7.1 Introduction

The additional information leading toward a more realistic description of regional climate compared to the global driving data is called "added value" within the regional climate modelling community. Added value studies are crucial in the evaluation of dynamical downscaling techniques and assessment of relative skill of RCMs compared to their forcing data (Di Luca et al., 2012). An analysis must be undertaken to decide whether the additional computational effort of RCM simulation is justified. The higher resolution does not automatically result in more realistic detail because many variables are spatially quite homogeneous and are already well described in coarser reanalyses (Prömmel et al., 2010). Thus, there is no added value of RCMs per se. The value of RCMs depends on the physical parameterizations, experimental setup, the analyzed variable and location (Feser et al., 2011).

Although a large number of studies have validated the RCM output and have demonstrated that RCMs can realistically simulate climate compared to observations (e.g., Früh et al., 2010), mostly they have not explicitly shown whether the capabilities of the RCM exceed those of global forcing data (Prömmel et al., 2010). At present, there are only a few added value assessments of RCMs. These assessments primarily concentrate on temperature, precipitation, sea level pressure, wind or mesoscale atmospheric circulation systems. More realistic detail compared to driving reanalyses was achieved on regional scales, e.g., in cases of temperature with complex orography (Prömmel et al., 2010), orographical induced wind systems (Winterfeldt et al., 2010) or North Atlantic polar lows and East Asian typhoons (Feser and von Storch, 2008; Zahn and von Storch, 2008).

This study analyzes the added value of a regional climate model hindcast with respect to snow water equivalent (SWE) for Siberia relative to the SWE estimate from the forcing NCEP-R1. In addition, this study examines the discrepancies of simulated SWE to further reanalyses products (NCEP-R2, NCEP-CFSR, ERA-Interim) which are characterized either by improved model version or by higher resolution compared to NCEP-R1. The objective is to introduce an alternative multi-decadal climatology of SWE over six decades that can be used to investigate long-term changes and trends. Therefore, the widely used reanalysis NCEP-R1 was taken as forcing which is the only reanalysis for downscaling purposes that extends back to 1948.

The question addressed is if CCLM can provide an added value on a large-scale because of its own model physics and finer resolution in space and time compared to the SWE estimate of the forcing. Because there were some issues with the snow information directly from NCEP-R1 that were partly related to an erroneous snow cover analysis (Kanamitsu et al.,

2002), the hindcast quality is also assessed relative to a set of further global reanalyses products (NCEP-R2, NCEP-CFSR and ERA-Interim) – even though they are not directly used as driving fields.

7.2 Data

7.2.1 Reanalyses

The general method of performing an added-value study is to assess the relative skill of RCM output against the considered parameter (the SWE, in this study) of the driving global reanalysis – here, NCEP-R1 (Kalnay et al., 1996; Kistler et al., 2001). For the inter-comparison period from 1987 to 2010, the SWE hindcast is additionally compared to a set of SWE fields from recent reanalyses, including the following: the updated NCEP/DOE or R2 (Kanamitsu et al., 2002), the newest generation climate forecast system reanalysis (CFSR) (Saha et al., 2010) and ERA-Interim produced by the European Center for Medium-Range Weather Forecasts (ECMWF) (Dee et al., 2011).

NCEP-R1

NCEP-R1 is available in a grid spacing of $1.875° \times 1.875°$ ($\sim 210\,\mathrm{km}$) and 6-hourly SWE is provided on T62 Gaussian grid (Kalnay et al., 1996; Kistler et al., 2001). Snow cover is based only on a weekly Northern Hemisphere snow cover analysis without snow depth. Therefore, maximum snow depth was set to 100 mm in an empirical formulation (liquid water equivalent) and no prediction of the snow accumulation by the model was used. Further errors in the snow cover analysis have been detected, such as the usage of the 1973 data for the period 1974-1994, an incorrect snowmelt term that led to an overestimation of the conversion of snow to water by a factor of 1000, and an erroneous moisture diffusion leading to incorrect snowfall in winter over valleys in high latitudes ('spectral snow' problem) (Kistler et al., 2001). Here the SWE data of NCEP-R1 are used for comparison, in spite of the aforementioned problems, to highlight the ability to add realistic detail to the global reanalysis via the technique of dynamical downscaling of atmospheric forcing fields using CCLM.

NCEP-DOE/ NCEP-R2

The errors discussed above in the NCEP-R1 were eliminated in the updated version of the NCEP-DOE or R2 reanalysis, covering the time period from 1979 to the present. Additionally, different snow budget diagnostics were introduced (Kanamitsu et al., 2002). The procedure to compute snow depth was handled differently than in R1. In the case of correspondence with snow cover observations (weekly Northern Hemisphere analyses of snow cover using satellite imagery), the snow depth of the model was used. Otherwise, the modeled snow depth was adjusted to the analysis. In that case, the snow was either

deleted or added by applying the same empirical formulation as in R1. Using this scheme has the advantage of accumulating deep snowpacks (Kanamitsu et al., 2002).

CFSR

The climate forecast system reanalysis (CFSR) is available from 1979 to 2010 (Saha et al., 2010). This latest reanalysis of NCEP offer a coupled atmosphere-ocean-land surface-sea ice system with a spatial resolution of ($\sim$38 km) (T382) and 64 vertical levels for the atmosphere. Additional new features include the assimilation of satellite radiances and the integration of observed greenhouse gases, aerosols and solar variations. To produce daily analyses of snow depth over land, data from the Air Force Weather Agency's SNODEP model (Kopp and Kiess, 1996) and the NESDIS Interactive Multisensor Snow and Ice Mapping System (IMS) (Helfrich et al., 2007) were used. Since February 1997, both analyses of SNODEP and IMS were used in combination for the Northern Hemisphere.

ERA-Interim

The ERA-Interim reanalysis is the latest version of the ECMWF forecast system that is available for 1979-2010 in spatial resolution of ($\sim$80 km) (T255) (Dee et al., 2011). It includes improvements such as a 4-D variational assimilation system, variational bias correction of satellite radiances, new humidity analysis and improved model physics compared to the former ERA40 reanalysis (Dee et al., 2011). These changes are expected to provide a better quality and more homogeneous analysis than that of the ERA40 reanalysis. Certain problems were documented with respect to the analyzed snow and data processing. Errors occurred in the Cressman-based interpolation scheme inducing snow-free patterns in periods in which only sparse observations were available. Since July 2003, the ERA-Interim snow analysis has been constrained with the satellite-derived NOAA/NESDIS daily IMS snow-cover dataset for the Northern Hemisphere. Shortcomings in the pre-processing of this dataset were addressed that led to mistaken locations of the data itself. Furthermore, issues with the used land-sea mask were mentioned. Dee et al. (2011) posited that this problem has caused errors in the snow analysis from July 2003 to February 2010.

7.2.2 Reference data

ESA GlobSnow

ESA GlobSnow is used for assessing the skill and added value of CCLM relative to global reanalyses for Siberia because of its more sophisticated approach to retrieve SWE from passive microwave satellite data than given in standalone algorithms. An important point in selecting this product was the availability of an uncertainty estimate and the advantage of it being a gridded dataset for the entire Northern Hemisphere compared to single point station measurements.

The brightness temperature derived from different channels of passive microwave sensors on satellites makes it possible to provide daily information on SWE, snow depth and snow mass of full spatial coverage under dry snow conditions beginning in 1978 (Derksen et al., 2012; Foster et al., 2005; Pulliainen, 2006). The SWE retrievals obtained by the space-borne passive microwave radiometer has the advantage of continuous wide swath, all-weather monitoring capabilities and being insensitive to cloud cover (Brown et al., 2010; Foster et al., 2005; Derksen et al., 2012).

However, standalone passive microwave SWE retrieval algorithms are highly uncertain, which limits the use of these datasets for model validation (Clifford, 2010; Takala et al., 2011). Certain snow properties affect microwave emission and scatter and make the extraction of SWE information difficult. For example, wet snow leads to increased microwave brightness temperature, whereas increases in snow grain size decrease the brightness temperature independent of any change in SWE. Additionally, vegetation cover, such as densely forested areas (e.g., the boreal forest in Siberia), can impact the accuracy of the SWE estimates and lead to underestimations (Foster et al., 2005). A common problem occurs with deep snow. The SWE retrievals tend to systematically underestimate the snowpack because of the changes in its microwave behavior (Foster et al., 2005; Pulliainen, 2006; Takala et al., 2011).

To overcome these problems, the GlobSnow consortium has introduced a new dataset of SWE that is based on an assimilation scheme that uses passive satellite microwave radiometer data and in situ measurements of snow depth (Pulliainen, 2006) in combination with a time-series melt-detection algorithm (Takala et al., 2009). The combination of these two algorithms yields information about SWE and of the extent of snow cover. The passive microwave data includes radiometer information of SSMR for 1979-1987, SSM/I for 1987-2002 and AMSR-E for the period 2003-2009. Additional station data of snow depth collected by ECMWF from national observing networks were used. The Helsinki University of Technology (HUT) semi-empirical snow emission model was used to interpret the passive microwave radiometer data and to calculate the SWE estimates. A detailed description of these methods was published by Takala et al. (2011).

SWE estimates together with the accuracy estimate and the information of snow extent were produced with a resolution of 25×25 km grid cells in a Lambert's equal-area azimuthal projection for the Northern Hemisphere land surface. Mountainous regions were masked out because of poor algorithm performance in regions with strong orographic complexity (Takala et al., 2011).

A validation study of the GlobSnow SWE retrievals was performed for the years 1980-2010 (Takala et al., 2011). The SWE estimates were compared for Eurasia against INTAS-SCCONE snow course measurements (Kitaev et al., 2002). This study demonstrated RMSE values of 30 to 40 mm for SWE values below 150 mm. The uncertainty of SWE es-

timates increased RMSEs up to 45 mm for Eurasia when the complete dataset was assessed. Takala et al. (2011) also compared the performance of the SWE assimilation technique against the SWE retrievals of NSIDC global monthly SWE climatology (Armstrong et al., 2007), which are obtained by a standalone passive microwave algorithm. They found a clear improvement in RMSE and bias error. In their study, they acknowledge that further improvement is needed to better account for land cover and forest properties and the effect of lakes.

FSUHSS Data

To cross-check whether the results are valid using reference data other than that of GlobSnow, the SWE estimate of CCLM is compared with in situ observations of SWE provided by Former Soviet Union Hydrological Snow Surveys (FSUHSS) (Krenke, 2004). This dataset provides SWE measurements over a snow course transect near World Meteorological Organization stations. The observations are available from 1966-1996, were taken 3 times per month and represent an average of 20 measuring points. However, the station-based comparison is restricted to single point measurements being sparse (particularly, in the northern parts of the model domain), snow measurements suffer from uncertainties as well, e.g., because of wind-induced redistribution. Additionally, the results can be affected by the grid box versus station comparison; one grid box represents a mean area of $\sim 2500\,\mathrm{km}^2$.

7.3 Methods

To assure reasonable comparison with model data, the daily L3A-product (v1.2) is used as one of the available products with no postprocessing applied (e.g., a 7-day sliding time window aggregation). This daily product of GlobSnow has the disadvantage that it contains several missing days, and in certain months, e.g., May, June and September, data availability is reduced to single days because the assimilation algorithm was not able to produce good SWE output. The reasons for erroneous retrievals include missing data of weather stations or unusable satellite data. Particularly in late spring and early autumn, problems with SWE retrieval occur because of difficulties in using radiometer data when a thin snow layer or wet snow is predominant.

Therefore, no standard seasons are considered; the analysis is restricted to single months. January and April are chosen as representative months of snow accumulation and the beginning of the melting period for the southern regions in which sufficient daily data over the long-term period of 1987-2010 is available. Unfortunately, no fall month representing the beginning of snow accumulation can be considered because of a shortage of daily data from GlobSnow over the considered years. Additional missing values occur over mountainous regions and water bodies.

The monthly mean values are calculated from daily SWE data. Missing values that occur in GlobSnow are excluded from all datasets before the monthly mean value of each dataset is calculated. This study uses daily data from 1987 until 2010. 1987 was the year when the Special Sensor Microwave/Imager (SSM/I) began to operate and daily data was available. Using SSM/I ascending and descending data, it is possible with daily data to cover all land areas north of $\sim 20\,^{\circ}$N. The SWE product of GlobSnow also includes the information about the snow cover's extent (SCE) where 0 mm denotes snow-free areas and >0.001 mm means areas with full snow cover (snow extent 100 %). A better choice would be to take a direct SCE dataset (e.g., the NOAA IMS SCE product) instead of using the GlobSnow SWE product to derive the SCE information because of the uncertainties in the wet/dry snow masking. However, as the NOAA IMS SCE dataset is used within the assimilation of ERA-Interim, for example, an independent intercomparison would not be possible.

The spatial distribution of SCE – here the frequency of snow-covered days during April averaged for 1987-2010 after masking all daily datasets according to the relevant criterion is considered first. With this information, it is possible to compare whether similar grid boxes are covered by snow or are snow-free. To obtain a quantitative comparison, the differences in snow cover frequency for all datasets are calculated against GlobSnow. Thus, all datasets are interpolated on the same spatial resolution as CCLM on a geographical grid.

To give an overview of the spatial distribution of SWE in that region, in a second step, spatial patterns of the mean monthly SWE for January and April of GlobSnow are shown, CCLM and ERA-Interim. As it is necessary to account for the underlying uncertainty information of the satellite-derived SWE, spatial monthly mean SWE fields of CCLM, ERA-Interim and reanalyses are not directly compared with GlobSnow. Instead, rather spatial averages were computed for several subregions for SWE and uncertainty estimates and this is compared to the different datasets within the calculated uncertainty range. Regional averaged analysis of SWE data is undertaken by decomposing the model domain into seven subdomains as presented in Fig. 2.1.

The GlobSnow SWE data is originally available in EASE-Grid projection and the SWE of CCLM is interpolated into the geographical coordinate system at 0.44 spatial resolution. The original projection and spatial resolution of reanalyses data are kept and masks are used for selecting single regions. Multi-year monthly means, standard deviation and temporal correlation are calculated for all the months in which more than 20 years of SWE of GlobSnow within the time period 1987-2010 are available. The time series presented here exclude the monthly mean if GlobSnow has more than 3 missing values. The uncertainty range of GlobSnow is calculated as the standard deviation of the accuracy estimates.

There are 2 types of data analyses conducted. On the one hand, the spatial patterns of snow cover frequency for April averaged over 1987-2010 are examined for all considered

datasets. Additionally, we present the spatial distribution of mean monthly SWE for GlobSnow, CCLM and ERA-Interim. On the other hand, we consider area averages of subregions to evaluate the regional variations of all the different datasets for monthly mean, multi-year monthly and multi-year monthly standard deviation of SWE in January and April.

To determine a direct measure of association to GlobSnow, the temporal correlation of monthly mean SWE is calculated using the Kendall rank correlation coefficient. This non-parametric correlation is applied because the monthly mean SWE of January and April does not follow a normal distribution. The statistical significance of the correlation coefficient is defined at the 95 % level. No temporal correlation of monthly mean SWE for April or January among the years is evident from the autocorrelation function of the observed dataset.

To compare in situ observations of SWE given by FSUHSS, we consider 2 subregions of the middle domain where most of the station data is available. Those stations that are within these subregions are selected and the corresponding nearest neighboring grid boxes of CCLM and ERA-Interim are extracted. The other subregions are disregarded due to limited station number. Only days with SWE measurements are extracted from the gridded datasets. Monthly averages are calculated and averaged over all available stations and grid boxes per subregion. The comparison starts 1979, when ERA-Interim begins, and ends with the data availability of FSUHSS in 1996.

7.4 Results and Discussion

7.4.1 Spatial patterns of snow cover frequency

The ability to reproduce the extent of the large-scale distribution of snow extent over Siberian land areas by CCLM and reanalyses is critical with respect to the surface albedo and, therefore, with respect to the amount of energy available to turbulent and radiant energy exchange. The onset and the melting of snow during the transition seasons of fall and spring is of particular concern. With respect to the fall season, the data coverage of GlobSnow was not sufficient throughout the years. Therefore, only the spring period, represented here through April, can be considered. In Fig. 7.1 the absolute frequency of snow covered days of April averaged over 1987-2010 is first illustrated for the whole model domain for GlobSnow. The other panels illustrate absolute differences in the frequency for the single datasets against GlobSnow. In some areas, e.g., the Sayan Mountains in the southwest, the white grid boxes indicate missing values because GlobSnow product does not deliver data that makes the evaluation for these regions impossible with this reference dataset. This is a significant disadvantage for this study because the potential of a RCM providing an added value is expected to be in areas with strong orography.

During April, GlobSnow shows a snow-cover frequency of 90-100 % for more than half of

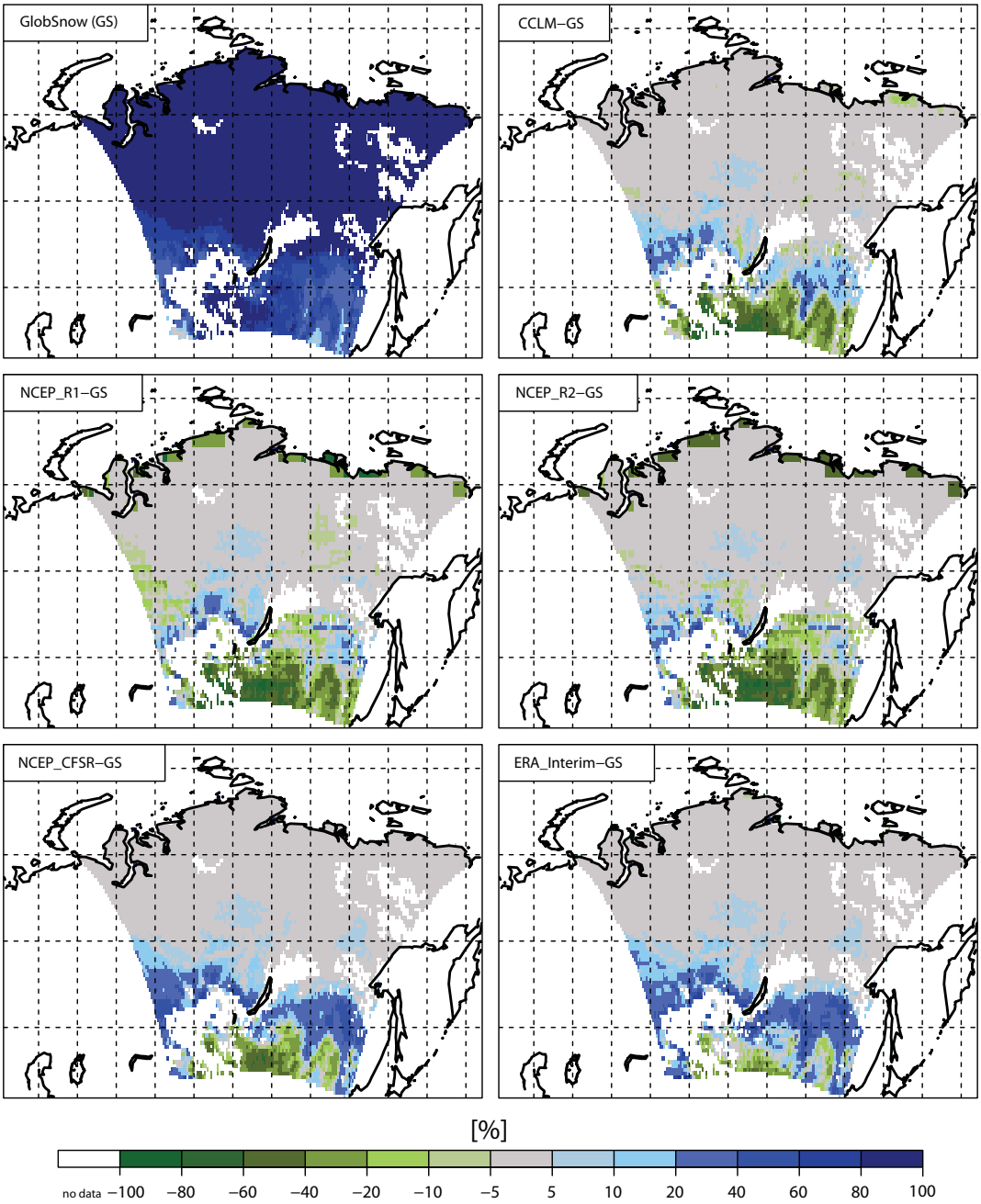

Figure 7.1: Absolute frequency of snow covered days over land points of model CCLM domain during April between 1987–2010 for GlobSnow (upper row left) and differences for the remaining datasets against GlobSnow. White boxes within the model domain indicate missing values given by GlobSnow.

the region down to ∼ 55 °N. West of Lake Baikal, the snow line is located more northward than eastward of the lake. This pattern is similar to the long-term (1966-2003) monthly snow cover frequency of the Northern Hemisphere for April provided by the NSIDC (not shown here) that is derived from the Northern Hemisphere EASE-Grid Weekly Snow Cover and Sea Ice Extent data set (Brodzik and Armstrong, 2013).

Absolute differences in the frequency of snow-covered days of CCLM to GlobSnow indicate that CCLM has up to 10 % more snow-covered days in the central section whereas it underestimates the frequency of snow-covered days by up to 10 % in the northwestern and northeastern parts of the Arctic and subarctic regions. These features are also visible for all the reanalyses when compared to GlobSnow. In general, the spatial pattern of the differences of snow-cover frequency that the CCLM hindcast illustrates is similar to that shown by NCEP-R1. Compared to NCEP-R1 and NCEP-R2, CCLM shows more grid boxes with 20-40 % of days that are additionally snow-covered south of 50 °N. CCLM, NCEP-R1 and NCEP-R2 underestimate the frequency of snow cover in South Siberia particularly in northern parts of Mongolia, south of Lake Baikal. Thus, the snow retreat takes place earlier than presented by GlobSnow.

A special feature of NCEP-R1 and NCEP-R2 becomes obvious for the coastal regions of Siberia in which the frequency of snow cover in April is lower than presented by GlobSnow, and some grid boxes show an underestimation. Here, CCLM can show an added value being in the same range of frequency of snow-covered grid boxes as GlobSnow. NCEP-CFSR and ERA-Interim with higher spatial resolution overestimate the snow cover frequency during April to be more pronounced at approximately 48-55°N. The overestimation in large parts of that region is approximately 20-40 % and even 40-60 %; this indicates that the snow-cover extent persists longer at these latitudes. In the southernmost parts NCEP-CFSR and ERA-Interim show an underestimation but less pronounced than CCLM, NCEP-R1 and NCEP-R2. Here, snow-covered-days are less frequent than in GlobSnow during April, which makes the melting stronger.

7.4.2 Spatial distribution of mean monthly SWE

Fig. 7.2 presents the spatial distribution of mean SWE during 1987-2010 for January and April for GlobSnow, CCLM and ERA-Interim. The uncertainty range of GlobSnow is disregarded, i.e., the SWE fields just serve as a general overview. During January almost the entire domain north of 50°N is covered by snow with more than 25 mm SWE. The highest values occur in the northwestern part of Siberia at up to 200 mm. Even higher values occur in that section during April with a slight northward shift. During April, the southern section with values from 0-25 mm are now more expanded to the north, which indicates the started melting period moving northward. It is evident in the GlobSnow data that the spatial patterns of SWE are very smooth with low spatial detail despite the

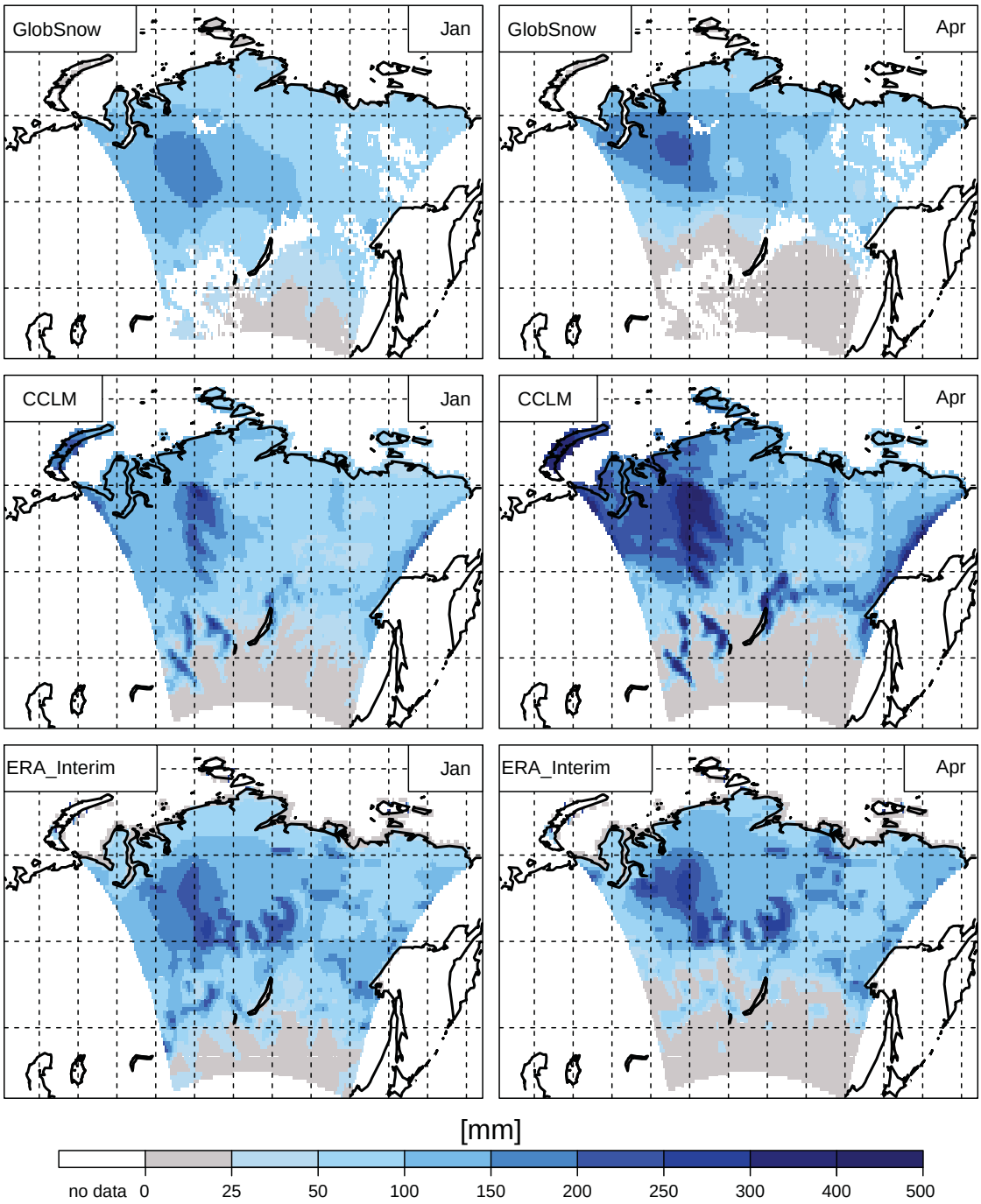

Figure 7.2: Long-term mean of SWE [mm] (1987–2010) of GlobSnow, CCLM and ERA-Interim for January and April. White boxes within the model domain indicate missing values of GlobSnow.

25 km original resolution. Matias Takala, one of the authors of the GlobSnow product, comments (personal communication, April 2013): "Although one underlying reason for the smoothness is the kriging interpolation one has to bear in mind that assimilation algorithm is adaptive and thus other factors also do contribute the final result. In fact it is possible to add more spatial details by giving more weight to satellite interpretation of SWE but we spent a considerable time to adjust the parameters to get the most accurate estimates of SWE. We are in the process of developing next version of GlobSnow product and it will, among other, implement new version of snow emission model, taking into account different land use (taiga and tundra for example) and also take into account variable snow density. I am quite confident that we get some improvement in terms of spatial details too."

By contrast, CCLM is able to add spatial detail. This is evident at the mountain ranges, e.g., at the highest elevation of the Central Siberian Plateau east of West Siberian Plain, the Stanovoy Range northeast of Lake Baikal, and the Verkhoyansk Mountains east of Lena river basin. Here, GlobSnow cannot deliver data because of shortcomings in data retrieval. During January and April, CCLM is able to locate the peaks of SWE as shown by GlobSnow. During January, CCLM mostly underestimates SWE – up to 25 mm with maximum values in the central part of the region. CCLM overestimates SWE in the coastal regions and along the border of Verkhoyansk Mountains. During April, the western part of the domain and Stanovoy Range is mainly characterized by a strong overestimation, compared to GlobSnow. The maximum values of SWE along the Central Siberian Plateau agree well with the maximum SWE pattern given by Bulygina et al. (2011), who analyzed SWE from snow course survey data collected at 958 meteorological stations in Northern Eurasia from 1966 to 2010. This coincides with the results noted by Brown and Mote (2009), who used the SWE climatology derived from the daily global snow depth from the Canadian Meteorological Centre. A more detailed comparison is restricted because of varying analyses and SWE patterns with less regional detail.

Less orographic detail within the SWE patterns is visible e.g., in the Lena river basin in ERA-Interim because of the coarser spatial resolution. During January, ERA-Interim has more pronounced maximum values in the northwest of the domain along the western border of the Central Siberian Plateau than GlobSnow. This peak of snow accumulation in that area coincides with the pattern of SWE climatology (1958-2002) during January for ERA-40 presented by Clifford (2010). In April, the spatial pattern of SWE distribution is in better agreement with GlobSnow than CCLM. During both months, ERA-Interim presents certain features with high SWE values within the model domain that are not given by GlobSnow and CCLM.

CCLM shows higher SWE values in mountainous terrain than ERA-Interim. This might be explained by the effect that precipitation increases with higher resolutions and improved

representation of complex orographical features as shown by Giorgi and Marinucci (1996) for Europe. Kunz and Kottmeier (2006) discussed the overestimation of precipitation with respect to orographic lifting. Also Rojas (2006) found large positive precipitation bias at high altitudes in South America. She suggested that this effect is related to better representation of steeper mountain slopes that influence the divergence of the horizontal wind flow, the vertical velocity, and the precipitation on the upward slope and at the top of the mountains.

7.4.3 Regional characteristics of SWE

To analyze the added value of the SWE hindcast relative to the forcing and the quality compared to more recent reanalyses, spatial averages for several subregions are considered. This makes it possible to analyze all the datasets together with the uncertainty range given by GlobSnow. The long-term means of January and April given by CCLM, GlobSnow and reanalyses averaged over 1987-2010, which represents a characteristic monthly SWE during snow accumulation and melting period are compared. Fig. 7.3a illustrates that all datasets show more SWE than presented by NCEP-R1 for all subregions except the southern domains. No latitudinal variation occurs in NCEP-R1 for January and only marginally in April in the southern regions. GlobSnow (as a reference), show the contrary, i.e., a north-south gradient from Arctic to the southern subregions with less SWE of arctic regions than in the middle domains and decreasing values southward.

In January, the higher values of AW compared to AE (which can be observed in all data sets except NCEP-R1) match with climate conditions during the winter in Siberia. From November to March, Siberia is dominated by the Siberian high pressure system centered southwest of Lake Baikal (Przybylak, 2003). The relatively infrequent eastward propagating cyclones with moist air masses from the Atlantic occur mainly in the northern regions. The decreasing moisture source explains the decline in snow and SWE eastwards of AW and MW. MW presents the highest value of SWE that is evident from GlobSnow, ERA-Interim and CCLM. This region is located in the West Siberian Lowlands in which the Central Siberian Highlands act as barrier and favor orographically induced solid and fluid precipitation. In the direct dataset comparison it is evident that CCLM reproduces SWE well for January compared to GlobSnow, whereas NCEP-R1 is clearly outside the uncertainty range given by GlobSnow, except for SW and SE. The poor performance of NCEP-R1 is related to erroneous snow analysis, which was previously documented by Kanamitsu et al. (2002) and further discussed in the study by Khan et al. (2008). However, this shows the added value of CCLM compared to NCEP-R1 for January and the benefit in using this RCM to generate more realistic SWE than its driving reanalysis provide.

NCEP-R2 is in better agreement with GlobSnow than NCEP-R1, except for SE. ERA-Interim reproduces the regional SWE distribution of satellite-derived SWE but tends to

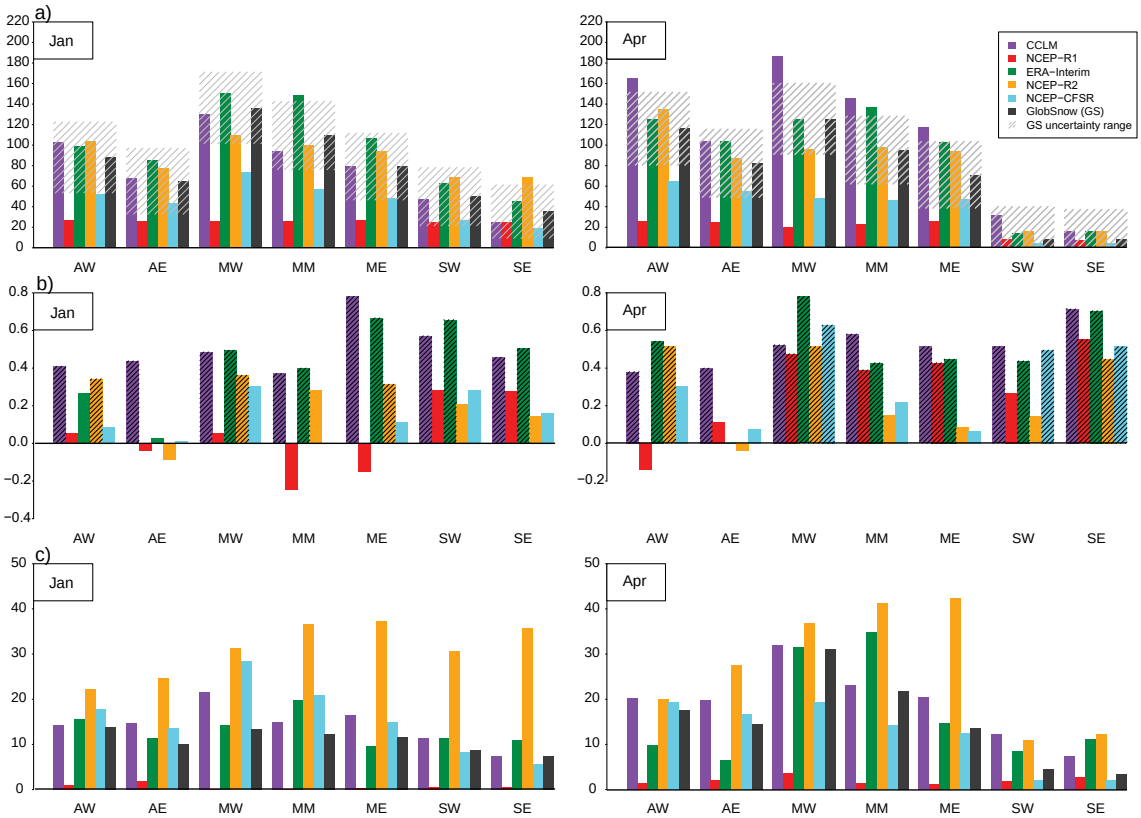

Figure 7.3: **(a)** Regional variations of multi-year (1987–2010) monthly mean of SWE [mm] for January and April for CCLM, NCEP-R1, NCEP-R2, NCEP-CFSR, ERA-Interim and GlobSnow. The gray shades with hachures represent the uncertainty range of GlobSnow; **(b)** temporal correlation of monthly mean of SWE (1987–2010) of each dataset versus GlobSnow, statistical significant coefficients defined at the 95 % level are marked with black hachures; **(c)** multi-year monthly standard deviation of SWE [mm] for 1987–2010. Locations of considered subregions (AW, AE, MW, MM, ME, SW and SE) are presented in Fig. 2.1.

overestimate SWE. The largest discrepancies occur for the Region MM, where ERA-Interim is outside the uncertainty range of GlobSnow. Except for AW, the ERA-Interim is in less agreement with GlobSnow than with the CCLM hindcast. In the subregion SE, SW and AW, NCEP-R2 presents higher SWE than ERA-Interim. This coincides with the results found for the Amur river basins in Khan et al. (2008), in which they compared the SWE of NCEP-R2 with ERA-40. NCEP-CFSR shows the regional variations of SWE but underestimates SWE for all subregions and is even outside the uncertainty range for the middle Siberian regions. Therefore, it can be concluded that CCLM for January provides an even more realistic datset than ERA-Interim and CFSR.

In April, CCLM overestimates SWE in all subregions compared to GlobSnow data. CCLM is even outside the uncertainty range of GlobSnow for the subregions AW, MW, MM and ME, which shows higher values than ERA-Interim. ERA-Interim is clearly in better agreement with the satellite-derived SWE data for AW, MW and SW, although SWE is overestimated as well. This overestimation is particularly pronounced in the regions MM and ME.

The best agreement between NCEP-R2 and ERA-Interim is evident for SE in April whereas the differences were higher in January. This is similar to the study by Khan et al. (2008) comparing NCEP-R2 and ERA-40 for the Amur River basin.

NCEP-R1 shows again almost no regional variations of SWE and is outside the uncertainty range of GlobSnow except that the regions SW and SE are close to the values presented by GlobSnow. In most regions south of the Arctic Circle, the beginning of the snowmelt period is indicated by decreasing SWE values of GlobSnow.

For all subregions, NCEP-R2 is in good agreement with GlobSnow and within the uncertainty range. For the regions MW, MM and ME, almost no variations are evident. Except for NCEP-R1, CFSR has the lowest SWE for all subregions and falls off the uncertainty estimate of GlobSnow for MW, MM and SW. Additionally, only small regional variations are obvious.

The overestimation during melting of the snow pack, which is the case in southern regions, is a common feature of climate models. Various state-of-the-art global climate models overestimate the snow mass of the Northern Hemisphere, particularly in spring (Clifford, 2010; Raeisaenen, 2008; Roesch, 2006). As noted by Roesch (2006), the reasons for the surplus of snow amount and delayed melt in spring might be excessive snowfall rate, temperature biases and poor representation of the snow melt processes. Another reason might be related to the absence of subgrid snow cover heterogeneities that lead to a snow cover that does not gradually abate (Liston, 2004). Deficiencies in the snow melting processes because of missing fractional snow cover leading to overly high albedo and the overestimation of precipitation (not shown here) are reasons that are evident in CCLM.

Even though CCLM produces considerably more SWE for several regions than GlobSnow, an added value can be observed in terms of the regional variations that are more realistically described in CCLM than in NCEP-R1. Nevertheless, it might also highlight shortcomings in snow cover simulations, especially during melting seasons, that must be addressed in future work. However, the overestimation might also be related to the bias for GlobSnow to underestimate SWE under deep snow conditions, as discussed by Takala et al. (2011). This aspect will be investigated in Section 7.4.4 by comparing with FSUHSS ground data.

To determine a measure of association provided for SWE between CCLM, reanalyses and GlobSnow, the temporal correlation of the monthly mean SWE using the Kendall rank correlation coefficient were calculated. Statistically significant coefficients at the 95 % level of confidence are marked with black hachures in Fig. 7.3b. In January for all subregions, CCLM shows significantly high correlations with a maximum of approximately 0.8 in ME. Except for SW and SE, ERA-Interim shows higher correlations than CCLM. We find lower correlations of NCEP-CFSR for all subregions. NCEP-R1 even shows negative correlations of approximately -0.2 in MM.

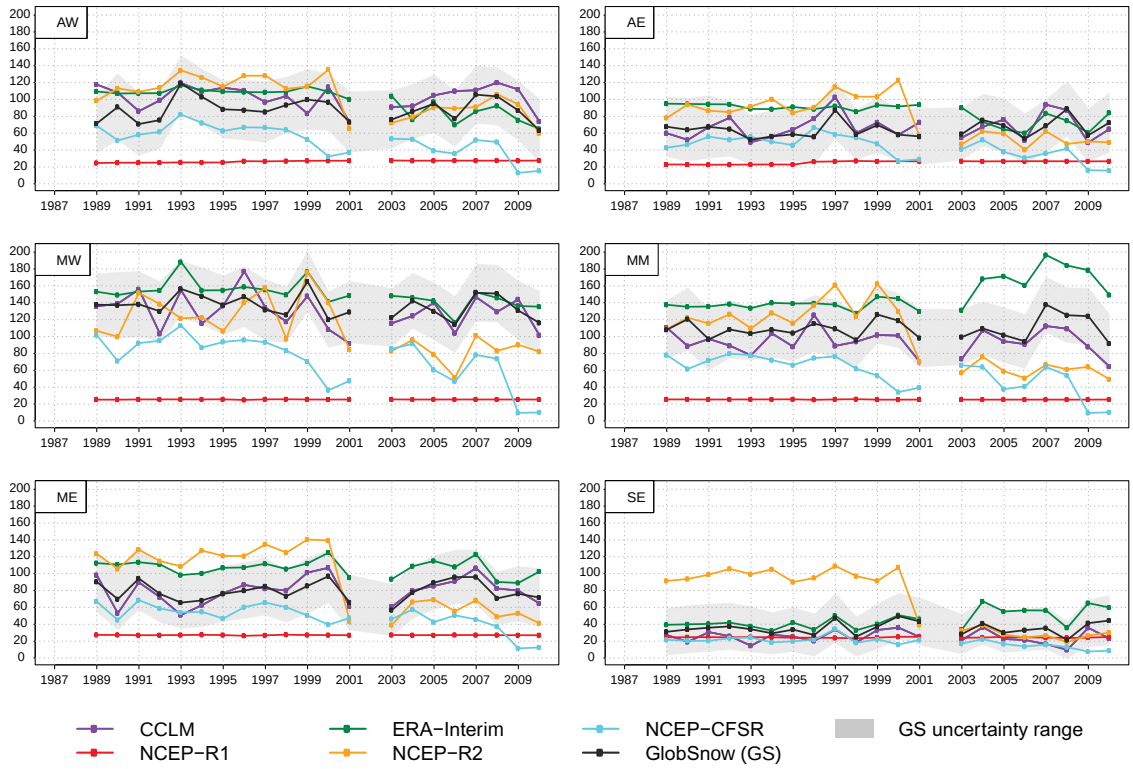

Figure 7.4: Time series of mean January SWE [mm] (1987–2010) for all considered datasets for different subregions. The gray shaded area represents the uncertainty range of GlobSnow. Data gaps occur where GlobSnow provides SWE with more than 3 missing days per month. These months are excluded in all datasets.

In April, CCLM shows statistically significant correlations between 0.3 and 0.7 for all subregions. Except for AW and MW, higher correlations are given by ERA-Interim, NCEP-R2 and CFSR. It is notable that CCLM shows higher rank correlation coefficients than ERA-Interim with GlobSnow because of better agreement in rank orders, although CCLM overestimates the multi-year mean SWE for April for MW, MM, ME, and SW. Despite the low long-term mean, for the April SWE of NCEP-R1 in certain regions, such as MW, ME and SE, there are correlations between 0.4 and almost 0.6.

7.4.4 Interannual variability of SWE

In the previous section, it was evident for the multi-year monthly means that CCLM is in good agreement with the remote-sensing-derived SWE during the cold season but overestimates SWE in April.

To assess the added value of CCLM in terms of interannual variations of these characteristic months, Fig. 7.3c provides the multi-year monthly standard deviation. In NCEP-R1 almost no interannual variations occur for January and April. The deviation of the long-term monthly mean in January is approximately 8-15 mm for GlobSnow. A good agree-

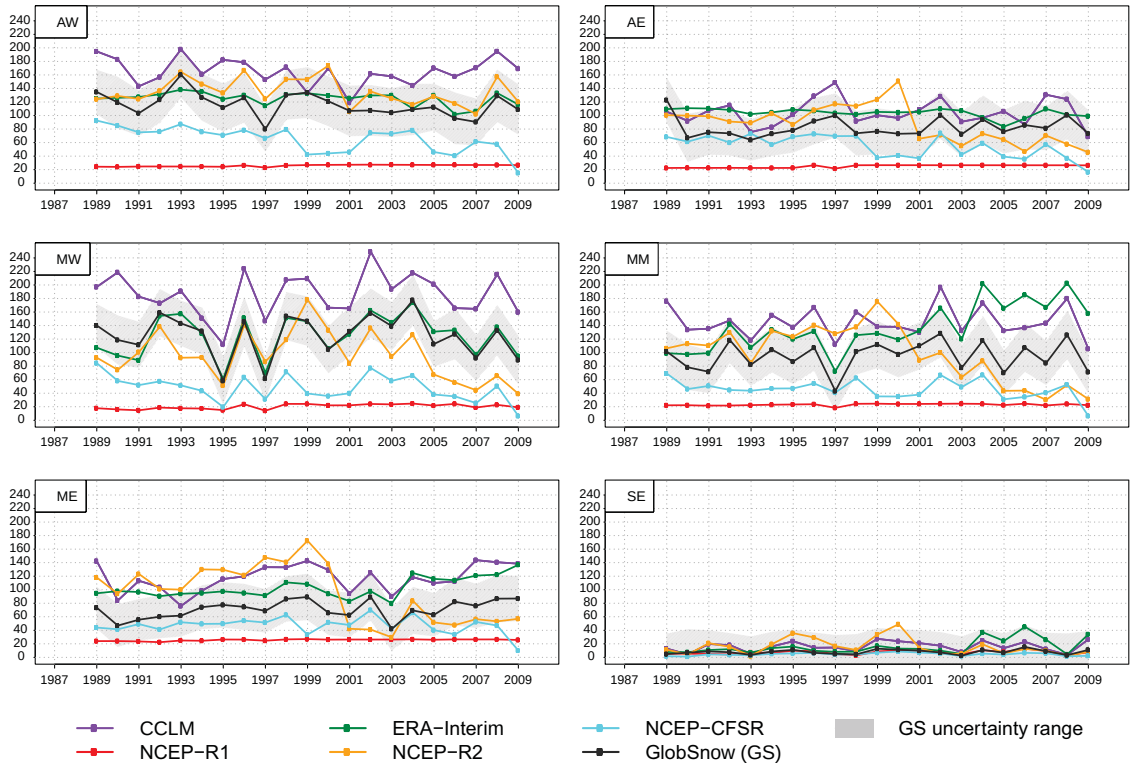

Figure 7.5: As Fig. 7.4. – mean April values are shown.

ment to GlobSnow is given by CCLM which tends to slightly overestimate the standard deviation, particularly for the MW region. CCLM captures the regional characteristics of long-term monthly standard deviation in April well, compared to GlobSnow who has an overall slight overestimation, particularly for AE, ME and SW. In terms of January and April CCLM provides more realistic detail, thus, it provides an added value to NCEP-R1 and a higher quality than NCEP-R2. NCEP-R2 illustrates the highest discrepancy compared to GlobSnow, which is particularly pronounced for ME in April. High standard deviations are also evident for NCEP-CFSR in January for the region MW and in April for ERA-Interim in the region MM.

To explain the long-term monthly standard deviations, Figures 7.4 and 7.5 presents the time series of monthly mean SWE. The high standard deviations in January and April of NCEP-R2 for all subregions are caused by the sudden change of SWE from 1999 or 2000 onwards, with lower SWE in the following years. A pronounced sudden jump is also obvious for ERA-Interim in 2004 for MM, which causes the high standard deviation in that region. Earlier, ERA-Interim reveals a pronounced overestimation and fewer interannual variations than were presented by GlobSnow and CCLM in all regions until 2001. After 2003, ERA-Interim moves closer to the satellite-derived SWE data for the regions AW, AE, and MW regions. The temporal inconsistency is very pronounced in MM and SE. An explanation of this sudden change might be the geolocation errors that have affected the

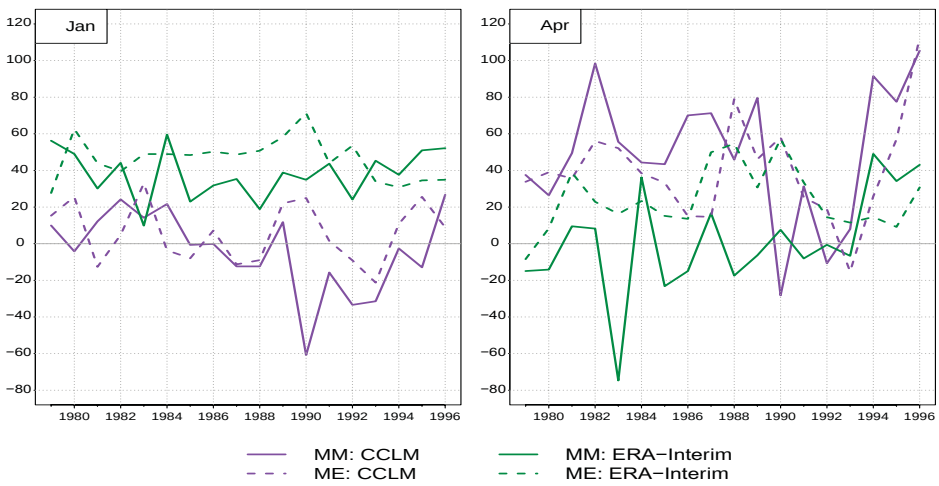

Figure 7.6: Differences of monthly mean SWE [mm] of CCLM and ERA-Interim compared to FSUHSS measurements for the subregions MM and ME for January and April. All available transect data and corresponding grid boxes are averaged over each considered subregion

ERA-Interim snow analyses from July 2003 onwards, as discussed by Dee et al. (2011). Unfortunately, the analysis of Khan et al. (2008) ends in 2000, so that no comparison can be made afterwards. They showed the averaged interannual variability of annual SWE for ERA40 and NCEP-R2 over the Amur river basin. During all the years, NCEP-R2 overestimates SWE, which is a similar feature that is illustrated in our comparison of NCEP-R2 and ERA-Interim for SE.

Deviations also occur in January in NCEP-CFSR in some regions with decreasing values of monthly SWE until the year 2000 and a more pronounced decrease in 2009. In general, NCEP-CFSR provides the lowest SWE throughout the years for January and April in all subregions, except for NCEP-R1.

CCLM tends to overestimate SWE in AW in most of the considered years, whereas, in ME and SE, SWE is underestimated by CCLM compared to GlobSnow. In general, CCLM follows the temporal evolution of SWE within the given uncertainty range of GlobSnow.

High discrepancies are shown by the NCEP-R1 SWE in comparison to all other datasets. Almost no variation occurs throughout all the years, with values of approximately 30 mm per month. Except for the southwest region where the SWE values from GlobSnow show the same range, NCEP-R1 is clearly outside the observed SWE uncertainty range. Because of the erroneous snow processing of NCEP-R1, as discussed in (Kanamitsu et al., 2002), the SWE for the entire considered Siberian region can be regarded as unrealistic. This shows a clear added value of CCLM during the cold season, with GlobSnow as reference data. The approach of dynamical downscaling of NCEP-R1 reanalysis using CCLM can add realistic details in terms of SWE because of its own model physics of 1987-2010 to NCEP-R1. Even compared to ERA-Interim for 2003-2010, NCEP-R2 and NCEP-CFSR CCLM is in

better agreement with GlobSnow. This clear added value cannot be observed in April. By contrast to January, the CCLM-simulated SWE for April shows an overestimation for all considered subregions. In most of the years, CCLM is even outside the uncertainty range of GlobSnow, except for the southeast region. Here, ERA-Interim is in better agreement with GlobSnow, whereas in certain subregions the sudden change in the presented time series is again visible after 2003, which leads to higher SWE values than estimated by GlobSnow. Even though CCLM overestimates SWE, this overestimation is consistent with time; this is by contrast to ERA-Interim and NCEP-R2, which show temporal inconsistencies in their SWE estimates.

As discussed in Section 2.3.1, the SWE estimate of GlobSnow might be problematic during the melting period. To confirm whether the overestimation of CCLM during April is not caused by the potential erroneous estimate of GlobSnow, the SWE hindcast and ERA-Interim was compared with in situ measurements of the FSUHSS dataset. Station data of the 2 subregions MM and ME are considered, as in that part of the region the overestimation of CCLM is pronounced and most of the station data is available. Unfortunately, the datasets end in 1996, i.e., the time series overlap only for 8 years.

Fig. 7.6 presents the differences of monthly mean SWE averaged from all available stations and the corresponding grid boxes selected for the subregions MM and ME for January and April 1979-1996. The number of stations with available data changes over time in MM (between 5 and 19 in January and between 8 and 19 in April) and ME (between 4 and 14 in both months). Throughout the considered time period, ERA-Interim mostly overestimates SWE in January, both in MM and ME, with a maximum in ME for 1990 of 70 mm. For the subregion ME, CCLM varies between an over- or underestimation within the range of -20 to 30 mm but is in general in better agreement with the FSUHSS data than does ERA-Interim. For MM, CCLM is more consistent with the station-derived spatial average than ERA-Interim, except for 1990-1993.

These features are consistent with the time series presented in Fig. 7.4 and 7.5 in which GlobSnow was used as reference data. More notable is that the overestimation of CCLM during April is also visible when FSUHSS transect measurements are used as a reference. Except for 1990-1993 in MM and 1993 in ME, CCLM presents higher SWE with a maximum in 1996 of more than 100 mm. It can be concluded that the overestimation of CCLM is a general feature and not dependent on the reference dataset of GlobSnow.

7.5 Summary and Conclusions

A regional climate model hindcast of CCLM has been obtained over the past 60 decades by means of dynamical downscaling of NCEP-R1. The aim was to provide a better gridded dataset with enhanced spatial resolution and temporal availability than that provided by satellites and global reanalyses in that data-sparse region of Siberia. This study demon-

strates the potential and limitations of the hindcast for the example of SWE as an important parameter in that domain. On the one hand, it contains an assessment of the added value with respect to the SWE estimate given by NCEP-R1 itself and, on the other hand, it provides an intercomparison between the CCLM data and further global reanalyses. The aspects examined in this paper include frequency of snow coverage, spatial distribution of mean monthly SWE, regional characteristics and interannual variability of SWE for January and April. As reference data, we choose a satellite-derived SWE product of ESA GlobSnow to perform the assessments of the regional SWE hindcast area-wide.

In terms of the spatial distribution of the frequency of snow cover during April, CCLM is in good agreement with GlobSnow presenting (particularly in the coastal areas) more days with snow cover than NCEP-R1 and NCEP-R2. The greatest discrepancies to GlobSnow occur at the southernmost extent of snow cover for ERA-Interim and NCEP-CFSR.

Compared to GlobSnow, CCLM indicates a clear added value in representing more realistic information for SWE compared to NCEP-R1, according to the spatial distribution of the considered mean monthly SWE. CCLM provides more spatial detail along the Lena river basin, for example, than GlobSnow and ERA-Interim. During January and April, CCLM captures the location of maximum snow accumulation given by GlobSnow but tends to overestimate SWE during April, mainly along the Central Siberian Plateau. This might be related to the effect of increased precipitation at higher resolutions or delayed melting and intensive snow accumulation because of the overestimation of snowfall rate or poor representation of the snow melting processes. The absence of fractional snow cover within CCLM might also be plausible.

The SWE product of NCEP-R1 does not represent any of the regional and temporal variations of SWE for the considered subregions, except for southern parts. Herein it is demonstrated that it is possible to provide more realistic historical SWE fields for the past 60 years than NCEP-R1 offers, which justifies the computational effort in applying a regional climate model. This added value compared to NCEP-R1 was expected because of erroneous SWE fields of NCEP-R1 that are already well documented. It also shows, however, that the technique of dynamical downscaling of atmospheric forcing fields (e.g., pressure, wind, etc.) provided by NCEP-R1 can be used to derive SWE fields back to 1948 with more realistic information than the reanalysis product itself can present. It is possible because of the model physics of the RCM, e.g., snow parameterization and finer resolved regional features, such as orography and land cover. This is evident for the entire SWE field even for mean values.

Because of the known poor quality of NCEP-R1 data, the output is additionally compared to the SWE fields of newer reanalyses datasets in order to assess the ability to compete with these datasets. The SWE of the regional hindcast is more homogeneous in time than ERA-Interim in presenting a spurious jump in 2003, obvious in certain subregions. A

temporal inconsistency is also evident in NCEP-R2 near 1999-2001, explaining the highest multi-year monthly standard deviation among the considered datasets. The CCLM hindcast of SWE can even compete with the newest generation of NCEP reanalysis (CFSR) at 38 km resolution that underestimates SWE in many subregions. Particularly in periods of snow accumulation, the CCLM hindcast is in better agreement with GlobSnow. However, as clearly shown by the SWE overestimation of CCLM in April (both compared to GlobSnow and to the snow survey measurements of FSUHSS), there is still an obvious model deficiency that must be addressed to justify the RCM application, even in snow-dominated cold regions such as Siberia.

It should be stressed that the results are dependent on the quality of the reference data of ESA GlobSnow. The used GlobSnow product show coarse SWE patterns that were, among others, caused by kriging interpolations methods. The spatial detail might be improved in future products in which, e.g., variable snow density and different land use types are be taken into account (Takala et al., 2011).

Nevertheless, this study shows that the regional CCLM hindcast of SWE can add more realistic information to the global product of NCEP-R1 and provide a better quality in temporal consistency compared to many of the recent reanalyses for the years after 1987. It is important to demonstrate the discrepancies between existing global reanalyses and to propose an alternative climatology of historical SWE. Using atmospheric fields of NCEP-R1, it is possible to derive a regional data set of historical SWE fields over the past decades that are not provided by newer reanalyses. Temporal inconsistencies of NCEP-R1 before 1987 due to changes in the observing systems (e.g. the use of satellite observations since the late 1970s) and their impact on the regional climate model hindcast were assessed in Chapter 5. In general, to assess long-term changes and trends with more spatial detail, a regional multi-decadal data set is necessary for that data-sparse region of Siberia.

8 Recent Changes of Siberian Snow Cover

8.1 Introduction

Amidst the context of amplified long-term temperature increase in northern high-latitudes of Eurasia compared to other regions (Serreze et al., 2009) and observed retreat of arctic sea ice extent (Serreze et al., 2007; Stroeve et al., 2012), contrasting trends in seasonal temperature and also snow cover have occurred in recent years over Siberia (Cohen et al., 2012).

Several studies exist that deal with snow cover changes mostly with respect to snow cover extent in Eurasia using satellite data (Dery and Brown, 2007; Derksen and Brown, 2012) but less studies focus on changes of other snow cover characteristics over Siberia such as snow amount or accumulation (snow depth or SWE), snow cover duration, timing of snow cover (onset and end of snow cover and melt). Results seem to be contrasting at first but discrepancies are related mostly due to their different behavior in change (Groisman and Gutman, 2012).

Whereas snow cover extent over Siberia has declined in spring, it has not decreased considerably during winter (e.g., Bulygina et al., 2011; Derksen and Brown, 2012; Groisman et al., 2006; Groisman and Gutman, 2012). According to Bulygina et al. (2011) who used snow survey data from 1966 to 2010, the duration of snow cover has decreased over west Siberia due to earlier onset of snowmelt (Bulygina et al., 2011). In contrast, maximum snow depth and the number of days with snow depth above 20 cm have increased over many parts in Siberia (Bulygina et al., 2009, 2011). Studies done by Bulygina et al. (2011) showed an overall tendency of increasing or steady maximum SWE during winter season since 1966.

In general, the response of snow amount to atmospheric and surface condition is complex and depends on the spatial and temporal scales with large regional and altitudinal variations (Brown and Mote, 2009; Callaghan et al., 2011; Bulygina et al., 2011). Most studies of accumulated snow amount are based on interpolated snow survey data which are limited by spatial and temporal gaps in the data coverage and are constrained by unevenly distributed in situ snow observations especially in mountainous areas and high latitudes.

To date, temporal dynamics and changes of snow cover over Siberia during the different snow seasons, especially of SWE which is important for water supply, have not been fully explored at regional scale. This section examines spatial and temporal patterns of seasonal SWE across the considered Siberian domain for recent decades together with trends of air temperature and precipitation to provide a regional detailed overview of recent changes and variability. As accumulated snow amount - here shown by SWE - demonstrate a different behavior in terms of interannual variations and change than snow extent (Ge and Gong, 2008; Roesch, 2006), additionally the variability of seasonal snow cover extent

(SCE) is investigated to gain a more precise overview of recent and ongoing changes in that region.

8.2 Data and Methods

In this study, spatio-temporal changes and interannual variability accumulated snow amount, as described by SWE, and of SCE are considered. SCE is derived by applying the threshold > 0.01 mm of SWE. SWE of both hindcast simulations are used when temporal variations are considered. In case recent changes from 1979-2010 are investigated, only the NCEP-R1 driven hindcast is used. As already stated in Chapter 6, before 1979 the hindcast data of CCLM-NCEP1 is uncertain due to temporal inconsistencies that are introduced by the NCEP-R1 reanalysis. In order to consider simulated SWE fields going back further in time, the ERA40-driven hindcast from 1968 to 2001 are additionally used.

Specific snow-related seasons for Siberia within the snow year (from July to June of the current year) defined by Bulygina et al. (2011) and Groisman and Rankova (2001) are assessed. These are fall (October to November), winter (December to March) and spring (April to May). Besides the consideration of spatial distribution of mean seasonal SWE and linear trends of 2 m air temperature and precipitation, regional averaged analysis of these three variables is carried out by the same seven subdomains as used in previous analyses which have already been presented in Fig. 1.

Trends in each season and variable are computed using a linear regression with the least squares method. Statistical significance is tested using the non-parametric Mann-Kendall trend test (Kendall, 1975; Mann, 1945) based on seasonal mean values to reduce autocorrelation. In a first step, the trend patterns of winter mean SWE derived from CCLM-NCEP1 hindcasts are compared to GlobSnow for the period 1987-2010. Afterwards, all three seasons are presented from CCLM-NCEP1 for the years 1981-2010. To examine the temporal variations of seasonal SWE and SCE, the 5 yr running means are calculated and included in the time series.

8.3 Results and Discussion

8.3.1 Spatial distribution of seasonal SWE

Before recent changes in mean seasonal SWE are addressed, long-term seasonal means (1981-2010) of SWE are presented. As snow cover is strongly related to temperature and precipitation, those fields are additionally depicted (Fig. 8.1).

There is a general increases in SWE from fall to winter and spring season north of 60°N as snow continues to accumulate until spring season. As illustrated in Fig. 8.1, mean SWE values during fall range mainly between 10 and 50 mm showing a strong north-south gradient. Snow accumulation increases from midlatitudes to the colder regions with

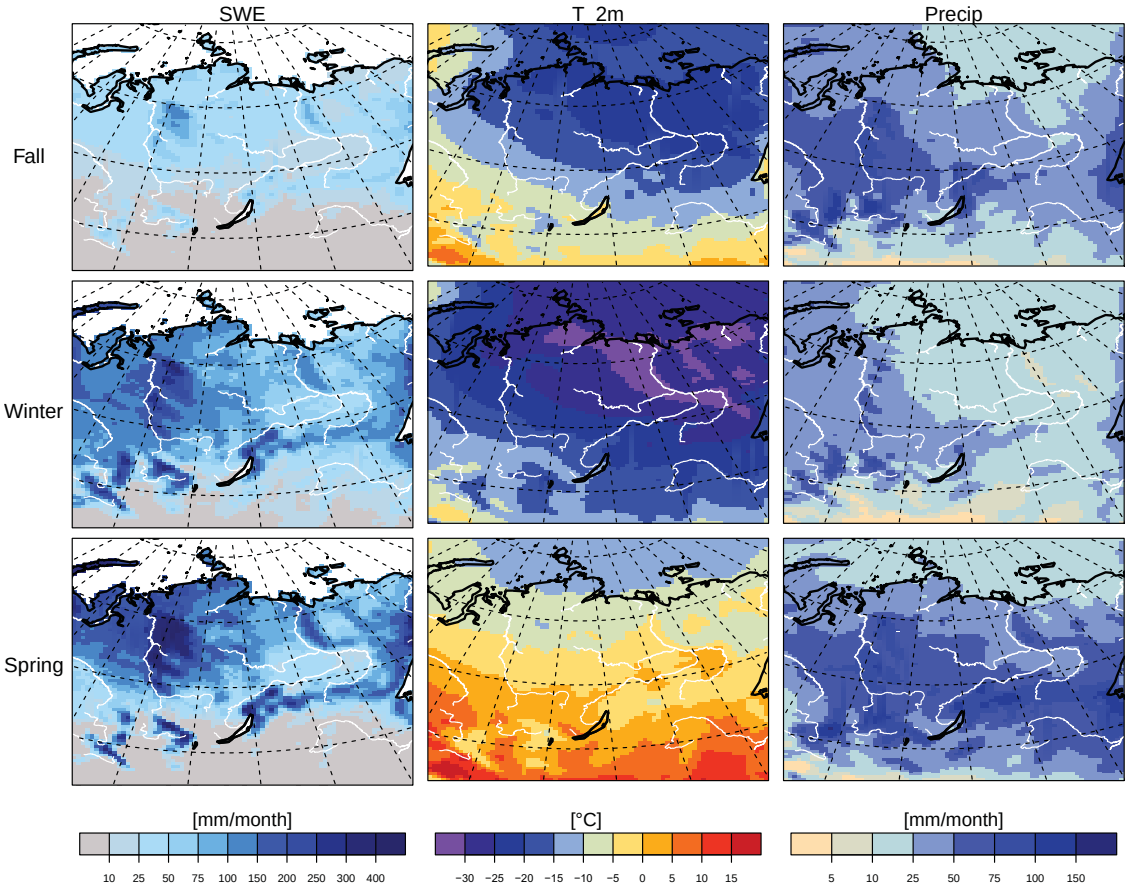

Figure 8.1: Mean seasonal patterns of SWE, 2 m air temperature (T_2m), Precipitation (Precip) averaged over the period 1981-2010 given by CCLM-NCEP1.

up to -30°C during fall of the high-latitudes. Local maxima of SWE, that ranges up to 150 mm, occur along the western border and elevated regions of the Central Siberian Plateau and Verkhoyansk Mountains north of 60°N where precipitation is increased by orographic lifting. During winter and spring season, snow accumulation is strongest in the western regions of Western Siberian Lowland and Central Siberian Plain and again in the elevated regions of Verkhoyansk Mountains, Stanovoy Range, Altai Mountains and along the border to the sea of Okhotsk. The coastal areas and northern lowlands during winter are characterized by low temperatures (minima can reach -35°C) and relatively dry conditions. Accumulated snow cover during winter season is therefore mainly a result of snowfall during fall especially in the eastern part of the region.

The zonal distribution of presented long-term values of mean SWE during winter with strongest accumulation along the Central Siberian Plateau is in agreement to the station-based results over Northern Eurasia for the period of 1966-2010 presented by Bulygina et al. (2011) and Kitaev et al. (2005). Bulygina et al. (2011), considered long-term mean of maximum winter season SWE and Kitaev et al. (2005) mean SWE in February. However, relative coarse spatial patterns of observed SWE have been illustrated due to limitations in

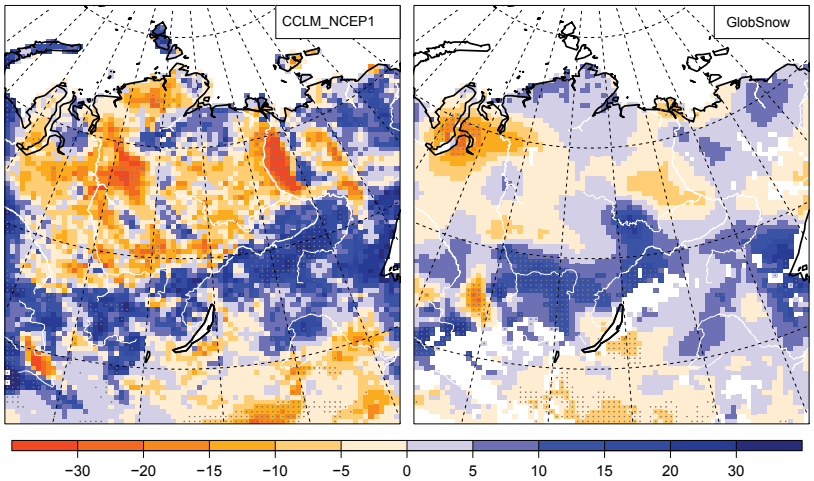

Figure 8.2: SWE trend pattern of winter (DJFM) [mm/decade] averaged over the period 1987-2010 given by CCLM-NCEP1 and GlobSnow. White boxes within the GlobSnow trends indicate missing values.

the coverage of snow survey data, so that a more precise comparison is restricted. Similar patterns were further illustrated by Callaghan et al. (2011) mean annual maximum SWE for 1998-2007 derived from the Canadian Meteorological Center snow depth analysis (Brasnett, 1999). Here, even more spatial detail is presented that show again more accumulation in the high elevations of Verkhoyansk Mountains. The overall decreasing maximum SWE from west to east can be partly related to the decreasing number of cyclones, as shown in Callaghan et al. (2011).

8.3.2 Variability and change of seasonal SWE

To compare the trend patterns from the hindcast and GlobSnow as observational based reference, the linear trend is calculated over the period of 1987 to 2010 in which GlobSnow data is available. GlobSnow provide best data coverage during winter as already discussed in Chapter 7. Consequently, the spatial patterns of GlobSnow are only presented for winter season (Fig. 8.2). Statistical significant trends at a 95% significance level are marked with grey dots. In general, the trend patterns show both in GlobSnow and the CCLM reconstructed SWE fields, a strong spatial variability. However, the magnitude of trends in GlobSnow is lower than in CCLM that partly corresponds to the smoother values already shown in Fig. 7.2. Furthermore, more regional detail is presented in CCLM.

Both datasets show a slight decrease in mean winter SWE in recent years south of Lake Baikal region in Northeast of Mongolia and northern China of 5 mm decade^{-1} that range to 10 mm decade^{-1} and even 20 mm decade^{-1} in the reconstructed data. This negative trend is, for certain grid boxes, statistically significant and does agree with the observed decreases of maximum SWE by Bulygina et al. (2011) for the period 1966-2010. A decrease in SWE is also visible at the eastern side of Central Siberian Plateau and most parts of West

Siberian Plain. Strong significant decreases of SWE during the winter seasons in the recent decades are evident according to CCLM in the most elevated parts at the Central Siberian Plateau and Verkhoyansk Mountains up to 40 mm decade^{-1}, which is less pronounced in GlobSnow.

Snow accumulation has increased strongest, according the presented two datasets, west, northwest and northeast of Lake Baikal and along the coast of Sea of Okhotsk. Along the Sayan Mountains and Stanovoy Range CCLM presents an increase up to 20-30 mm decade^{-1} and even to 40 mm in certain regions. Increases of SWE were also reported in the study by Bulygina et al. (2011). GlobSnow shows a similar pattern of SWE increase but again with a lower magnitude of 20 mm decade^{-1} than CCLM. Further regions that show increasing trends in winter season SWE are located in the Northeastern towards Siberia Far East ranging up to 10 mm decade^{-1} (GlobSnow) and up to 30 mm (CCLM-NCEP1), however these trends are not statistically significant. A more pronounced increase of 5-10 mm in GlobSnow and to 30 mm decade-1 in CCLM is illustrated on the eastside of the Verkhoyansk Mountains. Additionally, in the Northern Siberian Lowlands, CCLM shows a strong increase of mean winter season SWE which is less pronounced in GlobSnow.

Contrasting trends between GlobSnow and CCLM are illustrated e.g. along the northwestern side of Tymyr Peninsula where CCLM presents a decrease in snow accumulation (even statistically significant for certain grid boxes) and GlobSnow a slight increase of 5-10 mm decade^{-1}. Along the Lena river delta, CCLM shows a slight increase whereas SWE has decreased significantly by 5 mm decade^{-1} in GlobSnow. In the southern part of Yamal Peninsula, winter SWE has slightly but significantly decreased in CCLM but has increased a bit further east. In contrary, GlobSnow shows for this domain a decrease with more than 30 mm decade^{-1}. A similar heterogeneous pattern is also obvious in the southeastern part of the domain.

To provide trend patterns over the climatological standard period of 1981-2010 and related variables, trends of SWE, 2 m air temperature and precipitation of all 3 snow seasons provided by CCLM-NCEP1 are considered in Fig. 8.3. Trends of mean SWE for fall are very heterogeneous showing mainly a slight decline or increase of -5 to 5 mm decade^{-1} throughout the entire domain. Local maxima of increases in mean fall SWE occur along e.g. the Central Siberian Plateau, Sayan Mountains and Verkhoyansk Mountains. These regions correspond to regions where precipitation increases are predominant according to CCLM-NCEP1. Besides the presented increasing temperature trend, shown in Fig. 8.3(except in the Lake Baikal region that show a decreasing trend of 0.5°C decade^{-1}), the temperatures are still below 0°C during that season, so that precipitation increase might directly influence snow accumulation.

Trend patterns of SWE during winter over 1981-2010 are similar to the previously presented trend of 1987-2010 even though the magnitude is lower for certain areas. The

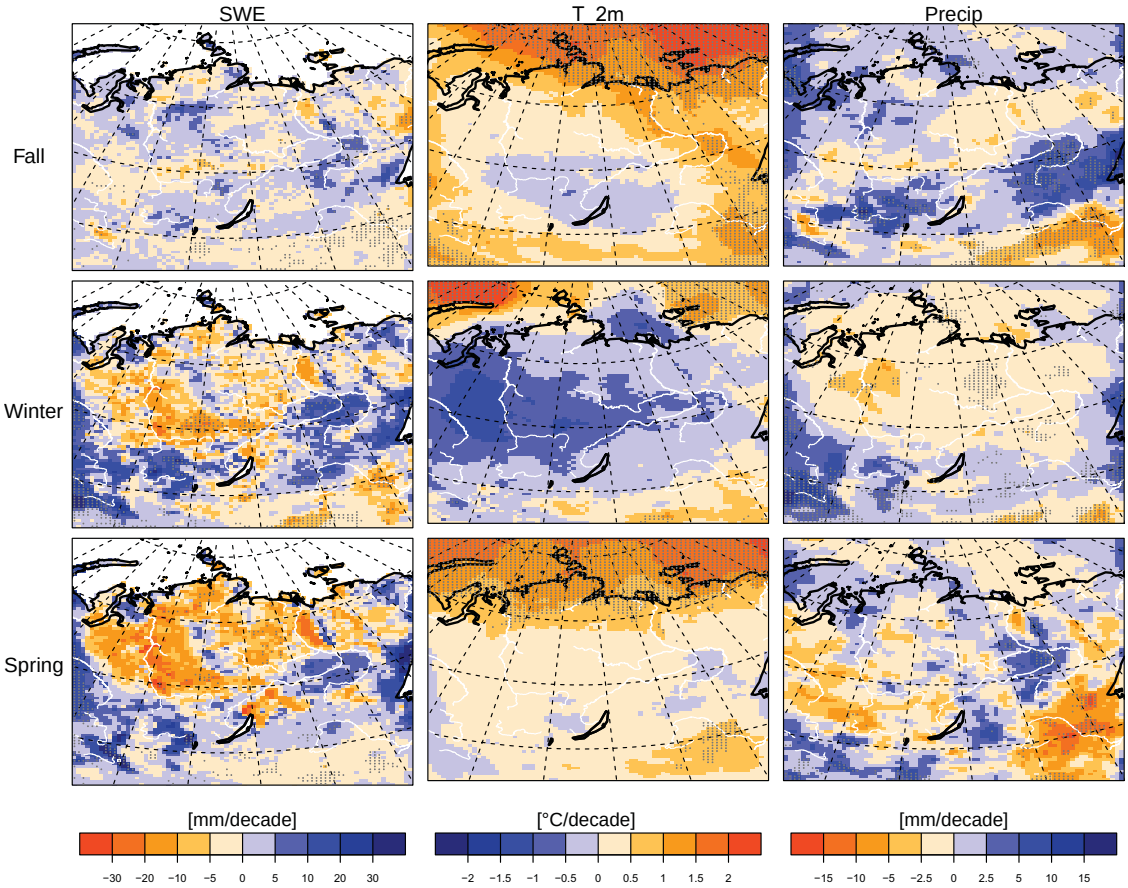

Figure 8.3: Seasonal trend patterns of SWE, T_2m and Precipitation averaged over the period 1981-2010 given by CCLM-NCEP1. Significant trends at the 95% level are indicated by gray dots.

amount of accumulated snow during winter includes snow from fall. This might be the reason of similar trend patterns between winter SWE and precipitation during fall. In general, during winter, temperature has decreased mainly by 0.5°C decade^{-1} and to 1.5°C decade^{-1} in the Western Siberian Lowland. However, these trends are not statistically significant. In contrast, positive temperature trends are obvious in the southeast. Precipitation shows a slight negative trend in the northern parts and slight positive trend along the western, eastern and southern parts of the model domain which are, in parts, statistically significant.

During spring north of 60°N, CCLM-NCEP1 mainly presents a negative trend in SWE except for Stanovoy Range and the lowland between Verkhoyansk and Chersky Range. West of Lake Baikal, mainly an increase of SWE is shown and in the southerneast region a negative trend which is presented in all three seasons. 2 m air temperature shows almost no or only slight increasing trend between 0 and 0.5°C and to 1 or 1.5 °C along the coastal regions and southeastern part. Certain domains present a slight negative trend.

These results obtained for winter mean SWE are in part consistent with the spatial patterns achieved by Bulygina et al. (2011) for maximum SWE. They documented increases

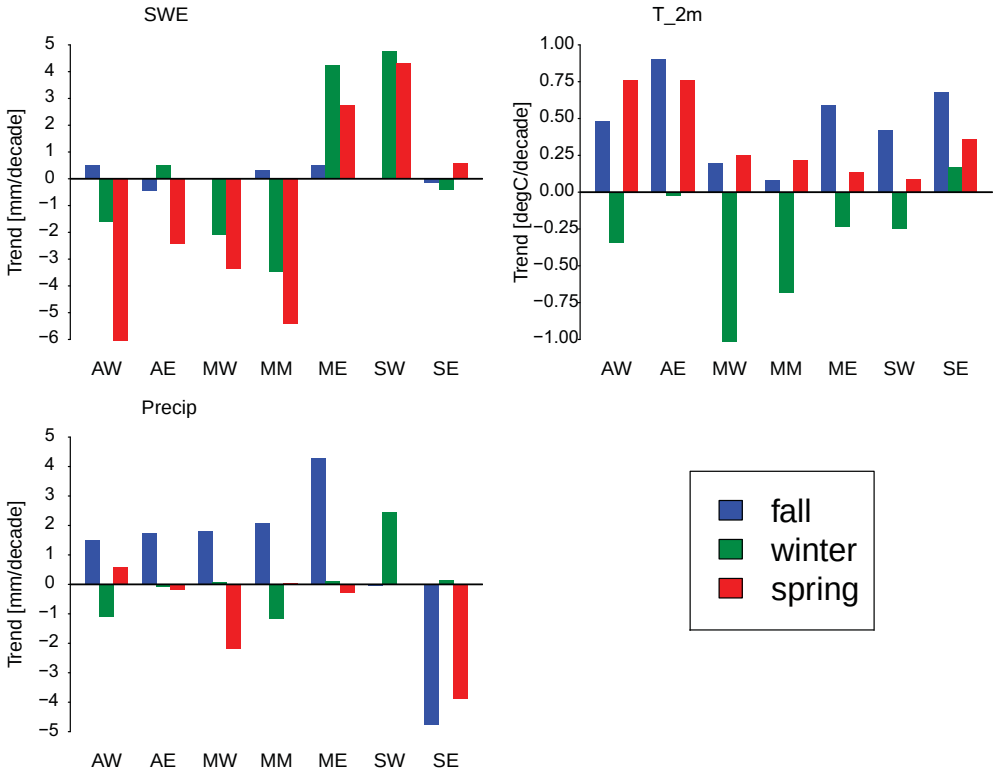

Figure 8.4: SWE, 2 m air temperature (T_2m) and precipitation trends averaged over seven subregions for the period of 1981-2010 derived from CCLM-NCEP1.

in central, northeastern and maritime eastern parts of Siberia, but decreases for the Baikal region and in the Western Siberian Lowland north of 60°N. However, the statistically significant decreases at the Central Siberian Plateau along 60°N are not in agreement with the study by Bulygina et al. (2011) that showed a positive trend for the same region. The reduction of snow accumulation at southeastern region might be due to reduction in solid precipitation that has also been stated by Bulygina et al. (2011) and Shmakin (2010), shown here during fall and less pronounced during winter. In addition, the temperature increase in fall might lead to less snowfall resulting in less accumulated snow during fall, winter and spring. Increased solid precipitation during fall along the northwestern part and along the coastal regions might be partly explained by enhanced water vapor that is available due to summertime sea ice reduction of Arctic Ocean which comes with easterly wind circulation during prevailing Siberian High. Ghatak et al. (2010) suggested a linkage between retreating Arctic sea ice and snow cover due to increasing snowfall as a consequence of enhanced availability of atmospheric moisture in association with rising temperatures (Ghatak et al., 2012). According to Honda et al. (2009), the reduction of summer sea ice might have impacts on the formation of stationary Rossby waves, which strengthen Siberian High and induce cold temperature conditions over Siberia as illustrated here in

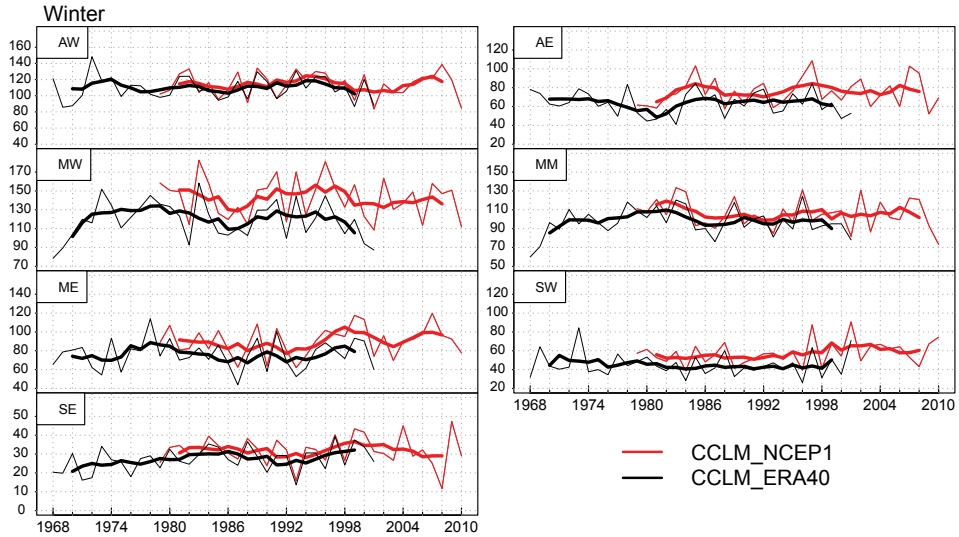

Figure 8.5: Interannual variation and 5 year running mean of SWE [mm] per subregion of both hindcasts for winter.

Fig. 8.3.

Spatial variability of changes in mean seasonal SWE is further determined by orographic features as the Verkhoyansk Mountains which are characterized by a reduction of snow accumulation mainly during winter and spring as well as the elevated parts of the western border of Central Siberian Plateau. In contrast, most of the elevated regions illustrate slight increases in mean SWE during fall season.

To get a general overview of interregional change patterns, trends averaged over single subregions for the period of 1981-2010 from CCLM-NCEP1 are presented in Fig. 8.4. During fall, only minor changes of SWE are evident whereas during winter and spring stronger changes occur. In winter, an increasing trend of mean SWE between 4 and 5 mm decade^{-1} in ME and SW and a slight one of 0.5 mm decade^{-1} in AE is presented. Strongest decreases are illustrated for MM with 3.5 mm decade^{-1}. During spring, SWE has decreased strongest within recent decades in the subregion AW by 6 mm decade^{-1} and MM by 5.5 mm decade^{-1}. An upward trend of SWE during spring is given in ME, SW and SE. The regional averaged trend patterns for 2 m temperature look somewhat different. In all subregions, 2 m air temperature increases are presented in fall and spring whereas a cooling is evident during winter in all subregions except in SE. Strongest temperature decreases are predominant in MW with 1°C decade^{-1}. Regional averages of precipitation present positive trends during fall in all subregions most pronounced in ME by 4.5 mm decade^{-1} except of SW (-5 mm decade^{-1}).

Compared to fall season, stronger increases and decreases of regional averaged trends of SWE are presented during winter and spring. Besides the presented trend patterns that are calculated from CCLM-NCEP1 over the period 1981-2010, by adding the time series of

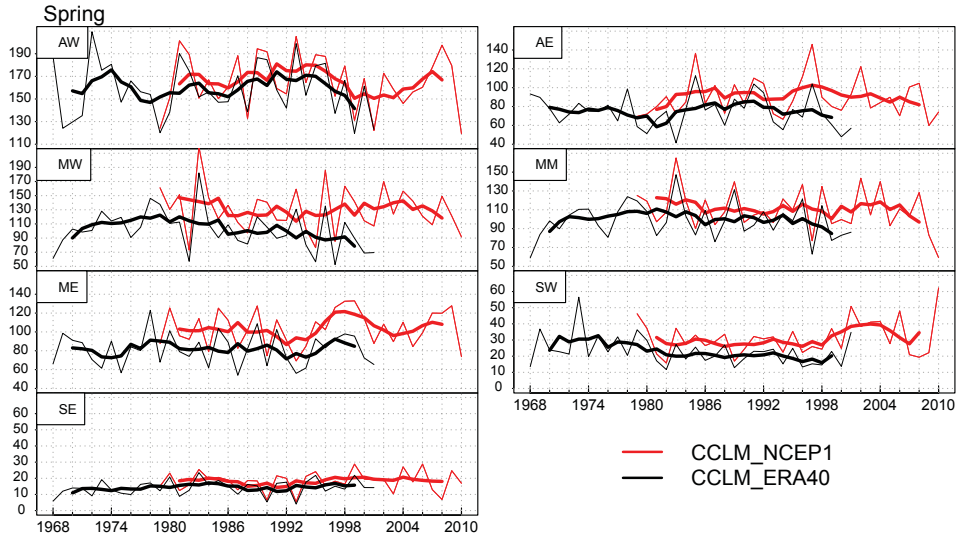

Figure 8.6: Interannual variation and 5 year running mean of SWE [mm] per subregion of both hindcasts for spring.

CCLM-ERA40 for these 2 seasons it is possible to show the variability in different regions going back to 1968 for both reconstructions. Fig. 8.5 describes the interannual variation of mean SWE during winter and Fig. 8.6 during spring for different subregions. Thick lines indicate the 5 year running means.

Both hindcasts show similar year-to-year variability of mean SWE. However, CCLM-NCEP1 presents higher SWE values. A strong year-to-year variability is evident that varies with region and season. Whereas in certain subregions such as e.g. SW, ME and AE, a gradual increase of wintertime snow accumulation occurs, other regions such as e.g. AW and MM vary considerably more showing a negative trend with especially pronounced reduction of SWE in recent years. For SW, ME, AW and MM this pattern is similar in spring season whereas in AE the tendency of decreasing SWE continues since 1997. In general, a strong spatial diversity of trend patterns and variability is obvious.

8.3.3 Temporal variations of seasonal snow cover extent

As mentioned in Section 4.1, the consideration of seasonal SCE is an additional important aspect when changes of snow cover are assessed. Fig. 8.7 shows the interannual variations of snow extent for fall, winter and spring season averaged over the entire model domain. Snow cover extent is derived from both hindcasts simulations. From 1968 to 2001 CCLM-ERA40 is illustrated and from 1979 to 2010 CCLM-NCEP1. Both hindcast simulations demonstrate similar year-to-year variations, whereas the snow cover extent derived by CCLM-NCEP1 is in general larger throughout all seasons.

To illustrate the tendencies of changes of snow cover extent for all three seasons, the 5 year running mean is denoted in solid lines. In fall, a slight increasing tendency is shown

from 1990 to 1998, and decreases in snow coverage to 2006 although a maximum in the seasonal value in 2003 occur. After 2006 the snow cover extent has increased with a yearly maximum in 2009 of 12.8 Mio km^2. The obtained time series is similar to the results presented in the study by Bulygina et al. (2011), who assessed interannual variations of fall SCE (per cent of the area) averaged over the Russian Federation derived from weekly NOAA/NESDIS satellite estimates. Around 2003 a record high is presented which is also reproduced by CCLM-NCEP1 followed by a decreasing snow cover extent until 2006.

Cohen et al. (2012) suggested potential links to increases in fall snow coverage in recent years to strong temperature warming trends during summer and increased losses of Arctic sea ice (Serreze et al., 2007). According to Cohen et al. (2012) and Stroeve et al. (2012), decreasing sea ice leads to enhanced latent heat flux which increases the lower tropospheric moisture which may impact cloud cover and precipitation and thus snowfall. Cohen et al. (2012) considered SCE only of October averaged over Eurasia, showing an increasing trend from 1988-2010. In that study they further mentioned potential links of increasing snow cover during fall to wintertime phase of AO due to stronger surface cooling and strengthening of Siberian High. This might lead to a weakening of polar vortex and westerlies but favor meridional flow and thus negative AO. Cohen et al. (2012) linked the presented negative trend in wintertime AO with the temperature cooling during winter in that region. However, these results are only based on analyses over recent years and should be accepted with some caution.

During winter, the snow cover extent shows only small variations in the time series of 5 year running mean compared to fall and spring season. From 1994 to 2003 snow cover has increased slightly. Afterwards, a slight reduction is presented in CCLM-NCEP1 to 2008. Since then, the reduction has ceased.

SCE varies strongest during spring season between both hindcasts. A decrease is evident from the beginning of the 1980s to 1998, an increase is denoted in the 5 year running mean from 1998 to 2004 and decreasing tendency afterwards. Over the entire period the smoothed time series show a slight decreasing tendency with 11.5 Mio km^2 in 1982 and 11.1 Mio km^2 2008. Only since 2008 has the decreasing extent again slowed, showing lately even decreases in the snow coverage. The presented SCE time series averaged over the Russian Federation by Bulygina et al. (2011) for April-May confirms the SCE retreat with a slowing decrease in the last two decades and an increasing tendency during the last years. This analysis is based on snow cover extent derived from weekly NOAA/NESDIS satellite estimates, extracted from the updated archive from Groisman et al. (1994). Similar results are obtained by Derksen and Brown (2012) showing snow cover extent anomaly time series from NOAA snow chart separately for April and May averaged over entire Eurasia. For both months the strongest positive anomalies are presented around 1980 and afterwards a negative trend which corresponds to the results obtained by CCLM. In April, around

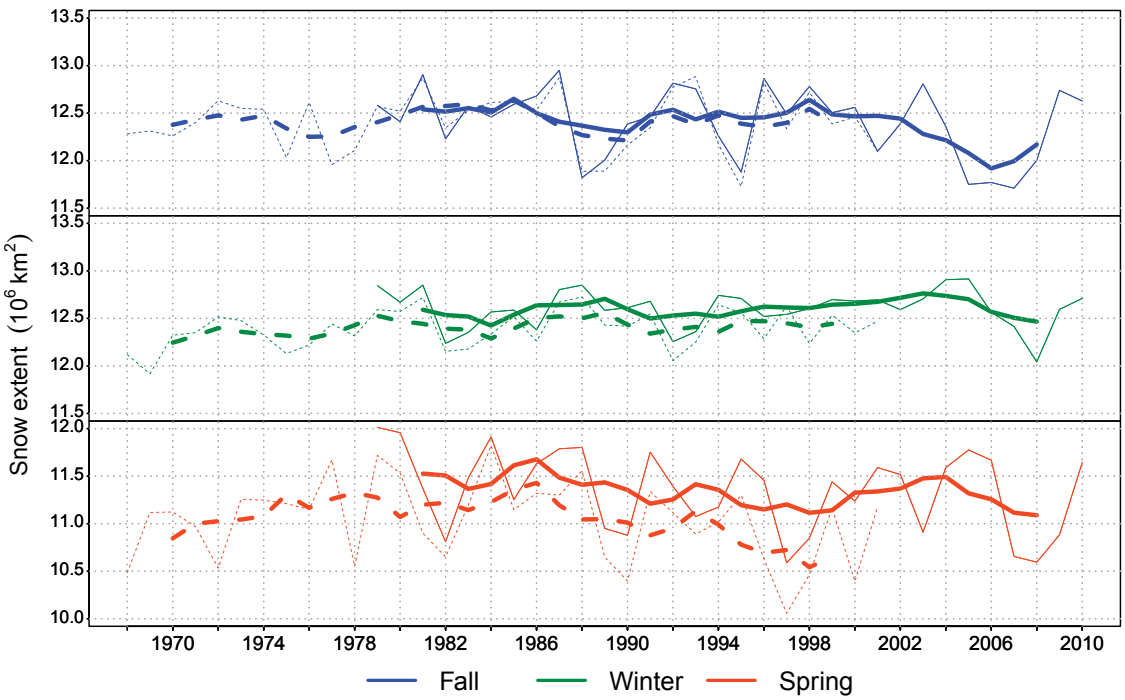

Figure 8.7: Interannual variations of snow cover extent [10^6 km^2] and 5 year running mean (thick lines) for 3 seasons (winter, fall, spring). Solid lines represent CCLM-NCEP1 and dotted CCLM-ERA40.

2010 the retreat ceased but at a less pronounced rate than presented in CCLM-NCEP1. According to Brown et al. (2007), the variability of SCE during spring is strongly determined by surface temperature variations. A strong correlation between trends of SCE and surface temperatures over Eurasia north of 60°N are found in May by (Derksen and Brown, 2012). This correlation exceeds the correlation between SCE and April temperatures (Derksen and Brown, 2012). They conclude that the retreat in spring SCE is caused by the positive temperature trend during spring, also presented in Fig. 8.3.

8.4 Conclusion

This study draws a detailed picture of recent regional changes and variations throughout the considered snow-related seasons for mean SWE together with 2 m air temperature and precipitation based on reconstructed climatologies from the RCM CCLM. Additionally, satellite-derived SWE estimates of ESA GlobSnow are added in the winter season. SCE, a further snow cover characteristic, is investigated for entire model domain.

Changes and interannual variations of mean SWE are characterized by strong spatial and seasonal variability. According to CCLM-NCEP1, regional averages for the period of 1981-2010 show only minor changes of SWE during fall, whereas during winter and spring stronger changes occur with varying patterns throughout the region.

A negative trend in mean winter and spring SWE is presented south of Lake Baikal region in northeast of Mongolia and northern China which is for certain grid boxes statistically

significant. A decrease in SWE is also visible at the eastern side of Central Siberian Plateau and most parts of West Siberian Plain. Strong significant decreases of SWE during the winter seasons in the recent decades are evident according to CCLM in the most elevated parts at the Central Siberian Plateau and Verkhoyansk Mountains up to 40 mm decade^{-1} and during in the Stanovoy Range during Spring. Snow accumulation has significantly increased strongest west of Lake Baikal. Additionally, a positive trend is illustrated in the eastern part, along the coast of Sea of Okhotsk, in the Sayan Mountains and northeast towards Siberia Far East even though these trends are not statistically significant. Increases are further shown in CCLM between the Verkhoyansk and Chersky Range.

Both hindcasts show stronger interannual variations of SCE during the transitions seasons of spring and fall than in winter. During spring a decreasing tendency is presented since the early 1980s which has ceased in recent years.

As Bulygina et al. (2011) stated, dynamics of snow cover are related to various factors associated with strong land-snow-atmosphere interactions. Different characteristics may react differently. To get a comprehensive overview of recent and ongoing changes in terrestrial snow cover, further characteristics such as the snow cover duration, the timing (onset and end of snow season) must be considered. In addition, to answer the underlying reasons for regional variations, the snow patterns should be related e.g. to atmospheric patterns (AO, NAO, SCAND), water vapor fluxes and changes in the cyclone tracks.

9 Conclusions and Outlook

9.1 Conclusions

Within this study, reconstructions of recent Siberian climate were obtained by means of dynamical downscaling of NCEP-R1 from 1948-2010 and ERA40 from 1958-2001 using the regional climate model CCLM. The aim was to provide consistent historical climatologies at approximately 50 km spatial resolution for different climate parameters to complement the limited availability of observational data in that region. Special emphasis was put on snow water equivalent (SWE), as one important parameter of the terrestrial snow cover, to investigate recent changes at regional scale.

For this purpose, a model configuration of CCLM for Siberia was defined, taking certain regional features into account. For the first time CCLM was used to conduct regional climate hindcast simulations over Siberia. According to the research questions in Chapter 1, the major findings within this study can be concluded as follows:

What does an optimized configuration of CCLM for Siberia look like?

First test simulations indicated a strong winter warm bias of 2 m air temperature in the arctic and central parts of the model domain which was only partly related to the driving fields. Performed sensitivity studies showed improved simulations after the reduction of minimal heat diffusion, increasing of the soil column depth and the application of multi-layer snow model with 2 snow layers. Lowering the minimal heat diffusion lead in general to the reduction of turbulent heat fluxes and vertical mixing in the model and to a better representation of the stable conditions predominant in the Siberian High pressure system.

To account for the distribution of energy within the deep reaching permafrost soils in that region, three more soil layers were added to the 10 standard layers with a depth of 11.5 m to deepen the soil column down to 92 m. However, even though an improvement in terms of 2 m air temperature could be achieved, a warm bias remained in certain regions.

How reliable are the derived regional climate model hindcasts and their forcings over Siberia with respect to their temporal consistency?

Both conducted hindcast simulations (CCLM-NCEP1 driven with NCEP-R1 and CCLM-ERA40 driven with ERA40) showed for a set of variables that they differ considerably in terms of interannual variability prior the 1970s in the southern parts of the model domain, especially during summer season. These large temporal discrepancies can be related to the varying large-scale atmospheric forcing of NCEP-R1 and ERA40. They showed inhomogeneities, spatial and temporal dissimilarities even for certain middle-tropospheric variables, such as the geopotential and horizontal wind components in 500 hPa, which are important to assess the effect of dynamical downscaling and spectral nudging. Con-

sequently, reanalyses cannot be assumed to be a 'perfect boundary' in southern Siberia. Further analyses were performed excluding data of CCLM-NCEP1 prior to 1979 and of CCLM-ERA40 prior 1968. This considerably shortened the originally 63 year hindcast of CCLM-NCEP1.

Is CCLM able to represent realistic climate conditions in Siberia of recent years?

Compared to station-related grid data of CRU3.2 and measurements provided by NCDC, CCLM reproduced seasonal temperature fields well with fewer differences during summer and spring but regional discrepancies in winter and fall. Despite the reduction of winter warm bias, an overestimation of 2 m air temperature is still evident in the subregion Arctic-East compared to CRU3.2 and NCDC and the subregion Mid-East during winter. CRU3.2 data show strong spatial variability in seasonal changes of 2 m air temperature over the years of 1981-2010, that is reproduced well by CCLM. The pattern of winter cooling is captured by CCLM as well as the temperature increase south and southeast of Lake Baikal during summer and fall. CCLM tends to overestimate seasonal precipitation in the southern and northeastern regions in winter, spring and fall whereas during summer an underestimation is evident in southern and western parts of the model domain.

How do snow water equivalent over Siberia by different reanalyses differ and can CCLM add value?

CCLM-NCEP1 showed a clear added value from 1987-2010 in representing realistic historical SWE estimates compared to the SWE product of NCEP-R1 when ESA GlobSnow was used as reference. The SWE product of NCEP-R1 does not represent any of the regional and temporal variations of SWE for the considered subregions, except for southern parts. However, this added value was not unexpected because of the errors of the SWE fields of NCEP-R1 already documented. Nevertheless, it was possible to illustrate that the technique of dynamical downscaling of atmospheric forcing fields provided by NCEP-R1 can be used to derive historical SWE fields with more realistic information than the reanalysis product itself can present. The SWE hindcast is in good agreement with GlobSnow in January (mid-winter), whereas it overestimates SWE during the melting season (both compared to GlobSnow and to the snow survey measurements of FSUHSS). CCLM is even is more homogeneous in time than ERA-Interim that shows a spurious jump in 2003 in certain subregions. A temporal inconsistency is also evident in NCEP-R2 near 1999-2001. The CCLM can even compete with the newest generation of NCEP reanalysis (CFSR) at 38 km resolution that underestimates SWE in many subregions. Particularly in periods of snow accumulation, the CCLM hindcast is in better agreement with GlobSnow. However, as clearly shown by the SWE overestimation of CCLM in April, there is still an obvious model deficiency. In general, the results are dependent on the quality of the reference data of ESA GlobSnow.

How do regional-scale change patterns of snow-cover characteristics over the past decades in Siberia look like?

Generally, changes and interannual variations of mean SWE are characterized by strong spatial and seasonal variability. According to CCLM-NCEP1, regional averages for the period of 1981-2010 show only minor changes of SWE in the fall, whereas during winter and spring stronger changes occur with varying patterns throughout the regions. Both hindcasts show stronger interannual variations of snow cover extent during the transition seasons spring and fall than in winter. During spring a negative tendency is presented since the early 1980s. This has ceased in recent years.

9.2 Outlook

To obtain historical consistent meteorological fields, the whole model system of CCLM including land-atmosphere interactions has been used after defining an appropriate model configuration for Siberia. Nevertheless, the presented reconstructions and analyses are not without their limitations.

After the reduction of NCEP-R1 driven hindcast from originally 1948-2010 to 1979-2010, the use of reanalyses with higher resolution might improve the model results. If a long-term reconstruction over 60 years is intended, the southern domain should be excluded in further simulation efforts. To better account for a stable stratified boundary layer in high pressure systems as the Siberian High, adjustments in the turbulence parameterization would be more advisable than tuning the current parameterization.

An additional limitation of CCLM is the overestimation of SWE during the melting season (April) in contrast to the relatively good agreement of CCLM-NCEP1 during January. The multi-layer snow model that has been introduced by DWD is only a preliminary version that is going to be improved in future work. Deficiencies in the snow's melting process might be partly related to the absence of fractional snow cover that could be examined in future work. One further aspect that has not been included so far is the blowing snow process. Especially in non-forested areas at northern high latitudes it has strong implications on e.g. snow density, SWE and sublimation and further physics of snow-cover evolution (Liston and Hiemstra, 2011). Therefore, the implementation of subgrid scale blowing snow parameterization within the snow model might be useful. However, additionally included processes in the model need to be in proportion to the computing time when long-term regional reconstructions are the goal.

The main objective of the present work was to derive a climate reconstruction using CCLM focusing on snow cover characteristics. Analyses have not addressed how snow cover at regional scale may change in future. This could be added and examined in future work. The present regional climate reconstructions have been conducted at a spatial resolution

of about 50 km. These relatively coarse simulations could be performed at much higher resolutions of e.g. 10 km. However, a satellite-based evaluation e.g. in terms of SWE using ESA GlobSnow, is restricted so far to 25 km resolution although the spatial patterns of SWE derived from GlobSnow look even coarser. However, some improvement with respect to spatial detail will be achieved within the next version of GlobSnow product. Therefore, it would be advisable to evaluate SWE of CCLM with the updated version of satellite-derived SWE estimate. Moreover, it would be advisable to evaluate more reconstructed climate variables with observations than presented here for 2 m air temperature, precipitation or SWE. However, the evaluation approach should try to address the observational uncertainties in that region.

In terms of permafrost, the evaluation of soil temperature compared to in situ measurements should be a next step. One potential data source might be the Russian Historical Soil Temperature Data provided the National Snow and Ice Data Center (Zhang et al., 2006). In addition, the consideration of vertical varying soil properties would be of interest to assess the effect of a top organic layer on the climate simulations.

Further parameters such as e.g. maximum SWE, snow cover duration, the timing (start and end dates) of any snow on the ground or continuous snow cover would be interesting to investigate to obtain a more extended overview of recent and ongoing changes of snow cover.

In addition, some aspects relating to the external data would be of interest to assess. The characteristic plant parameters (maximal and minimal plant cover, LAI) are derived by external land cover datasets and might be different in other datasets as e.g. from the ESA GlobCover project (Bicheron et al., 2011). Especially for large areas dominated by tundra and taiga, variations in these plant parameters might alter e.g. the surface energy balance.

Future research will improve the ability to derive model-based climate reconstructions over Siberia to provide regional detailed datasets and information of various climate parameters including those for snow cover. This may help to improve the understanding of snow-climate relations among the atmosphere, hydrosphere and biosphere, in a region in which snow has the potential to feed back to the climate of the whole Northern Hemisphere

A Appendix

Nomenclature

AE ..... Subregion: Arctic-East
AMSR-E ..... Advanced Microwave Scanning Radiometer - EOS
AO ..... Arctic Oscillation
AW ..... Subregion: Arctic-West
CCLM ..... The RCM COSMO-CLM
CCLM-ERA40 ... CCLM hindcast simulation driven by ERA40
CCLM-NCEP1 .. CCLM hindcast simulation driven by NCEP-R1
CFSR ..... Climate Forecast System Reanalysis
crmsd ..... centered root-mean-square difference
CRU ..... Climate Research Unit
DWD ..... Deutscher Wetterdienst
ECMWF ..... European Centre for Medium-Range Weather Forecasts
ECMWF ..... European Centre for Medium-Range Weather Forecasts
ERA-Interim .... ECMWF Re-analysis
ERA40 ..... ECMWF 40 Year Re-analysis Data Archive
ETCCDMI ..... Expert Team on Climate Change Detection, Monitoring and Indices
FSUHSS ..... Former Soviet Union Hydrological Snow Surveys
GCM ..... Global Climate Model
GPCC ..... Global Precipitation Climatology Center
IMS ..... Ice Mapping System
ME ..... Subregion: Mid-East
MM ..... Subregion: Mid-Mid
MSLP ..... Mean sea level pressure
MW ..... Subregion: Mid-West
NAO ..... North Atlantic Oscillation
NCDC ..... National Climatic Data Center
NCEP-CFSR .... NCEP Reanalysis CFSR
NCEP-R1 ..... NCEP Reanalysis 1
NCEP-R2 ..... NCEP Reanalysis 2/DOE
NOAA ..... National Oceanic and Atmospheric Administration
PBL ..... planetary boundary layer
RCM ..... Regional Climate Model
RMSE ..... Root Mean Square Error
SCAND ..... Scandinavian pattern
SCE ..... Snow cover extent

SE ..... Subregion: South-East
SSM/I ..... Special Sensor Microwave/Imager
SSMR ..... Scanning Multichannel Microwave Radiometer
SW ..... Subregion: South-West
SWE ..... Snow water equivalent
SWIPA ..... Snow, Water, Ice and Permafrost in the Arctic
TERRA-ML ..... Multi-layer soil and vegetation model

References

ACIA: Arctic Climate Impact Assessment, Cambridge University Press, 2005.

Adam, J. C. and Lettenmaier, D. P.: Application of New Precipitation and Reconstructed Streamflow Products to Streamflow Trend Attribution in Northern Eurasia, Journal of Climate, 21, 1807–1828, 2008.

Alexander, M. A., Tomas, R., Deser, C., and Lawrence, D. M.: The Atmospheric Response to Projected Terrestrial Snow Changes in the Late Twenty-First Century, J. Climate, 23, 6430–6437, 2010.

Alexandru, A., de Elia, R., Laprise, R., Separovic, L., and Biner, S.: Sensitivity Study of Regional Climate Model Simulations to Large-Scale Nudging Parameters, Mon. Wea. Rev., 137, 1666–1686, doi:10.1175/2008MWR2620.1, 2009.

Alexeev, V., Esau, I., Polyakov, I., Byam, S., and Sorokina, S.: Vertical structure of recent arctic warming from observed data and reanalysis products, Climatic Change, 111, 215–239, 2012.

Alexeev, V. A., Nicolsky, D. J., Romanovsky, V. E., and Lawrence, D. M.: An evaluation of deep soil configurations in the CLM3 for improved representation of permafrost, Geophys. Res. Lett., 34, L09 502–, 2007.

Allen, R. J. and Zender, C. S.: The role of eastern Siberian snow and soil moisture anomalies in quasi-biennial persistence of the Arctic and North Atlantic Oscillations, J. Geophys. Res., 116, D16 125–, URL `http://dx.doi.org/10.1029/2010JD015311`, 2011.

Anisimov, O. and Reneva, S.: Permafrost and Changing Climate: The Russian Perspective, AMBIO: A Journal of the Human Environment, 35, 169–175, doi:10.1579/0044-7447(2006)35[169:PACCTR]2.0.CO;2, 2006.

Armstrong, R. L., Brodzik, M. J., Knowles, K., and Savoie, M.: Global Monthly EASE-Grid Snow Water Equivalent Climatology, Tech. rep., Boulder, Colorado USA: National Snow and Ice Data Center. Digital media., 2007.

Bengtsson, L., Hagemann, S., and Hodges, K. I.: Can climate trends be calculated from reanalysis data?, J. Geophys. Res., 109, 1–22, URL `http://dx.doi.org/10.1029/2004JD004536`, 2004.

Bicheron, P., Amberg, V., Bourg, L., Petit, D., Huc, M., Miras, B., Brockmann, C., Hagolle, O., Delwart, S., Ranera, F., Leroy, M., and Arino, O.: Geolocation Assessment

of MERIS GlobCover Orthorectified Products, Geoscience and Remote Sensing, IEEE Transactions on, 49, 2972–2982, 2011.

Brands, S., Gutiérrez, J. M., Herrera, S., and Cofiño, A. S.: On the Use of Reanalysis Data for Downscaling, J. Climate, 25, 2517–2526, doi:10.1175/JCLI-D-11-00251.1, URL http://dx.doi.org/10.1175/JCLI-D-11-00251.1, 2011.

Brasnett, B.: A Global Analysis of Snow Depth for Numerical Weather Prediction, J. Appl. Meteor., 38, 726–740, doi:10.1175/1520-0450(1999)038<0726:AGAOSD>2.0.CO;2, 1999.

Brodzik, M. and Armstrong, R.: Northern Hemisphere EASE-Grid 2.0 Weekly Snow Cover and Sea Ice Extent. Version 3. [indicate subset used], Boulder, Colorado USA: National Snow and Ice Data Center, 2013.

Bromwich, D. H. and Fogt, R. L.: Strong Trends in the Skill of the ERA-40 and NCEP-NCAR Reanalyses in the High and Midlatitudes of the Southern Hemisphere, 1958-2001*, J. Climate, 17, 4603–4619, doi:10.1175/3241.1, URL http://dx.doi.org/10.1175/3241.1, 2004.

Bromwich, D. H., Fogt, R. L., Hodges, K. I., and Walsh, J. E.: A tropospheric assessment of the ERA-40, NCEP, and JRA-25 global reanalyses in the polar regions, J. Geophys. Res., 112, D10 111–, 2007.

Bromwich, D. H., Hines, K. M., and Bai, L.-S.: Development and testing of Polar Weather Research and Forecasting model: 2. Arctic Ocean, J. Geophys. Res., 114, 1–22, URL http://dx.doi.org/10.1029/2008JD010300, 2009.

Brooks, R. H. and Corey, A. T.: Properties of porous media affecting fluid flow, Journal of the Irrigation and Drainage Division, ASCE, 72, 61–88, 1966.

Brown, R., Derksen, C., and Wang, L.: Assessment of spring snow cover duration variability over northern Canada from satellite datasets, Remote Sens. Environ., 111, 367–381, 2007.

Brown, R., Derksen, C., and Wang, L.: A multi-data set analysis of variability and change in Arctic spring snow cover extent, 1967-2008, J. Geophys. Res., 115, D16 111–, URL http://dx.doi.org/10.1029/2010JD013975, 2010.

Brown, R. D. and Mote, P. W.: The Response of Northern Hemisphere Snow Cover to a Changing Climate*, J. Climate, 22, 2124–2145, URL http://dx.doi.org/10.1175/2008JCLI2665.1, 2009.

Brown, R. D., Brasnett, B., and Robinson, D.: Gridded North American monthly snow depth and snow water equivalent for GCM evaluation, Atmosphere-Ocean, 41, 1–14, URL http://dx.doi.org/10.3137/ao.410101, 2003.

Brun, E., Vionnet, V., Boone, A., Decharme, B., Peings, Y., Valette, R., Karbou, F., and Morin, S.: Simulation of northern Eurasian local snow depth, mass and density using a detailed snowpack model and meteorological reanalysis, J. Hydrometeor, doi: 10.1175/JHM-D-12-012.1, URL http://dx.doi.org/10.1175/JHM-D-12-012.1, 2012.

Brun, E., E., David, P., Sodul, M., and Brunot, G.: A numerical model to simulate snow-cover stratigraphy for operational avalanche forecasting, Journal of Glaciology, 38, 13–28, 1992.

Bulygina, O. N., Razuvaev, V. N., and Korshunova, N.: Changes in snow cover over Northern Eurasia in the last few decades, Environmental Research Letters, 4, 045 026, 2009.

Bulygina, O. N., Groisman, P. Y., Razuvaev, V. N., and Korshunova, N. N.: Changes in snow cover characteristics over Northern Eurasia since 1966, Environmental Research Letters, 6, 045 204–, URL http://stacks.iop.org/1748-9326/6/i=4/a=045204, 2011.

Byrkjedal, O., Esau, I., and Kvamtso, N.: Sensitivity of simulated wintertime Arctic atmosphere to vertical resolution in the ARPEGE/IFS model, 30, 687–701–, URL http://dx.doi.org/10.1007/s00382-007-0316-z, 2008.

Callaghan, T. V., Johansson, M., Brown, R. D., Groisman, P., Ya, L. N., Radionov, V., and Contributing, A.: Snow, Water, Ice and Permafrost in the Arctic (SWIPA), chap. Changing Snow Cover and its Impacts, p. 59, AMAP, 2011.

Clifford, D.: Global estimates of snow water equivalent from passive microwave instruments: history, challenges and future developments, International Journal of Remote Sensing, 31, 3707–3726, URL http://dx.doi.org/10.1080/01431161.2010.483482, 2010.

Cohen, J. L., Furtado, J. C., Barlow, M. A., Alexeev, V. A., and Cherry, J. E.: Arctic warming, increasing snow cover and widespread boreal winter cooling, Environmental Research Letters, 7, 014 007, 2012.

Cook, B., Bonan, G., Levis, S., and Epstein, H.: The thermoinsulation effect of snow cover within a climate model, Climate Dynamics, 31, 107–124, URL http://dx.doi.org/10.1007/s00382-007-0341-y, 2008.

Cosby, B. J., Hornberger, G. M., Clapp, R. B., and Ginn, T. R.: A Statistical Exploration of the Relationships of Soil Moisture Characteristics to the Physical Properties of Soils, Water Resour. Res., 20, 682–690, 1984.

Cuxart, J., Holtslag, A., Beare, R., Bazile, E., Beljaars, A., Cheng, A., Conangla, L., Ek, M., Freedman, F., Hamdi, R., Kerstein, A., Kitagawa, H., Lenderink, G., Lewellen, D., Mailhot, J., Mauritsen, T., Perov, V., Schayes, G., Steeneveld, G.-J., Svensson, G., Taylor, P., Weng, W., Wunsch, S., and Xu, K.-M.: Single-Column Model Intercomparison for a Stably Stratified Atmospheric Boundary Layer, 118, 273–303–, URL http://dx.doi.org/10.1007/s10546-005-3780-1, 2006.

Dankers, R., Burke, E. J., and Price, J.: Simulation of permafrost and seasonal thaw depth in the JULES land surface scheme, The Cryosphere, 5, 773–790, URL http://www.the-cryosphere.net/5/773/2011/, 2011.

Davies, H. C.: A laterul boundary formulation for multi-level prediction models, Quarterly Journal of the Royal Meteorological Society, 102, 405–418, doi:10.1002/qj.49710243210, URL http://dx.doi.org/10.1002/qj.49710243210, 1976.

Dee, D. P., Uppala, S. M., Simmons, A. J., Berrisford, P., Poli, P., Kobayashi, S., Andrae, U., Balmaseda, M. A., Balsamo, G., Bauer, P., Bechtold, P., Beljaars, A. C. M., van de Berg, L., Bidlot, J., Bormann, N., Delsol, C., Dragani, R., Fuentes, M., Geer, A. J., Haimberger, L., Healy, S. B., Hersbach, H., Hólm, E. V., Isaksen, L., Kållberg, P., Köhler, M., Matricardi, M., McNally, A. P., Monge-Sanz, B. M., Morcrette, J.-J., Park, B.-K., Peubey, C., de Rosnay, P., Tavolato, C., Thépaut, J.-N., and Vitart, F.: The ERA-Interim reanalysis: configuration and performance of the data assimilation system, Q.J.R. Meteorol. Soc., 137, 553–597, URL http://dx.doi.org/10.1002/qj.828, 2011.

Derksen, C. and Brown, R.: Spring snow cover extent reductions in the 2008-2012 period exceeding climate model projections, Geophys. Res. Lett., 39, L19 504–, URL http://dx.doi.org/10.1029/2012GL053387, 2012.

Derksen, C., Toose, P., Lemmetyinen, J., Pulliainen, J., Langlois, A., Rutter, N., and Fuller, M.: Evaluation of passive microwave brightness temperature simulations and snow water equivalent retrievals through a winter season, Remote Sensing of Environment, 117, 236–248, URL http://www.sciencedirect.com/science/article/pii/S0034425711003488, 2012.

Dery, S. J. and Brown, R. D.: Recent Northern Hemisphere snow cover extent trends and implications for the snow-albedo feedback, Geophys. Res. Lett., 34, L22 504–, URL http://dx.doi.org/10.1029/2007GL031474, 2007.

Dewdney, J.: A geography of the Soviet Union, Pergamon Press, URL http://books.google.de/books?id=EzJpAAAAMAAJ, 1971.

Di Luca, A., de Elia, R., and Laprise, R.: Potential for added value in precipitation simulated by high-resolution nested Regional Climate Models and observations, Climate Dynamics, 38, 1229–1247, doi:10.1007/s00382-011-1068-3, URL http://dx.doi.org/10.1007/s00382-011-1068-3, 2012.

Doms, G., J., F., Heise, E., Herzog, H.-J., Mrionow, D., Raschendorfer, M., Reinhart, T., Ritter, B., Schrodin, R., Schulz, J.-P., and Vogel, G.: A Description of the Nonhydrostatic Regional COSMO Model. Part II: Physical Parameterization, Tech. rep., Deutscher Wetterdienst, URL http://www.cosmo-model.org/content/model/documentation/core/cosmoPhysParamtr.pdf, 2011.

Ershov, E. D.: General Geocryology (Studies in Polar Research), Cambridge Univ. Press, 1998.

Feser, F. and von Storch, H.: Regional modelling of the western Pacific typhoon season 2004, Meteorologische Zeitschrift, 17, 519–528, doi:10.1127/0941-2948/2008/0282, 2008.

Feser, F., Rockel, B., von Storch, H., Winterfeldt, J., and Zahn, M.: Regional Climate Models Add Value to Global Model Data: A Review and Selected Examples, Bull. Amer. Meteor. Soc., 92, 1181–1192, URL http://dx.doi.org/10.1175/2011BAMS3061.1, 2011.

Flerchinger, G. and Saxton, K.: Simultaneous heat and water model of freezing snow-residue-soil system. I. Theory and development, Transactions of the ASEA, 32, 565–571, 1989.

Foster, J. L., Sun, C., Walker, J. P., Kelly, R., Chang, A., Dong, J., and Powell, H.: Quantifying the uncertainty in passive microwave snow water equivalent observations, Remote Sensing of Environment, 94, 187–203, 2005.

Frauenfeld, O. W., Zhang, T., Barry, R. G., and Gilichinsky, D.: Interdecadal changes in seasonal freeze and thaw depths in Russia, J. Geophys. Res., 109, D05 101–, URL http://dx.doi.org/10.1029/2003JD004245, 2004.

Früh, B., Feldmann, H., Panitz, H. J., Schaedler, G., Jacob, D., Lorenz, P., and Keuler, K.: Determination of Precipitation Return Values in Complex Terrain and Their Evaluation, Journal of Climate, 23, 2257–2274, 2010.

Gao, Q., Guan, Z., Du, N., and Hu, T.: Comparison of in situ station data and reanalysis data in winter and summer temperature in China, vol. 7083, pp. 708 313–708 313–12, doi:10.1117/12.794474, URL http://dx.doi.org/10.1117/12.794474, 2008.

Ge, Y. and Gong, G.: Observed Inconsistencies between Snow Extent and Snow Depth Variability at Regional/Continental Scales, J. Climate, 21, 1066–1082, URL http://dx.doi.org/10.1175/2007JCLI1829.1, 2008.

Ghatak, D., Frei, A., Gong, G., Stroeve, J., and Robinson, D.: On the emergence of an Arctic amplification signal in terrestrial Arctic snow extent, J. Geophys. Res., 115, D24 105–, URL http://dx.doi.org/10.1029/2010JD014007, 2010.

Ghatak, D., Deser, C., Frei, A., Gong, G., Phillips, A., Robinson, D. A., and Stroeve, J.: Simulated Siberian snow cover response to observed Arctic sea ice loss, 1979-2008, J. Geophys. Res., 117, D23 108–, URL http://dx.doi.org/10.1029/2012JD018047, 2012.

Giorgi, F.: Simulation of Regional Climate Using a Limited Area Model Nested in a General Circulation Model, J. Climate, 3, 941–963, 1990.

Giorgi, F. and Marinucci, M. R.: An investigation of the sensitivity of simulated precipitation to model resolution and its implications for climate studies, 124(1), URL http://nldr.library.ucar.edu/repository/collections/WOS-000-000-006-111, 1996.

Giorgi, F. and Mearns, L. O.: Introduction to special section: Regional climate modeling revisited, Journal Of Geophysical Research-Atmospheres, 104, 6335–6352, 1999.

Groisman, P. and Amber, J. S.: Ongoing climatic change in Northern Eurasia: justification for expedient research, Environmental Research Letters, 4, 045 002, 2009.

Groisman, P. and Gutman, G.: Regional Environmental Changes in Siberia and Their Global Consequences, Springer, URL http://books.google.de/books?id=6uaNnUiYUTwC, 2012.

Groisman, P. Y. and Rankova, E. Y.: Precipitation trends over the Russian permafrost-free zone: removing the artifacts of pre-processing, International Journal of Climatology, 21, 657–678, URL http://dx.doi.org/10.1002/joc.627, 2001.

Groisman, P. Y., Karl, T. R., Knight, R. W., and Stenchikov, G. L.: Changes of Snow Cover, Temperature, and Radiative Heat Balance over the Northern Hemisphere, J. Climate, 7, 1633–1656, doi:10.1175/1520-0442(1994)007<1633:COSCTA>2.0.CO;2, 1994.

Groisman, P. Y., Knight, R. W., Razuvaev, V. N., Bulygina, O. N., and Karl, T. R.: State of the Ground: Climatology and Changes during the Past 69 Years over Northern Eurasia for a Rarely Used Measure of Snow Cover and Frozen Land, J. Climate, 19, 4933–4955, doi:10.1175/JCLI3925.1, URL http://journals.ametsoc.org/doi/abs/10.1175/JCLI3925.1, 2006.

Helfrich, S. R., McNamara, D., Ramsay, B. H., Baldwin, T., and Kasheta, T.: Enhancements to, and forthcoming developments in the Interactive Multisensor Snow and Ice Mapping System (IMS), Hydrol. Process., 21, 1576–1586, URL http://dx.doi.org/10.1002/hyp.6720, 2007.

Hillel, D.: Applications of Soil Physics, Academic Press , New York, 1980.

Honda, M., Inoue, J., and Yamane, S.: Influence of low Arctic sea-ice minima on anomalously cold Eurasian winters, Geophys. Res. Lett., 36, L08 707–, URL http://dx.doi.org/10.1029/2008GL037079, 2009.

Huang, W.-R., Wang, S.-Y., and Chan, J. C. L.: Discrepancies between global reanalyses and observations in the interdecadal variations of Southeast Asian cold surge, Int. J. Climatol., 31, 2272–2280, URL http://dx.doi.org/10.1002/joc.2234, 2011.

Hurrell, J. W.: Decadal Trends in the North Atlantic Oscillation: Regional Temperatures and Precipitation, Science, 269, 676–679, 1995.

Inoue, T. and Matsumoto, J.: A Comparison of Summer Sea Level Pressure over East Eurasia between NCEP-NCAR Reanalysis and ERA-40 for the Period 1960-99, Journal of the Meteorological Society of Japan, 82, 951–958, 2004.

Kalnay, E., Kanamitsu, M., Kistler, R., Collins, W., Deaven, D., Gandin, L., Iredell, M., Saha, S., White, G., Woollen, J., Zhu, Y., Chelliah, M., Ebisuzaki, W., Higgins, W., Janowiak, J., Mo, K. C., Ropelewski, C., Wang, J., Leetmaa, A., Reynolds, R., Jenne, R., and Joseph, D.: The NCEP/NCAR 40-year reanalysis project, Bulletin of the American Meteorological Society, 77, 437–471, URL http://dss.ucar.edu/datasets/ds090.0/docs/bams/bams1996mar/bamspapr-bm.pdf, 1996.

Kanamitsu, M., Ebisuzaki, W., Woollen, J., Yang, S.-K., Hnilo, J. J., Fiorino, M., and Potter, G. L.: NCEP–DOE AMIP-II Reanalysis (R-2), Bulletin of the American Meteorological Society, 83, 1631–1643, 2002.

Karl, T., Nicholls, N., and Ghazi, A.: Clivar/GCOS/WMO Workshop on Indices and Indicators for Climate Extremes Workshop Summary, 42, 3–7, 1999.

Kendall, M. G.: Rank Correlation Methods, Charles Griffin, 1975.

Khan, V., Rubinshtein, K., and Shmakin, A.: Comparison of seasonal and interannual variability of snow cover in Russian watersheds according to observations and reanalyses, 43, 59–69, 2007.

Khan, V., Holko, L., Rubinstein, K., and Breiling, M.: Snow Cover Characteristics over the Main Russian River Basins as Represented by Reanalyses and Measured Data, J. Appl. Meteor. Climatol., 47, 1819–1833, 2008.

Kiehl, J. T. and Gent, P. R.: The Community Climate System Model, Version 2, J. Climate, 17, 3666–3682, doi:10.1175/1520-0442(2004)017<3666:TCCSMV>2.0.CO;2, 2004.

Kistler, R., Kalnay, E., Collins, W., Saha, S., White, G., Woollen, J., Chelliah, M., Ebisuzaki, W., Kanamitsu, M., Kousky, V., van den Dool, H., Jenne, R., and Fiorino, M.: The NCEP-NCAR 50-year reanalysis: Monthly means CD-ROM and documentation, Bulletin of the American Meteorological Society, 82, 247–267–, URL `http://nldr.library.ucar.edu/repository/collections/AMS-PUBS-000-000-000-091`, 2001.

Kitaev, L., Kislov, A., Krenke, A., Razuvaev, V., Martuganov, R., and Konstantinov, I.: The snow characteristics of northern Eurasia and their relationship to climatic parameters, Boreal Environment Research, 7, 437–445, 2002.

Kitaev, L., Forland, E., Razuvaev, V., Tveito, O. E., and Krueger, O.: Distribution of snow cover over Northern Eurasia, Nordic Hydrology, 36(4-5), 311–319, 2005.

Kopp, T. J. and Kiess, R. B.: The Air Force Global Weather Central snow analysis model., in: Preprints, 15th Conf. on Weather Analysis and Forecasting, Norfolk, VA, Amer. Meteor. Soc., 1996.

Krenke, A.: Former Soviet Union hydrological snow surveys, 1966–1996., Tech. rep., National Snow and Ice Data Center/World Data Center for Glaciology, Boulder, 2004.

Kunz, M. and Kottmeier, C.: Orographic Enhancement of Precipitation over Low Mountain Ranges. Part II: Simulations of Heavy Precipitation Events over Southwest Germany, J. Appl. Meteor. Climatol., 45, 1041–1055, doi:10.1175/JAM2390.1, URL `http://dx.doi.org/10.1175/JAM2390.1`, 2006.

Lachenbruch, A. and Marshall, V.: Changing Climate: Geothermal Evidence from Permafrost in the Alaskan Arctic, Science, 234, 689–696, 1986.

Lawrence, D. and Slater, A.: Incorporating organic soil into a global climate model, 30, 145–160–, URL `http://dx.doi.org/10.1007/s00382-007-0278-1`, 2008.

Lawrence, D. M., Slater, A. G., Romanovsky, V. E., and Nicolsky, D. J.: Sensitivity of a model projection of near-surface permafrost degradation to soil column depth and representation of soil organic matter, J. Geophys. Res., 113, F02 011–, URL `http://dx.doi.org/10.1029/2007JF000883`, 2008a.

Lawrence, D. M., Slater, A. G., Tomas, R. A., Holland, M. M., and Deser, C.: Accelerated Arctic land warming and permafrost degradation during rapid sea ice loss, Geophys. Res. Lett., 35, L11 506–, URL `http://dx.doi.org/10.1029/2008GL033985`, 2008b.

Liston, G. E.: Representing Subgrid Snow Cover Heterogeneities in Regional and Global Models, J. Climate, 17, 1381–1397, 2004.

Liston, G. E. and Hiemstra, C. A.: The Changing Cryosphere: Pan-Arctic Snow Trends (1979-2009), J. Climate, 24, 5691–5712, doi:10.1175/JCLI-D-11-00081.1, URL http://dx.doi.org/10.1175/JCLI-D-11-00081.1, 2011.

Liu, Z., Xu, Z., Yao, Z., and Huang, H.: Comparison of surface variables from ERA and NCEP reanalysis with station data over eastern China, 107, 611–621–, URL http://dx.doi.org/10.1007/s00704-011-0501-1, 2012.

Louis, J.-F.: A parametric model of vertical eddy fluxes in the atmosphere, 17, 187–202–, URL http://dx.doi.org/10.1007/BF00117978, 1979.

Lydolph, P.: Geography of the U.S.S.R., John Wiley & Sons, URL http://books.google.de/books?id=03YIAAAAIAAJ, 1977.

Mann, H. B.: Non-parametric test against trend, Econometrica, 13, 245–259, 1945.

Meissner, C. S., Panitz, H.-J. F., and Kottmeier, C.: High-resolution sensitivity studies with the regional climate model COSMO-CLM, metz, 18, 543–557, URL http://dx.doi.org/10.1127/0941-2948/2009/0400, 2009.

Mellor, G. L. and Yamada, T.: Development of a turbulence closure model for geophysical fluid problems, Rev. Geophys., 20, 851–875, URL http://dx.doi.org/10.1029/RG020i004p00851, 1982.

Miguez-Macho, G., Stenchikov, G. L., and Robock, A.: Regional Climate Simulations over North America: Interaction of Local Processes with Improved Large-Scale Flow, J. Climate, 18, 1227–1246, doi:10.1175/JCLI3369.1, URL http://dx.doi.org/10.1175/JCLI3369.1, 2005.

Mitchell, T. D. and Jones, P. D.: An improved method of constructing a database of monthly climate observations and associated high-resolution grids, International Journal of Climatology, 25, 693–712, URL http://dx.doi.org/10.1002/joc.1181, 2005.

Müller, B.: Eine regionale Klimasimulation für Europa zur Zeit des späten Maunder-Minimums 1675-1705, Ph.D. thesis, GKSS, 2004.

Nicolsky, D. J., Romanovsky, V. E., Alexeev, V. A., and Lawrence, D. M.: Improved modeling of permafrost dynamics in a GCM land-surface scheme, Geophys. Res. Lett., 34, L08 501–, URL http://dx.doi.org/10.1029/2007GL029525, 2007.

Peterson, T.: Climate Change Indices, WMO Bulletin, 54, 83–86, 2005.

Prömmel, K., Geyer, B., Jones, J. M., and Widmann, M.: Evaluation of the skill and added value of a reanalysis-driven regional simulation for Alpine temperature, Int. J. Climatol., 30, 760–773, URL http://dx.doi.org/10.1002/joc.1916, 2010.

Przybylak, R.: The Climate of the Arctic, Kluwer Academic Publishers, 2003.

Pulliainen, J.: Mapping of snow water equivalent and snow depth in boreal and sub-arctic zones by assimilating space-borne microwave radiometer data and ground-based observations, Remote Sensing of Environment, 101, 257–269, 2006.

Raeisaenen, J.: Warmer climate: less or more snow?, Climate Dynamics, 30, 307–319–, 2008.

Rinke, A., Dethloff, K., Cassano, J., Christensen, J., Curry, J., Du, P., Girard, E., Haugen, J.-E., Jacob, D., Jones, C., Koltzow, M., Laprise, R., Lynch, A., Pfeifer, S., Serreze, M., Shaw, M., Tjernstrom, M., Wyser, K., and Zagar, M.: Evaluation of an ensemble of Arctic regional climate models: spatiotemporal fields during the SHEBA year, Climate Dynamics, 26, 459–472, URL http://dx.doi.org/10.1007/s00382-005-0095-3, 2006.

Rinke, A., Kuhry, P., and Dethloff, K.: Importance of a soil organic layer for Arctic climate: A sensitivity study with an Arctic RCM, Geophys. Res. Lett., 35, L13 709–, URL http://dx.doi.org/10.1029/2008GL034052, 2008.

Rinke, A., H, M., and K, D.: Regional characteristics of Arctic temperature variability: comparison of observations with regional climate simulations, Clim Res, 41, 177–192, URL http://www.int-res.com/abstracts/cr/v41/n3/p177-192/, 2010.

Rockel, B., Will, A., and Hense, A.: The Regional Climate Model COSMO-CLM (CCLM), Meteorologische Zeitschrift, 17, 347–348, 2008.

Roeckner, E.: Allgemeine Zirkulationsmodelle, Atmosphäre, Numerische Klimamodelle, Teil II: Modellierung natürlicher Klimaschwankungen, 29, 6–14, 2003.

Roesch, A.: Evaluation of surface albedo and snow cover in AR4 coupled climate models, J. Geophys. Res., 111, D15 111–, URL http://dx.doi.org/10.1029/2005JD006473, 2006.

Rojas, M.: Multiply Nested Regional Climate Simulation for Southern South America: Sensitivity to Model Resolution, Mon. Wea. Rev., 134, 2208–2223, doi:10.1175/MWR3167.1, URL http://dx.doi.org/10.1175/MWR3167.1, 2006.

Roshydromet, ed.: Assessment report on climate change and its consequences in Russian Federation, 2008.

Saha, S., Moorthi, S., Pan, H.-L., Wu, X., Wang, J., Nadiga, S., Tripp, P., Kistler, R., Woollen, J., Behringer, D., Liu, H., Stokes, D., Grumbine, R., Gayno, G., Wang, J., Hou, Y.-T., Chuang, H.-Y., Juang, H.-M. H., Sela, J., Iredell, M., Treadon, R., Kleist, D., Van Delst, P., Keyser, D., Derber, J., Ek, M., Meng, J., Wei, H., Yang, R., Lord, S., Van Den Dool, H., Kumar, A., Wang, W., Long, C., Chelliah, M., Xue, Y., Huang, B., Schemm, J.-K., Ebisuzaki, W., Lin, R., Xie, P., Chen, M., Zhou, S., Higgins, W., Zou, C.-Z., Liu, Q., Chen, Y., Han, Y., Cucurull, L., Reynolds, R. W., Rutledge, G., and Goldberg, M.: The NCEP Climate Forecast System Reanalysis, Bull. Amer. Meteor. Soc., 91, 1015–1057, 2010.

Saha, S. K.: The influence of an improved soil scheme on the arctic climate in a regional climate model (RCM), Reports on polar and marine research, Bremerhaven, Alfred Wegener Institute for Polar and Marine Research, 2006.

Saito, K., Kimoto, M., Zhang, T., Takata, K., and Emori, S.: Evaluating a high-resolution climate model: Simulated hydrothermal regimes in frozen ground regions and their change under the global warming scenario, J. Geophys. Res., 112, F02S11–, URL `http://dx.doi.org/10.1029/2006JF000577`, 2007.

Salstein, D. A., Ponte, R. M., and Cady-Pereira, K.: Uncertainties in atmospheric surface pressure fields from global analyses, J. Geophys. Res., 113, D14 107–, URL `http://dx.doi.org/10.1029/2007JD009531`, 2008.

Schaettler, U., Doms, G., and Schraff, C.: A Description of the Nonhydrostatic Regional COSMO-Model Part VII: User's Guide, Tech. rep., Deutscher Wetterdienst, 2008.

Schneider, U., Becker, A., Finger, P., Meyer-Christoffer, A., Ziese, M., and Rudolf, B.: GPCC's new land surface precipitation climatology based on quality-controlled in situ data and its role in quantifying the global water cycle, pp. 1–26–, URL `http://dx.doi.org/10.1007/s00704-013-0860-x`, 2013.

Screen, J. A. and Simmonds, I.: Erroneous Arctic Temperature Trends in the ERA-40 Reanalysis: A Closer Look, J. Climate, 24, 2620–2627, doi:10.1175/2010JCLI4054.1, URL `http://dx.doi.org/10.1175/2010JCLI4054.1`, 2010.

Serreze, M. C. and Barry, R. G.: The Arctic Climate System, Cambridge University Press, 2005.

Serreze, M. C. and Hurst, C. M.: Representation of Mean Arctic Precipitation from NCEP-NCAR and ERA Reanalyses, J. Climate, 13, 182–201, doi:10.1175/1520-0442(2000)013<0182:ROMAPF>2.0.CO;2, URL `http://dx.doi.org/10.1175/1520-0442(2000)013<0182:ROMAPF>2.0.CO;2`, 2000.

Serreze, M. C., Clark, M. P., and Bromwich, D. H.: Monitoring Precipitation over the Arctic Terrestrial Drainage System: Data Requirements, Shortcomings, and Applications of Atmospheric Reanalysis;, Journal of Hydrometeorology, 4, 387–407, 2003.

Serreze, M. C., Barrett, A. P., and Lo, F.: Northern High-Latitude Precipitation as Depicted by Atmospheric Reanalyses and Satellite Retrievals, Mon. Wea. Rev., 133, 3407–3430, doi:10.1175/MWR3047.1, URL http://dx.doi.org/10.1175/MWR3047.1, 2005.

Serreze, M. C., Holland, M. M., and Stroeve, J.: Perspectives on the Arctic's Shrinking Sea-Ice Cover, Science, 315, 1533–1536, URL http://www.sciencemag.org/content/315/5818/1533.abstract, 2007.

Serreze, M. C., Barrett, A. P., Stroeve, J. C., Kindig, D. N., and Holland, M. M.: The emergence of surface-based Arctic amplification, The Cryosphere, 3, 11–19, URL http://www.the-cryosphere.net/3/11/2009/, 2009.

Shaw, D.: Russia in the Modern World: A New Geography, Wiley, 1999.

Shkolnik, I. M., Nadyozhina, E. D., Pavlova, T. V., Molkentin, E. K., and Semioshina, A. A.: Snow cover and permafrost evolution in Siberia as simulated by the MGO regional climate model in the 20th and 21st centuries, Environmental Research Letters, 5, 015 005–, URL http://stacks.iop.org/1748-9326/5/i=1/a=015005, 2010.

Shmakin, A.: Climatic characteristics of snow cover over North Eurasia and their change during the last decades, Ice and Snow, 1, 43–57, 2010.

Shmakin, A. and Popova, V.: Dynamics of climate extremes in northern Eurasia in the late 20th century, 42, 138–147, 2006.

Shulgina, T. M., Genina, E. Y., and Gordov, E. P.: Dynamics of climatic characteristics influencing vegetation in Siberia, Environmental Research Letters, 6, 045 210–045 215, 2011.

Simmons, A. J., Jones, P. D., da Costa Bechtold, V., Beljaars, A. C. M., Kållberg, P. W., Saarinen, S., Uppala, S. M., Viterbo, P., and Wedi, N.: Comparison of trends and low-frequency variability in CRU, ERA-40, and NCEP/NCAR analyses of surface air temperature, J. Geophys. Res., 109, D24 115–, URL http://dx.doi.org/10.1029/2004JD005306, 2004.

Slater, A. G., Schlosser, C. A., Desborough, C. E., Pitman, A. J., Henderson-Sellers, A., Robock, A., Vinnikov, K. Y., Entin, J., Mitchell, K., Chen, F., Boone, A., Etchevers, P., Habets, F., Noilhan, J., Braden, H., Cox, P. M., de Rosnay, P., Dickinson, R. E., Yang, Z.-L., Dai, Y.-J., Zeng, Q., Duan, Q., Koren, V., Schaake, S., Gedney, N., Gusev, Y. M., Nasonova, O. N., Kim, J., Kowalczyk, E. A., Shmakin, A. B.,

Smirnova, T. G., Verseghy, D., Wetzel, P., and Xue, Y.: The Representation of Snow in Land Surface Schemes: Results from PILPS 2(d), J. Hydrometeor, 2, 7–25, doi: 10.1175/1525-7541(2001)002<0007:TROSIL>2.0.CO;2, 2001.

Steppeler, J., Doms, G., Schättler, U., Bitzer, H., Gassmann, A., Damrath, U., and Gregoric, G.: Meso-gamma scale forecasts using the nonhydrostatic model LM, Meteorology and Atmospheric Physics, 82, 75–96, doi:10.1007/s00703-001-0592-9, 2003.

Sterl, A.: On the (In)Homogeneity of Reanalysis Products, J. Climate, 17, 3866–3873, doi:10.1175/1520-0442(2004)017<3866:OTIORP>2.0.CO;2, 2004.

Stieglitz, M., Déry, S. J., Romanovsky, V. E., and Osterkamp, T. E.: The role of snow cover in the warming of arctic permafrost, Geophys. Res. Lett., 30, 1721–, URL `http://dx.doi.org/10.1029/2003GL017337`, 2003.

Stroeve, J., Serreze, M., Holland, M., Kay, J., Malanik, J., and Barrett, A.: The Arctic's rapidly shrinking sea ice cover: a research synthesis, 110, 1005–1027–, URL `http://dx.doi.org/10.1007/s10584-011-0101-1`, 2012.

Sturaro, G.: A closer look at the climatological discontinuities present in the NCEP/NCAR reanalysis temperature due to the introduction of satellite data, 21, 309–316–, URL `http://dx.doi.org/10.1007/s00382-003-0334-4`, 2003.

Sturm, M. andSchimel, J., Mechaelson, G., Welker, J., Oberbauer, S., Liston, G. E., Fahnestock, J., and Romanovsky, V., V. E.: Winter Biological Processes Could Help Convert Arctic Tundra to Shrubland, BioScience, 55, 17–26, 2005.

Takala, M., Pulliainen, J., Metsamaki, S., and Koskinen, J.: Detection of Snowmelt Using Spaceborne Microwave Radiometer Data in Eurasia From 1979 to 2007, Geoscience and Remote Sensing, IEEE Transactions on, 47, 2996 –3007, doi:10.1109/TGRS.2009.2018442, 2009.

Takala, M., Luojus, K., Pulliainen, J., Derksen, C., Lemmetyinen, J., Kärnä, J.-P., Koskinen, J., and Bojkov, B.: Estimating northern hemisphere snow water equivalent for climate research through assimilation of space-borne radiometer data and ground-based measurements, Remote Sensing of Environment, 115, 3517–3529, URL `http://www.sciencedirect.com/science/article/pii/S0034425711003166`, 2011.

Tang, Q. and Leng, G.: Damped summer warming accompanied with cloud cover increase over Eurasia from 1982 to 2009, Environmental Research Letters, 7, 014 004, URL `http://stacks.iop.org/1748-9326/7/i=1/a=014004`, 2012.

Thompson, D. W. J. and Wallace, J. M.: The Arctic oscillation signature in the wintertime geopotential height and temperature fields, Geophys. Res. Lett., 25, 1297–1300, 1998.

Thorne, P. W. and Vose, R. S.: Reanalyses Suitable for Characterizing Long-Term Trends, Bull. Amer. Meteor. Soc., 91, 353–361, doi:10.1175/2009BAMS2858.1, URL http://dx.doi.org/10.1175/2009BAMS2858.1, 2010.

Troy, T. J., Sheffield, J., and Wood, E. F.: The role of winter precipitation and temperature on northern Eurasian streamflow trends, J. Geophys. Res., 117, D05 131–, URL http://dx.doi.org/10.1029/2011JD016208, 2012.

Uppala, S., Kallberg, P., Simmons, A., Andrae, U., da Costa Bechtold, V., Fiorino, M., Gibson, J., Haseler, J., Hernandez, A., Kelly, G., Li, X., Onogi, K., Saarinen, S., Sokka, N., Allan, R., Andersson, E., Arpe, K., Balmaseda, M., Beljaars, A., van de Berg, L., Bidlot, J., Bormann, N., Caires, S., Chevallier, F., Dethof, A., Dragosavac, M., Fisher, M., Fuentes, M., Hagemann, S., Holm, E., Hoskins, B., Isaksen, L., Janssen, P., Jenne, R., McNally, A., Mahfouf, J.-F., Morcrette, J.-J., Rayner, N., Saunders, R., Simon, P., Sterl, A., Trenberth, K., Untch, A., Vasiljevic, D., Viterbo, P., and Woollen, J.: The ERA-40 re-analysis, Quart. J. Roy. Meteor. Soc., 131, 2961–3012, 2005.

Vavrus, S.: The role of terrestrial snow cover in the climate system, Climate Dynamics, 29, 73–88, URL http://dx.doi.org/10.1007/s00382-007-0226-0, 2007.

Viterbo, P., Beljaars, A., Mahfouf, J.-F., and Teixeira, J.: The representation of soil moisture freezing and its impact on the stable boundary layer, Q.J.R. Meteorol. Soc., 125, 2401–2426, URL http://dx.doi.org/10.1002/qj.49712555904, 1999.

von Storch, H., Langenberg, H., and Feser, F.: A Spectral Nudging Technique for Dynamical Downscaling Purposes, Monthly Weather Review, 128, 3664–3673, 2000.

Waldron, K. M., Peagle, J., and Horel, J. D.: Sensitivity of a spectrally filtered and nudged limited area model to outer model options., Mon. Wea. Rev., 124, 529–547, 1996.

Waliser, D., Kim, J., Xue, Y., Chao, Y., Eldering, A., Fovell, R., Hall, A., Li, Q., Liou, K., McWilliams, J., Kapnick, S., Vasic, R., Sale, F., and Yu, Y.: Simulating cold season snowpack: Impacts of snow albedo and multi-layer snow physics, 109, 95–117–, URL http://dx.doi.org/10.1007/s10584-011-0312-5, 2011.

Warrach, K.: Gefrorener Boden und Schneebedeckung unter besonderer Berücksichtigung des hydrologischen Verhaltens der Landoberfläche, Ph.D. thesis, GKSS, 2000.

Weisse, R. and Feser, F.: Evaluation of a method to reduce uncertainty in wind hindcasts performed with regional atmosphere models, Coastal Engineering, 48, 211–225, URL http://www.sciencedirect.com/science/article/pii/S0378383903000279, 2003.

Winterfeldt, J., Geyer, B., and Weisse, R.: Using QuikSCAT in the added value assessment of dynamically downscaled wind speed, Int. J. Climatol., 31, 1028–1039, 2010.

Wood, A.: Siberia: Problems and Prospects for Regional Development, Croom Helm, 1987.

Wu, R., Kinter, J. L., and Kirtman, B. P.: Discrepancy of Interdecadal Changes in the Asian Region among the NCEP-NCAR Reanalysis, Objective Analyses, and Observations, J. Climate, 18, 3048–3067, doi:10.1175/JCLI3465.1, URL http://dx.doi.org/10.1175/JCLI3465.1, 2005.

Yang, D., Robinson, D., Zhao, Y., Estilow, T., and Ye, B.: Streamflow response to seasonal snow cover extent changes in large Siberian watersheds, J. Geophys. Res., 108, 4578–4592, 2003.

Ye, H. and Fetzer, E. J.: Atmospheric moisture content associated with surface air temperatures over northern Eurasia, Int. J. Climatol., 30, 1463–1471, URL http://dx.doi.org/10.1002/joc.1991, 2010.

Zahn, M. and von Storch, H.: A long-term climatology of North Atlantic polar lows, Geophysical Research Letters, 35, L22 702, doi:10.1029/2008GL035769, 2008.

Zhang, T., Frauenfeld, O. W., Serreze, M. C., Etringer, A., Oelke, C., McCreight, J., Barry, R. G., Gilichinsky, D., Yang, D., Ye, H., Ling, F., and Chudinova, S.: Spatial and temporal variability in active layer thickness over the Russian Arctic drainage basin, J. Geophys. Res., 110, D16 101–, 2005.

Zhang, T., Barry, R., and Gilichinsky, D.: Russian Historical Soil Temperature Data, Boulder, Colorado USA: National Snow and Ice Data Center. CD-ROM., 2006.

Zhao, T. and Fu, C.: Comparison of products from ERA-40, NCEP-2, and CRU with station data for summer precipitation over China, 23, 593–604–, URL http://dx.doi.org/10.1007/s00376-006-0593-1, 2006.

Zhao, T. and Fu, C.: Intercomparison of the summertime subtropical high from the ERA-40 and NCEP/NCAR reanalysis over East Eurasia and the western North Pacific, 26, 119–131–, URL http://dx.doi.org/10.1007/s00376-009-0119-8, 2009.

Acknowledgements

During my PhD work I received a lot of support by many persons to whom I am deeply thankful either for their scientific help or their contribution in every-day life. First of all, I would like to thank the members of my supervising panel, Prof. Hans von Storch, Prof. Eva Pfeiffer and Dr. Burkhardt Rockel for their scientific advice.

Special thanks to Prof. Hans von Storch, and Dr. Burkhardt Rockel for giving me the possibility to work on this interesting topic.

In particular, I have to thank my supervisor Dr. Burkhardt Rockel for a good and productive collaboration. I appreciated his scientific guidance and support especially during the long-lasting period of model configuration.

I am very grateful to Dr. Beate Geyer for her comments, suggestions and scientific support throughout all the period. Thanks for the patience in answering all my questions concerning the data analysis.

Another thank-you goes to Dennis Bray for his 'english look' to the different parts of my thesis.

Furthermore, I would like to thank my colleagues of the 'Regional Atmospheric Modelling' group and the colleagues from the Institute of Coastal Research for a nice working atmosphere and helpful talks. I am very grateful to those colleagues who gave me a ride from Hamburg to Geesthacht. It was a great help for me.

I would also thank all of my friends for their patience and for all the nice moments beyond my PhD work.

Finally, I would like to say thank-you to my parents and family for their encouragement and continuous understanding in all these years.

Declaration

(Eidesstattliche Erklärung)

Hiermit erkläre ich an Eides statt, dass ich die vorliegende Dissertationsschrift selbst verfasst und keine anderen als die angegebenen Quellen und Hilfsmittel benutzt habe.

Hamburg, den 2. Dezember 2013

Katharina Klehmet